

"Common sense is the collection of prejudices acquired by age eighteen"

-Albert Einstein

University of Alberta

Pipeline Transport of Wheat Straw Slurry

by

Jason Luk

A thesis submitted to the Faculty of Graduate Studies and Research
in partial fulfillment of the requirements for the degree of

Master's of Science
in
Engineering Management

Department of Mechanical Engineering

©Jason Luk
Fall 2010
Edmonton, Alberta

Permission is hereby granted to the University of Alberta Libraries to reproduce single copies of this thesis and to lend or sell such copies for private, scholarly or scientific research purposes only.

Where the thesis is converted to, or otherwise made available in digital form, the University of Alberta will advise potential users of the thesis of these terms.

The author reserves all other publication and other rights in association with the copyright in the thesis and, except as herein before provided, neither the thesis nor any substantial portion thereof may be printed or otherwise reproduced in any material form whatsoever without the author's prior written permission.

Examining Committee

Amit Kumar, Mechanical Engineering

Mike Lipsett, Mechanical Engineering

Rajender Gupta, Chemical and Materials Engineering

Abstract

This study experimentally evaluated wheat straw slurry pipelines. Tests were conducted to determine the particle properties of the biomass mixed in water over time. The saturated particle density of $1,060\text{kg/m}^3$ was reached after 24 hours, while the saturated moisture contents of 78.5% and 79.5% were later reached for particle sizes of 1/8" and 3/4" respectively.

A pipeline loop was redesigned to operate with 1/8", 1/4", and 3/4" straw particle slurries at up to 30% wet basis concentrations. The modifications allowed measurements of pressure loss through a length of pipe.

These measurements which show the influences of drag reducing fibre suspension. Straw particles added to water lowered the pressure loss, by suppressing turbulence at lower concentrations or higher velocities. Additional straw further improved the result, until the maximum concentration was reached. High concentrations create plugs, increasing the pressure loss. Longer straw particles can further reduce losses, but have lower maximum concentrations.

Acknowledgements

The greatest debt of gratitude is owed to the guidance of supervisor Dr. Amit Kumar, which began years in advance of this thesis project. Dr. Sean Sanders provided critical insights into the nuances of experimental pipeline research. Mr. Curt Stout inspired with innovative design concepts. Credit is extended to Dr. Andre MacDonald for shaping the author's communication skills, however limited it may be. If it were not for whom, this paper may have descended into a highly unreadable state of perpetual revisions.

Peers have also played a tremendous role in the fruition of this project; most notably Hossein Safaei Mohamadabadi, for his ongoing support and mentoring. Appreciation is also extended to Victor Jaimes, Henrique Fernandes, Susanjib Sarkar, and Mahdi Vaezi whose aid, inquisition and friendship have been invaluable.

By far the largest sacrifices have been made by Kaye Yu and my family, for which I am forever grateful.

Table of Contents

Chapter I: Introduction	1
1. Background.....	1
2. Pipeline Transportation	3
3. Objectives	4
4. Scope and Limitations.....	5
5. Organization of the Thesis	6
Chapter II: Particle Characterization	7
1. Background.....	7
2. Methodology	8
3. Results and Discussion.....	16
3.1. Particle Size Comparison.....	21
3.2. Preliminary Results Comparison	27
Chapter III: Hydraulic Transport Design.....	29
1. Background.....	29
2. Methodology	29
2.1. Design Intent.....	30
2.2. Original Design	34
2.3. Modified Design	45
3. Results and Discussion.....	64
Chapter IV: Hydraulic-transport Characterization.....	69
1. Methodology	69
1.1. Operating Conditions	69
1.2. Material Introduction	70

1.3. Sample Preparation	71
1.4. Data Collection	72
2. Results and Discussion.....	75
2.1. Concentration Comparison	91
2.2. Particle Size Comparison.....	93
2.3. Drag Reducing Fibre Suspension	96
2.4. Other Drag Reducing Mechanisms	98
2.5. Efficiency Comparison	102
2.6. Effective Viscosity	105
2.7. Uncertainty Analysis	106
Chapter V: Conclusions	110
1. Particle Characterization	110
2. Hydraulic-transport Design.....	111
3. Hydraulic-transport Characterization	112
4. Recommendations for Future Work.....	117
Bibliography.....	119
Appendix: Detailed Design Drawings.....	128

List of Tables

Table 1: Straw particle size classification.....	8
Table 2: Straw conditions at different moisture levels	10
Table 3: Moisture content sample results for 1/8" particle size.....	17
Table 4: Moisture content sample results for 3/4" particle size.....	18
Table 5: Particle density sample results for 1/8" particle size	19
Table 6: Particle density sample results for 3/4" particle size	20
Table 7: Experimental design considerations.....	30
Table 8: System components	45
Table 9: Minor loss coefficients.....	46
Table 10: Major loss factors.....	46
Table 11: 3 m/s System Head Loss	50
Table 12: Power law approximation for pressure loss gradients	75
Table 13: 1/8" 30% Concentration slurry pressure drop data	76
Table 14: 1/8" 25% Concentration slurry pressure drop data	77
Table 15: 1/8" 20% Concentration slurry pressure drop data	78
Table 16: 1/8" 15% Concentration slurry pressure drop data	79
Table 17: 1/8" 10% Concentration slurry pressure drop data	80
Table 18: 1/8" 5% Concentration slurry pressure drop data	81
Table 19: 1/4" 25% Concentration slurry pressure drop data	82
Table 20: 1/4" 20% Concentration slurry pressure drop data	83
Table 21: 1/4" 15% Concentration slurry pressure drop data	84
Table 22: 1/4" 10% Concentration slurry pressure drop data	85
Table 23: 1/4" 5% Concentration slurry pressure drop data	86

Table 24: 3/4" 10% Concentration slurry pressure drop data	87
Table 25: 3/4" 5% Concentration slurry pressure drop data	88
Table 26: Optimum conditions to minimize specific pumping requirements.....	116

List of Figures

Figure 1: Wet straw between layers of towel.....	11
Figure 2: Wheat straw mass over time in drying oven.....	12
Figure 3: Mesh cylinder fabricated for particle density experiments	13
Figure 4: Flowchart depicting experimental methodology for measuring particle properties	15
Figure 5: Moisture content over time in mixing tank	21
Figure 6: Particle density over time in mixing tank	22
Figure 7: Carrier fluid impurities concentrated on the surface of wet straw	23
Figure 8: Mesh cylinder suspended in water.....	26
Figure 9: Saturated particle properties.....	27
Figure 10: Particle density of 1/8" average particle size straw.....	28
Figure 11: Physical constraints of laboratory floor space	32
Figure 12: Centrifugal pump curve.....	33
Figure 13: Godwin CD80M pump	34
Figure 14: Schematic of original system layout.....	35
Figure 15: Upstream and downstream pressure transducer noise	36
Figure 16: Correlation of pressure transducer and flow rate noise	38
Figure 17: Air bubbles seen in viewing section	40
Figure 18: Slurry splashing caused by mixer and mixing tank inlet	41
Figure 19: Slurry viscosity experienced by viscometer.....	42
Figure 20: Temperature escalation of ice water pumped in pipeline loop.....	44
Figure 21: Schematic of modified system layout.....	51
Figure 22: Pressure taps and flow meter are placed away from bends	52

Figure 23: Mechanical pressure gauges adjoined by bleed valves	53
Figure 24: Coils of long radius hose in line with pipeline	54
Figure 25: Mixing tank inlet submerged to allow air bubbles to dissipate	55
Figure 26: Air dissipating from slurry accumulates as bubbles on surface	56
Figure 27: Hose bend in wide radius connects the pump to mixing tank	58
Figure 28: Slurry cycles through the entire system during normal operation	59
Figure 29: A siphon reverses the slurry in the return line during discharge	59
Figure 30: The dilution tank is elevated above the mixing tank	60
Figure 31: Transparent PVC return line links discharge valve to mixing tank	61
Figure 32: PVC hose, cam lock and ball valve in-line with steel pipe	62
Figure 33: Insulated 90 gallon water bath	63
Figure 34: Theoretical and experimental friction factors.....	64
Figure 35: Inner diameter of cam lock fittings are 1/4" less than steel pipe	66
Figure 36: Maximum flowable concentration at different particle sizes	67
Figure 37: 40% concentration slurries are not flowable.....	68
Figure 38: Flowchart depicting experimental methodology for measuring hydraulic transport properties	74
Figure 39: 30% 1/8" Average size woodchip and straw slurries	89
Figure 40: Maximum flowable slurry concentration pressure losses.....	90
Figure 41: 1/8" Particle slurry pressure losses, exhibiting 25% & 30% plugs	92
Figure 42: 1/4" Particle slurry pressure losses, exhibiting 25% plug	92
Figure 43: 3/4" Particle slurry pressure losses, exhibiting 10% plug.....	92
Figure 44: 5% Relative pressure losses, exhibiting no plugs	94
Figure 45: 10% Relative pressure losses, exhibiting 3/4" plug	94
Figure 46: 15% Relative pressure losses, exhibiting no plugs.....	94

Figure 47: 20% Relative pressure losses, exhibiting no plugs.....	95
Figure 48: 25% Relative pressure losses, exhibiting 1/8" & 1/4" plugs	95
Figure 49: 30% Relative pressure losses, exhibiting 1/8" plug	95
Figure 50: a) nylon, b) asbestos fibres and c) wood pulp	97
Figure 51: Specific pressure loss by concentration at 1.5 m/s.....	102
Figure 52: 1/8" particle size specific pumping requirements by velocity	103
Figure 53: 1/8" particle size specific pumping requirements, per unit time	104
Figure 54: Effective viscosity of 1/8" average particle size straw slurry	105
Figure 55: Coefficient of determination by wet basis concentration.....	106
Figure 56: Relative pressure drop 95% confidence interval at 3 m/s.....	107
Figure 57: A mix of straw reveals green and golden material.....	108
Figure 58: Pressure loss of maximum flowable concentrations.....	112
Figure 59: Pressure loss of 1/4" particle size slurry.....	113
Figure 60: Pressure loss of 10% concentration slurry	114
Figure 61: Pumping requirements of 1.5 m/s slurry.....	115
Figure 62: Assembly of loop	129
Figure 63: 5260 mm pipe section.....	130
Figure 64: 1110 mm pipe section.....	131
Figure 65: 740 mm pipe section.....	132
Figure 66: 9770 mm pipe section.....	133
Figure 67: Discharge outlet.....	134
Figure 68: Return line	135
Figure 69: Mixing tank	136
Figure 70: Discharge tank stand.....	137
Figure 71: Water bath tank	138

List of Nomenclature

C_{dry}	Concentration, dry mass basis (%)
C_{wet}	Concentration, wet mass basis (%)
C_{vol}	Concentration, volume basis (dimensionless)
ρ_{slurry}	Density of slurry (kg/m ³)
ρ_{water}	Density of water (kg/m ³)
D_{pipe}	Diameter of pipe (internal) (m)
ρ	Density of fluid (kg/m ³)
f	Friction factor (dimensionless)
g	Gravity acceleration (m/s ²)
h	Head loss (m of water)
$m_{straw,air}$	Mass of air dry straw (kg)
$m_{straw,wet}$	Mass of wet straw (kg)
$m_{straw,oven}$	Mass of oven dry straw (kg)
$m_{straw,wet}$	Mass of wet straw (kg)
$m_{straw,water}$	Mass (apparent) of wet straw sample in water (kg)
m_{water}	Mass of water added to slurry (kg)
$u_{m_{straw,wet}}$	Mass of wet straw uncertainty (kg)
K	Minor head loss coefficient (dimensionless)
MC_{straw}	Moisture content of straw sample (%)
MC_{air}	Moisture content of air dry straw (%)
u_{MC}	Moisture content uncertainty (%)
ρ_{straw}	Particle density of wet straw (kg/m ³)
u_{ρ}	Particle density uncertainty (kg/m ³)
i_m	Pressure drop of slurry (m of water per m of pipe length)
i	Pressure drop of clear water (m of water per m of pipe length)
k	Ratio of particle dimensions to diameter of pipe (dimensionless)
Re	Reynolds's number (dimensionless)
v_m	Velocity of slurry (mean) (m/s)
ν	Viscosity of carrier fluid (kinematic) (m ² /s)
μ	Viscosity of liquid (Pa*s)

Chapter I:

Introduction

1. Background

A concerted effort to address global warming could alter the world economy. A transformation of the energy sector in particular will be required to manage overall greenhouse gas emissions. Potential solutions not only must meet economic and environmental benchmarks, but also address political and technical challenges.

Biofuels are increasingly used as an alternative to traditional energy sources derived from fossil fuels. As with wind and solar power, it can be nearly carbon neutral and renewable (Chum and Overend, 2001). However, liquid biofuels are also more readily stored and integrated into existing transport infrastructure based on liquid petroleum fuels. Conversely, the widespread use of electric vehicles would require substantial investments in power generation and transmission (Hajimiragha et al., 2010). A more near term transition to plug in hybrid electric vehicles would still require the availability of liquid fuels. Economic wind and solar energy sources can also be more geographically limited (National Energy Board 2006).

Domestic production of biofuels is a means of economic diversification. For net importing countries such as the United States, it provides energy security while acknowledging climate change concerns (Farrell et al., 2006). For emerging

nations such as Brazil, biofuel exports contribute economic growth (Geller et al., 2004; Oosterveer and Mol, 2010). While this growth has been accelerated by government mandated use of renewable fuels (Libecap, 2003), it has been met with industry investment. The nature of the technology has allowed both established agricultural and petro-chemical industry leaders, as well as regional competitors to enter the market (Gnansounou, 2010; Canadian Renewable Fuels Association, 2009).

Cellulosic ethanol, a second generation biofuel, may allow the industry to expand beyond its current niche role. It will enable the use of abundant, low value, non-food crops such as grasses, or food crop by-products such as straw (Bi et al., 2009; Singh et al., 2010). Despite the rapid developments, the technology is currently only realized at small scale productions (Gnansounou and Dauriat, 2010; Banerjee et al., 2010; Canadian Renewable Fuels Association, 2009).

Bio-refineries produce fuels at capacities significantly below that of petroleum refineries. Thus capital costs per unit output are disproportionately high due to economies of scale, with the scale factor typically being between 0.6-0.9 (Kumar et al., 2003). The capacity is constrained by the substantial transportation costs of biomass feedstock (Kumar et al., 2004; Searcy et al., 2007). Low energy densities require a high mass of feedstock to be shipped, which is further exacerbated by low bulk densities of the baled material. Limited crop yields require the biomass to be collected over vast areas, increasing transport distances.

The conventional means of transportation introduces further constraints. Large scale truck transportation effectively has a fixed cost per tonne which is independent of the distance of transport and the scale of the field sourced biorefinery (Searcy et al., 2007). Financial considerations aside, there are practical limitations as well. A large theoretical cellulosic ethanol plant would require 15 trucks per hour, to deliver the 2M dry tonnes of feedstock required per year to producing only 960 ML annually (Kumar et al., 2005b). Thus traffic congestion alone prevents production capacities from reaching that of existing petroleum refineries. The GS Caltex Yeosu Complex has a production capacity over 100 ML daily (GS Caltex, 2005), which is several orders of magnitude greater.

2. Pipeline Transportation

Pipeline transportation enables petroleum refineries to achieve these capacities. It is a well-established technology, which benefits from economies of scale and is not limited by traffic congestion (Ghafoori et al., 2007). Fine slurry pipelines have been successfully used in the mining industry to transport solids over long distances. The Black Mesa Coal Slurry Pipeline is 439 km in length (Liu, 2003).

A preliminary body of work has been developed on wood chip biomass slurries (Hunt, 1976; Elliot and Montmorency, 1963). It has been found to be competitive with truck transportation at high concentrations and large capacities (Kumar et al., 2004). However, other biomass materials have yet to be investigated.

Alternatively pneumatic pipelines would also be able to transport biomass solids. However, this technology would utilize lower density air to carry materials and requires significantly higher velocities, over 10 m/s, than slurry pipelines (Liu, 2003; Pryfogle, 2009). As power consumption increases to the third power with respect to pump speed (Energy Manager Training, n.d), slower slurry transportation results in lower operating costs. Pneumatic pipelines would not be practical over the long distances, which would be of interest to biomass transportation.

Further, the water absorption by the biomass materials destined for ethanol production in a slurry pipeline is not a concern, and may even be advantageous. This feedstock is ultimately prepared into slurry form to allow fermentation and other processes, regardless of the means of transportation (Kumar et al., 2005a). The slurry can be prepared at satellite locations and pumped to a large scale pipeline which can deliver the lignocellulosic biomass to a biorefinery. This helps in accumulation of the biomass and hence large scale transport. Also, pipeline gives an opportunity to do pre-processing of biomass before ethanol production in the plant.

3. Objectives

The overall objective of this research work is to understand the rheological characteristics of pipeline transport of biomass slurries. The focus of this phase of research is to study the agricultural biomass (i.e. wheat straw) based slurry.

Slurry is formed by mixing chopped straw in water. Following are the specific objectives of this thesis:

- Study the characteristics of the wheat straw slurry in terms of changes in its physical properties due to water absorption in a mixing tank.
- Redesign and fabrication of the earlier designed loop to handle high concentrations.
- Study the pressure drop profile of the slurry in the pipeline with respect to:
 - Changes in concentration
 - Changes in velocity in the pipeline
 - Changes in particle size
- Compare the pressure drop of wheat straw based slurry with water.
- Determine the optimum operating conditions in the pipeline for the transport of wheat straw slurry to minimize specific pumping requirements.

4. Scope and Limitations

The study was limited to only wheat straw based as the feedstock. Only water was studied as the carrier fluid in this research work. The study used a pipeline loop of 2" in diameter and 45 m long. The loop was made of carbon steel. The particle size of straw was limited to three particle sizes including 1/8", 1/4" and 1/8". The measurement of physical characteristics would include water absorption characteristics in terms of moisture content at different particle density and concentrations.

5. Organization of the Thesis

This thesis contains five chapters in addition to a table of contents, a list of tables, a list of figures, a list of abbreviations, and an appendix. This study is divided into three main phases, each of which comprise of its own chapter in this thesis.

Chapter 1 includes the background of this study, objectives of the study definition of the problem, and limitations of the study.

In Chapter 2 particle characterization experiments to determine slurry preparation requirements is explained. This characterization includes moisture content and particle density measurement at various time intervals in exposing straw with water in a mixing tank.

In Chapter 3 describes the methodology of redesigning an existing laboratory pipeline system to optimize its use for biomass slurry experimentation and its fabrication.

Chapter 4 examines the hydraulic transport characteristics of the slurry samples pumped through the pipeline system. This chapter details the pressure drop in the pipeline due to the wheat straw based water slurry at various concentrations, slurry velocities and particle sizes.

Finally conclusions and recommendations based on the results of research work and future recommendations of for research are given in Chapter 5.

Chapter II:

Particle Characterization

1. Background

Particle characterization experiments were conducted to provide a better understanding of biomass slurry. Dry biomass materials absorb a significant amount of water when used for preparation of slurry (Kumar and Flynn, 2006). The slurries with straw absorbing water at a rapid rate are more susceptible to congestion in pipelines. During the experimental phase straw was saturated with water. On an industrial scale it is necessary to determine the amount of time straw should be prepared in a mixing tank before being introduced into the pipeline, to introduce near constant concentration of slurry in the pipeline. These saturated properties are also pertinent to the end user of the material after pipeline transportation, to understand the delivered conditions.

Preliminary results of moisture content and particle density during mixing, was reviewed from earlier work done by Mohamadabadi (2009). This work was refined, to explore the accuracy of those results. An understanding of the statistical significance of physical characterization conclusions were gained from this study.

2. Methodology

Table 1: Straw particle size classification

Screen Size	Estimated Average Particle Size
3/4"	n/a, discarded
1/2"	n/a, discarded
1/4"	n/a, discarded
5/32"	3/4"
1/8"	1/4"
1/20"	1/8"
Pan	n/a, discarded

The following is a brief description of the processes used to determine the particle density and moisture content of wheat straw in a mixing tank over time. A more detailed explanation can be found in an earlier study by Mohamadabadi (2009). Any differences in the methodology are clearly noted.

The wheat straw feedstock, which is readily available lignocellulosic biomass in Western Canada, was collected near Westlock, Alberta (Desseault Farms, 2009). The 15-20kg bales of straw were chopped using a cutting mill (Retsch, 2007), producing a particle size distribution from less than 1 mm to over 25 mm. On an industrial scale, this narrow gradient may be insignificant when pumped within a pipeline several feet in diameter. However on a laboratory scale system, which in this case had a 2" diameter pipeline, a smaller tolerance was desired.

The chopped wheat straw was passed through a chip classifier (BM&M Screening Solutions, 2007). A stack of 6 screens of descending square openings were used. The shaker was operated for 2 minutes as per ASABE standard (ASABE, 2007), for each load. The material collected on lower 3 screens were

collected for testing, and are referred to by their approximate average particle sizes of 3/4", 1/4", and 1/8" respectively, as shown in Table 1.

This dry wheat straw was then prepared into dilute slurries. It maintained a $1\pm 0.5\%$ dry basis concentration by mass, as calculated by Equation 1 and Equation 2, using Mohamadabadi's finding of 6% air dry moisture content (Mohamadabadi, 2009). Wet straw samples were taken out, leaving behind the carrier fluid in the mixing tank. This allows the large mixing tank volume of 80 ± 10 gallons to be maintained, allowing similar agitation throughout the test, which is provided by a 280 rpm impeller further described in Chapter 3. The large volume of slurry reduces the change in concentration as samples are removed.

Equation 1: Dry basis concentration by mass

$$C_{dry} = \frac{m_{straw,oven}}{m_{water} + m_{straw,air}} * 100\%$$

Where:

C_{dry} : Concentration, dry mass basis (%)

$m_{straw,oven}$: Mass of oven dry straw (kg)

$m_{straw,air}$: Mass of air dry straw (kg)

m_{water} : Mass of water added to slurry (kg)


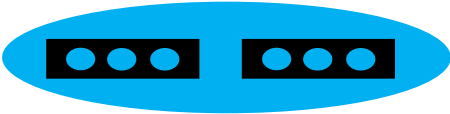



Equation 2: Oven dry mass of air dry straw

$$m_{straw,oven} = m_{straw,air} * (100\% - MC_{air})$$

Where:

MC_{air} : Moisture content of air dry straw (%)

Table 2: Straw conditions at different moisture levels

Condition	Description	Illustration
Air Dry	Limited internal moisture after storage in ambient air	
Saturated Slurry	Fully submerged in carrier fluid, maximum internal moisture	
Saturated Strained	Residual moisture left on surface, maximum internal moisture	
Saturated Surface Dry	No residual moisture left on surface, maximum internal moisture	
Oven Dry	No internal or surface moisture after drying in 110 + 5 °C heat	

These samples are taken from the mixing tank in 8 time intervals; 1, 3, 6, 12, 24, 48, 96 and 144 hours after preparation. Although Mohamadabadi (2009) included a 196 hour tests, he found identical properties as the 144 hour results, and thus were excluded in this set of experiments for practical reasons. Each time sample was approximately 4 kg of wet straw. Excess moisture between particles was strained with a 1/4" square screen. After this process, surface moisture not absorbed within the straw remained. The moisture sitting on the surface was then removed to create surface dry conditions, which is required to accurately measure the properties of the straw itself. Ideal straw conditions are explained in Table 2.



Figure 1: Wet straw between layers of towel

In an effort to more accurately achieve a surface dry material, the surface drying methodology was more thorough than that of Mohamadabadi (2009). The wet straw was spread across an area of commercial paper towel 4 times larger, at approximately 40 square feet. Further, to prevent over saturation of the drying medium, the paper towel was placed over a layer of ribbed microfiber towel. Upon this microfiber and paper towel base, the wet straw was padded down by an additional layer of paper towel, and gently rolled to remove moisture on all straw surfaces. This is shown in Figure 1.

The surface dry straw was then suitable for experimentation. The time sample was subdivided into 6 test samples to determine particle density and moisture content.

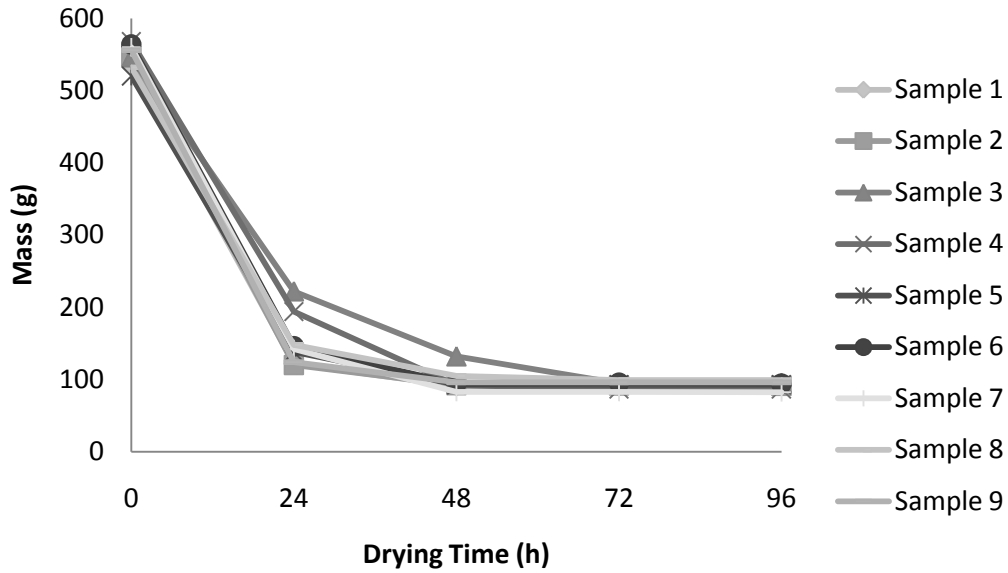


Figure 2: Wheat straw mass over time in drying oven

Moisture content was measured according to ASABE (ASABE, 2008) and ASTM (ASTM, 2004) standards. Three test samples of wet straw of at least 500 g were placed in individual paper bags and weighed to the nearest 2 g. The wet straw are then dried in a ventilated oven at $110 \pm 5^\circ\text{C}$. The test samples remained in the oven until further drying would not result in additional decrease mass. When the 3260 W Aminco test unit (Newport Scientific, n.d.), was filled with 9 sample bags, it was found to require 72 hours of drying time, as seen in Figure 2. The dry samples were then weighed to within 2 g, and the wet basis moisture content was calculated by Equation 3.



Figure 3: Mesh cylinder fabricated for particle density experiments

Equation 3: Moisture content equation

$$MC_{straw} = \frac{m_{straw,wet} - m_{straw,oven}}{m_{straw,wet}} * 100\%$$

Where:

MC_{straw} : Moisture content of straw sample (%)

$m_{straw,wet}$: Mass of wet straw (kg)

Particle density was evaluated according to ASTM standards (ASTM, 2007). The cylinder in Figure 3, with a 150 mm diameter and height, manufactured with a 1/16" mesh material, was loosely filled with wet straw. The mass of straw is weighed within 2 g in air, and when submerged in water. The difference between the two values is due to the displaced volume of water, which provides a buoyant force against the material. Particle density was calculated with Equation 4.

Equation 4: Particle density equation

$$\rho_{straw} = \frac{m_{straw,wet} * \rho_{water}}{(m_{straw,wet} - m_{straw,water})}$$

Where:

ρ_{straw} : Particle density of wet straw (kg/m³)

ρ_{water} : Density of water (kg/m³)

$m_{straw,water}$: Mass (apparent) of wet straw sample in water (kg)

Both of these two experiments were conducted on all three test samples, for each of the 8 time samples, of each of the slurries examined. The process was repeated twice for a total of 3 trials. Thus a total of 9 data points were collected at each time interval, for each test. A summary of the methodology is summarized as a flow chart in Figure 4.

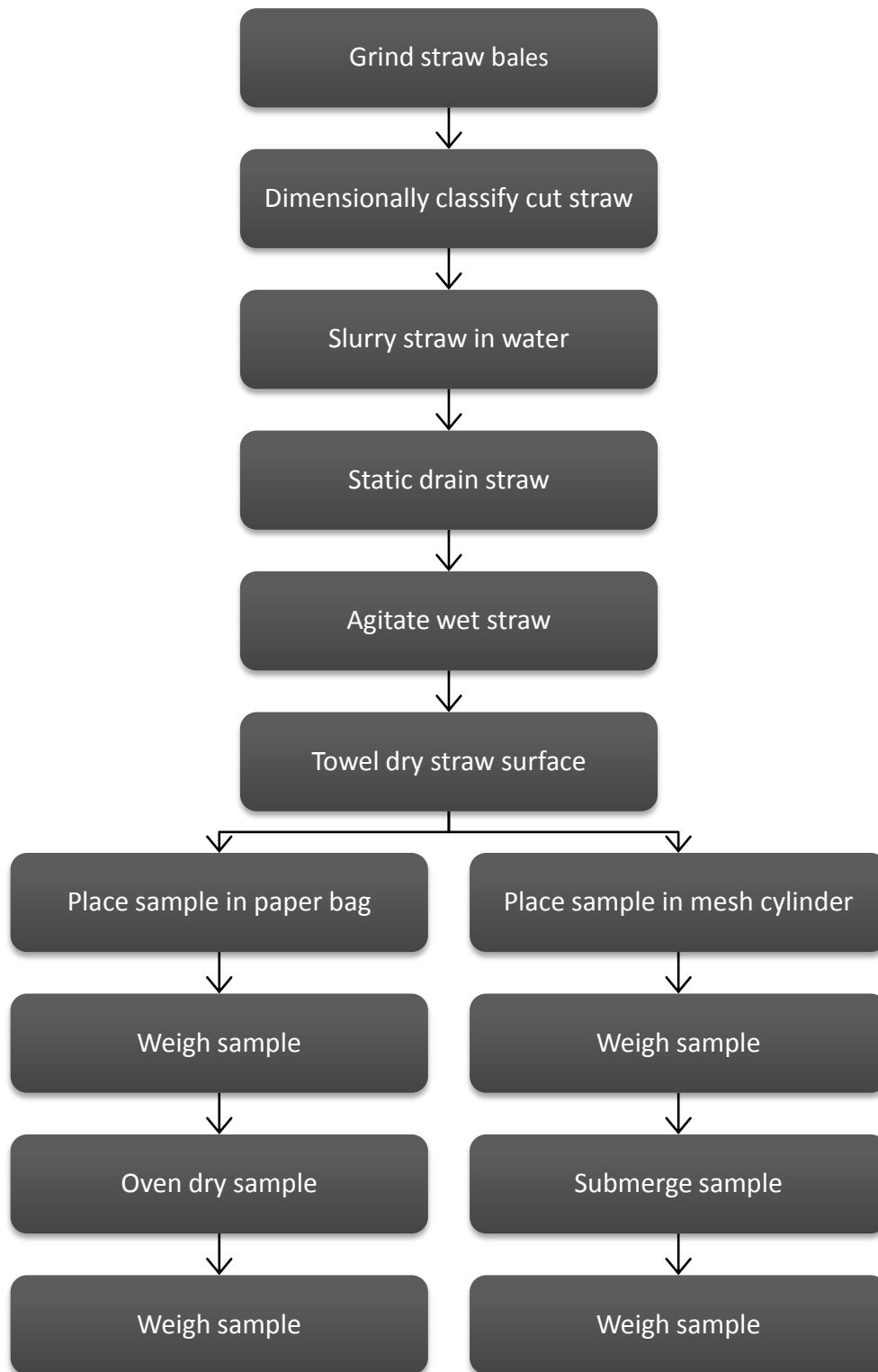


Figure 4: Flowchart depicting experimental methodology for measuring particle properties

3. Results and Discussion

The physical characterization results of 1/8" and 3/4" particles are itemized in Table 3 through Table 6. The confidence intervals are based on the student-t test. The data was plotted to a resolution of 0.5% moisture content and 10 kg/m³ particle density. The resolutions selected are loosely based on the standard deviation of the values at each time interval. Fine differences from reporting more precise measurements would not be statistically significant, as can be seen with the 95% confidence intervals plotted in subsequent figures. The confidence intervals are based on the student-t test.

Table 3: Moisture content sample results for *1/8" particle size

Time (hour)	Sample	Trial A	Trial B	Trial C	Average	95% Confidence Interval
1	A	74.9%	73.1%	73.3%	74.0%	±0.6%
	B	74.7%	73.0%	73.5%		
	C	74.5%	73.3%	73.5%		
3	A	76.4%	74.3%	75.2%	75.5%	±0.7%
	B	76.7%	74.5%	75.2%		
	C	76.6%	75.0%	75.0%		
6	A	76.6%	75.4%	75.8%	76.0%	±0.4%
	B	76.7%	75.8%	75.9%		
	C	76.8%	75.2%	76.0%		
12	A	77.1%	77.0%	76.2%	76.5%	±0.3%
	B	77.2%	76.9%	76.1%		
	C	77.0%	76.5%	76.2%		
24	A	77.2%	78.2%	76.9%	77.5%	±0.4%
	B	77.2%	78.0%	76.8%		
	C	77.5%	78.0%	76.9%		
48	A	78.8%	78.9%	76.9%	78.0%	±0.7%
	B	78.6%	78.8%	76.8%		
	C	78.3%	78.7%	77.0%		
96	A	79.2%	79.1%	77.3%	78.5%	±0.8%
	B	79.1%	78.9%	77.2%		
	C	79.3%	79.2%	76.9%		
144	A	79.3%	79.6%	77.4%	78.5%	±0.8%
	B	79.5%	79.2%	77.5%		
	C	79.5%	79.6%	77.2%		

*Average particle size sample as classified in Table 1

Table 4: Moisture content sample results for *3/4" particle size

Time (hour)	Sample	Trial A	Trial B	Trial C	Average	95% Confidence Interval
1	A	76.0%	74.8%	76.0%	75.5%	±0.4%
	B	75.8%	74.6%	76.1%		
	C	75.6%	75.2%	76.2%		
3	A	77.6%	77.4%	77.2%	77.5%	±0.3%
	B	77.6%	78.1%	77.3%		
	C	77.9%	77.6%	77.1%		
6	A	77.2%	77.6%	78.4%	78.0%	±0.3%
	B	77.5%	78.0%	77.9%		
	C	77.4%	77.6%	78.2%		
12	A	77.9%	77.9%	79.4%	78.5%	±0.5%
	B	78.2%	77.5%	79.4%		
	C	78.2%	77.7%	78.8%		
24	A	78.7%	79.4%	79.8%	79.0%	±0.4%
	B	78.7%	79.8%	78.9%		
	C	78.5%	79.3%	79.4%		
48	A	79.0%	79.7%	79.4%	79.5%	±0.2%
	B	79.4%	79.4%	79.2%		
	C	78.9%	79.8%	79.1%		
96	A	79.2%	79.6%	79.4%	79.5%	±0.2%
	B	78.8%	79.6%	79.4%		
	C	78.9%	79.4%	79.3%		
144	A	79.2%	79.7%	79.6%	79.5%	±0.2%
	B	79.3%	79.1%	79.1%		
	C	79.3%	79.6%	79.8%		

*Average particle size sample as classified in Table 1

Table 5: Particle density sample results for *1/8" particle size

Time (hour)	Sample	Trial A (kg/m ³)	Trial B (kg/m ³)	Trial C (kg/m ³)	Average (kg/m ³)	95% Confidence Interval (kg/m ³)
1	A	944	939	948	950	±5
	B	946	938	951		
	C	950	939	957		
3	A	977	988	979	980	±10
	B	983	945	988		
	C	986	978	984		
6	A	1001	1011	1011	1010	±7
	B	1012	988	1014		
	C	1008	998	1015		
12	A	1011	1049	1027	1030	±11
	B	1020	1052	1043		
	C	1016	1026	1040		
24	A	1040	1062	1066	1060	±9
	B	1049	1071	1069		
	C	1047	1070	1067		
48	A	1038	1070	1070	1060	±10
	B	1051	1071	1075		
	C	1048	1071	1072		
96	A	1036	1074	1066	1060	±11
	B	1047	1075	1072		
	C	1054	1076	1074		
144	A	1033	1059	1070	1060	±9
	B	1060	1061	1072		
	C	1059	1066	1071		

*Average particle size sample as classified in Table 1

Table 6: Particle density sample results for *3/4" particle size

Time (hour)	Sample	Trial A (kg/m ³)	Trial B (kg/m ³)	Trial C (kg/m ³)	Average (kg/m ³)	95% Confidence Interval (kg/m ³)
1	A	906	878	887	890	±12
	B	915	884	885		
	C	908	872	873		
3	A	951	912	913	930	±16
	B	957	916	923		
	C	956	925	906		
6	A	968	960	935	960	±8
	B	962	960	955		
	C	965	959	951		
12	A	990	986	984	990	±4
	B	998	994	984		
	C	990	994	990		
24	A	1054	1058	1049	1060	±5
	B	1058	1060	1047		
	C	1066	1056	1049		
48	A	1049	1061	1055	1060	±4
	B	1059	1059	1064		
	C	1059	1066	1056		
96	A	1063	1065	1041	1060	±7
	B	1061	1064	1053		
	C	1066	1071	1053		
144	A	1063	1054	1045	1060	±5
	B	1065	1052	1051		
	C	1062	1058	1048		

*Average particle size sample as classified in Table 1

3.1. Particle Size Comparison

Figure 5 shows smaller particles consistently having lower moisture content. The 1/8" particles required 4 days to reach its 78.5% saturated moisture content. The larger 3/4" samples only required 2 days to achieve its higher 79.5% saturation level. This may be due to the increased number of exposed pores at the surface of the smaller particles. Mohamadabadi concluded that the larger pieces of straw may have more enclosed internal pores to absorb additional moisture (Mohamadabadi, 2009).

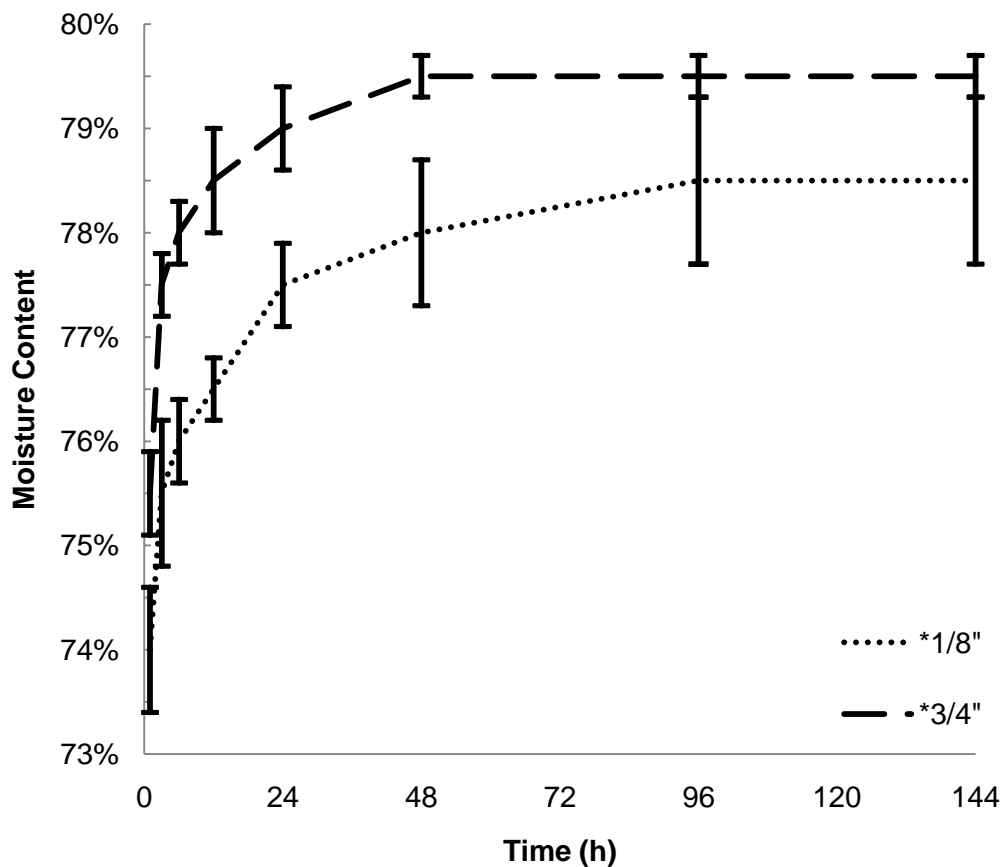


Figure 5: Moisture content over time in mixing tank

*Average particle size sample as classified in Table 1

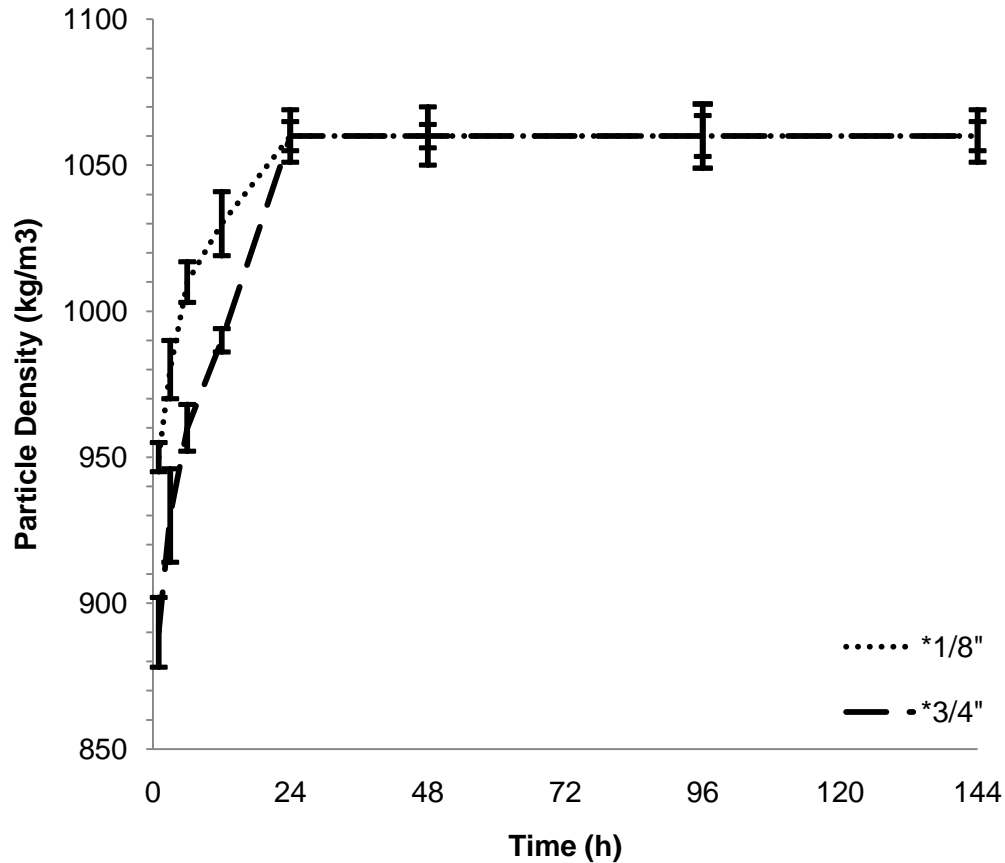


Figure 6: Particle density over time in mixing tank

In Figure 6, the saturated particle density of the two straw sizes were identical, within 10 kg/m^3 the resolution. As well, both reached 1060 kg/m^3 saturation level after 24 hours. Before that time, the smaller particles had a higher particle density with the difference significant at the 95% confidence interval. This again may be due to the decreased number of enclosed pores in the smaller particles. Internal pores void of high density moisture, decrease the density of the straw. Upon saturation of these additional pores, the significance of particle size on particle density was negligible.



Figure 7: Carrier fluid impurities concentrated on the surface of wet straw

Smaller particles have greater uncertainty, as they have increased surface area for surface moisture to reside on. This alone makes it more difficult to achieve surface dry conditions. However, it is compounded by the fact that smaller particles can also breakdown to release more fine material into the carrier fluid than larger particles (Sebastian et al., 2006). These impurities concentrate upon the surface during straining, creating a more viscous layer of surface moisture, resulting in further uncertainty in determining whether surface dry conditions have been met. An exaggerated example of this phenomenon is shown in Figure 7, where high concentration slurry has been dewatered after 8 days.

There are two main differences between the moisture content and the particle density results. First, the particle density tests appear to reach saturation after 24 hours, whereas the moisture content continues to increase thereafter. Second, the moisture content saturation levels have a statistically significant difference between the two particle sizes, while the saturated particle density is the equal.

This is due to the inability for particle density measurements to distinguish small differences. The saturated density of 1,060 kg/m³ is approximately only 6% greater than the density of water. Wet straw is primarily comprised of the water absorbed, thus the minor differences in pore structures are not evident. A finer resolution than the 10 kg/m³ used would be required to detect nuances. However it would not be meaningful in this study, as the level of uncertainty would eclipse the precision of the resolution.

The moisture content calculations capture more subtleties, but as a result it is also greater impacted by errors. Equation 5 calculates the moisture content uncertainty from wet straw mass error, due to non-dry surface conditions. It is transformed into Equation 6 when percentage errors are used.

Equation 5: Moisture content uncertainty from wet straw mass error

$$u_{MC} = \frac{100\%}{m_{straw,wet}} u_{m_{straw,wet}}$$

Where:

u_{MC} : Moisture content uncertainty (%)

$u_{m_{straw,wet}}$: Wet straw mass uncertainty (kg)

Equation 6: Moisture content percentage uncertainty from wet straw mass percentage error

$$\frac{u_{MC}}{MC_{straw}} = \frac{100\%}{MC_{straw}} \left(\frac{u_{m_{straw,wet}}}{m_{straw,wet}} \right)$$

Similarly, in Equation 7 and Equation 8, particle density uncertainty due to wet straw mass error is determined.

Equation 7: Particle density uncertainty from wet straw mass error

$$u_{\rho} = \frac{\rho_{water} * m_{straw,water}}{\rho_{straw} * (m_{wet} - m_{straw,water})^2} u_{m_{straw,wet}}$$

Where:

u_{ρ} : Particle density uncertainty (kg/m³)

Equation 8: Particle density percentage uncertainty from wet straw mass percentage error

$$\frac{u_{\rho}}{\rho_{straw}} = \frac{\rho_{water} * m_{straw,water} * m_{straw,wet}}{\rho_{straw} * (m_{straw,wet} - m_{straw,water})^2} \left(\frac{u_{m_{straw,wet}}}{m_{straw,wet}} \right)$$

As an example, the variables were substituted for the values obtained in third sample, of the third trial, at the final time interval, of 1/8" straw particles. The wet straw mass error is set at be 1%. The result is that for every 1% error in the mass of surface dry straw weighed in the air, is the equivalent of a 1.30% error in the resultant moisture content calculated. Conversely, the same 1% error contributes to a 0.07% error in particle density. The difference in the error of the resultant physical characteristic properties is two orders of magnitude.



Figure 8: Mesh cylinder suspended in water

Note that excess surface moisture does not have an effect on the mass of wet straw in water. Once suspended in the water, as shown in Figure 9, the surface moisture would simply dissipate out of the mesh cylinder, into the surrounding water. Thus, only the mass of wet straw in air is impacted.

Similarly, subtle discrepancies between the saturation rate and saturation level of different particle sizes, are magnified in the moisture content calculations, and deemphasized in particle density evaluations.

3.2. Preliminary Results Comparison

The preliminary findings indicated higher moisture content but lower particle density for smaller particles, as compared in Figure 9. While the natural variations feedstock collected from different harvests will affect the results, this statistically significant pattern is also accounted for by the difficulty in achieving surface dry conditions. An increase in the mass of wet straw from surface moisture decreases the measured particle density. This is because the excess mass is only realized when weighed in air, but dissipates when weighed in water. The calculated volume is thus larger than actual.

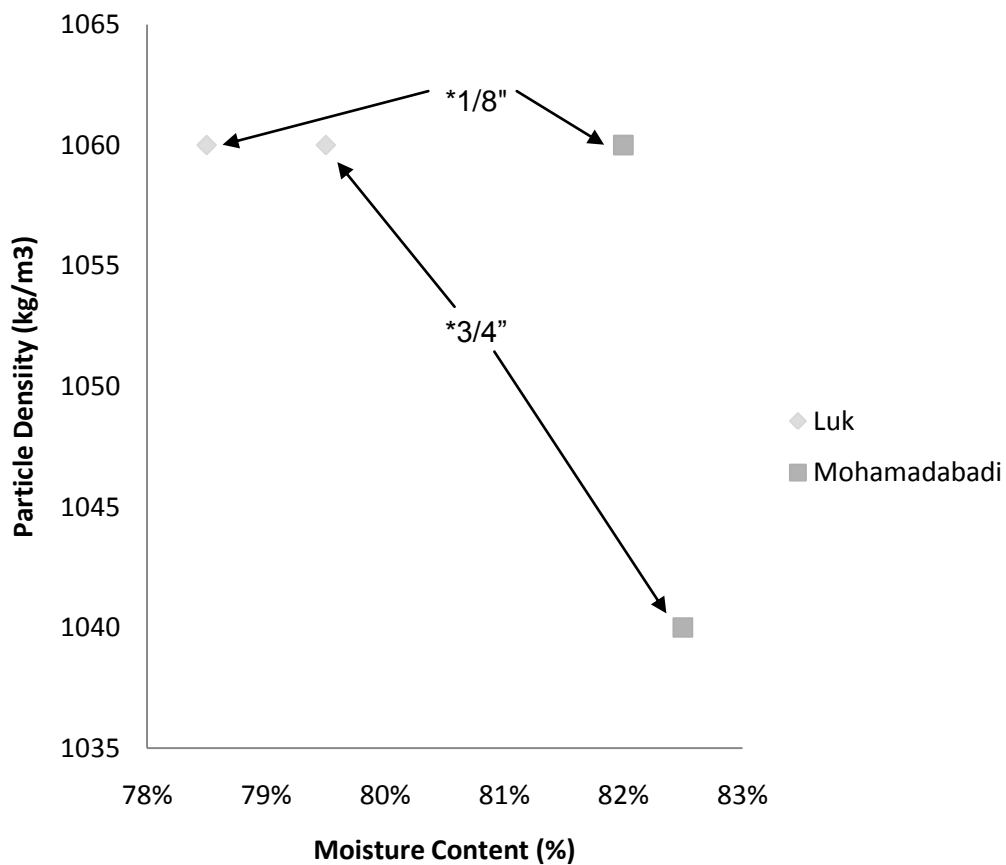


Figure 9: Saturated particle properties

**Average particle size sample as classified in Table 1*

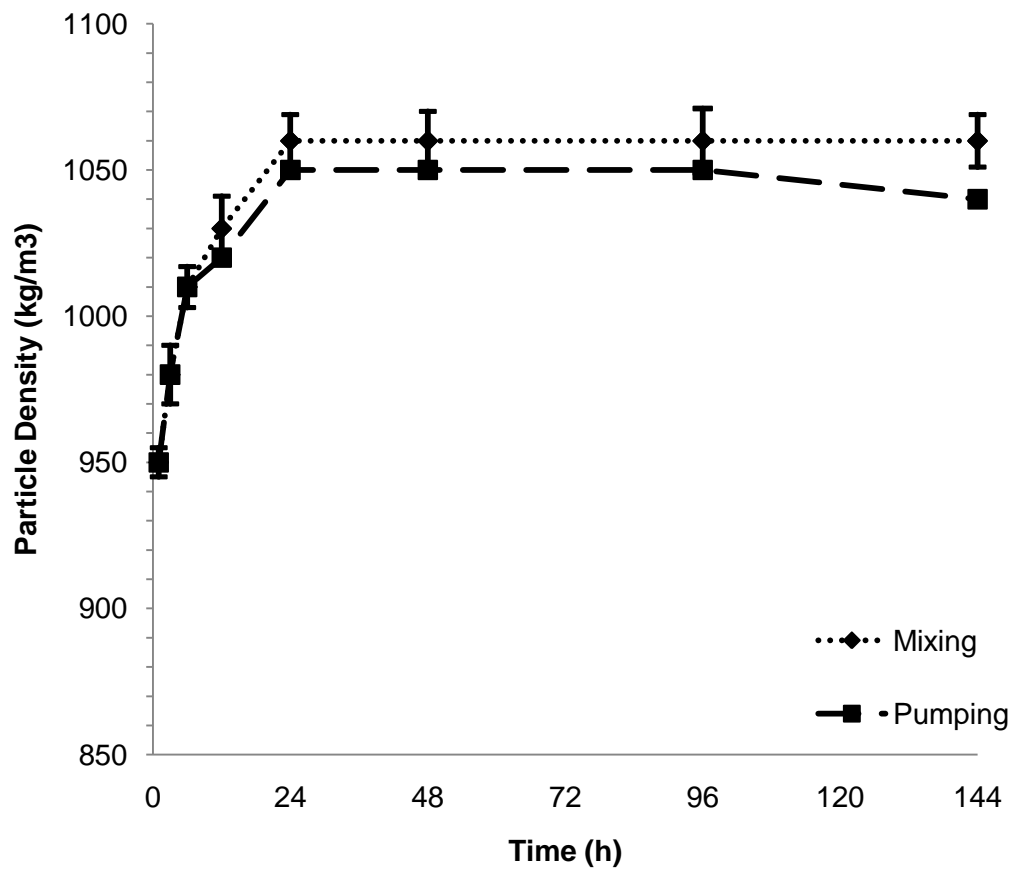


Figure 10: Particle density of *1/8" average particle size straw

Preliminary results were also recorded in Figure 10 for pumped, as opposed to mixed wet straw (Luk et al., 2009). For the 1/8" particle density measurements, it can be seen to be statistically similar to the results of this study, until 96 hours. After 96 hours the pumping results infer a decrease in particle density. This is likely again attributed to excess surface moisture, as the amount of impurities in the carrier fluid increases with time, making it more difficult to achieve surface dry conditions at later time intervals.

**Average particle size sample as classified in Table 1*

Chapter III:

Hydraulic Transport Design

1. Background

In order to determine the hydraulic transport requirements of the wheat straw slurries, an experimental pipeline was constructed. A laboratory scale system designed earlier was partially successful in pumping high concentration slurries (Mohamadabadi, 2009). However there were some limitations with the results from the instrumentation readings. Additionally, some components were found to be highly susceptible to congestion. Using the lessons learned from this original system, it was dismantled and redesigned to improve the accuracy of the measurements and reduce congestion.

2. Methodology

This design process can be broken down into three phases. First a thorough discussion of the experimental design intent and constraints. Second, the original system was closely inspected to isolate specific limitations and determine means of improvement. Finally a design was fully itemized and drawn for construction purposes.

An explanation of the system modification is provided here. The selection of existing equipment is not elaborated. Detailed explanation of the original system design process can be found in an earlier study (Mohamadabadi, 2009).

2.1. Design Intent

Table 7: Experimental design considerations

	Considerations	Comment
Responding Variables	Pressure Drop	Create pressure drop gradient
Manipulated Variables	Flow Rate	1.5-3.0 m/s
	Slurry Concentration	5% - 30% wet basis
	Particle Size	*1/8", *1/4" and *3/4"
Controlled Variables	Pipeline Material	Commercial steel
	Pipeline Diameter	2"
	Temperature	Ambient (20-25°C)
Constraints	Room Dimensions	8.7 x 8.3 x 3.3 m
	System Operation	Congestion remediation
	Air Content	Minimize
	Total Head	Godwin CD80M

Before addressing the limitations of the original system, the experimental variables and constraints are detailed in Table 7. The responding variable is the pressure loss of slurry. The data is required to approximate the pumping requirements of a full size industrial system. To minimize the sources of uncertainty, it is only measured over given length of straight pipe.

There were three manipulated variables to be examined. The average flow velocity was to be a minimum of 1.5 m/s, which was found by Mohamadabadi (2009) to be the critical velocity before particles lose suspension due to insufficient turbulence and begin to settle at the bottom of the pipeline. The maximum of 3 m/s was arbitrarily set to be sufficient to understand the pressure drop gradients, which is the change in pressure loss at different flow rates. The particle size used would be 1/8" to 3/4", which are the sizes produced by the methodology previously described in Chapter 2.

**Average particle size sample as classified in Table 1*

The slurry concentrations were to range from a high of 30% wet basis concentration, which was the highest achieved by Mohamadabadi (2009), and a minimum 5% wet basis concentration. The wet basis concentrations are calculated using Equation 9 and Equation 10, and using anticipated moisture content results from the physical characterization experiments in Chapter 2.

Equation 9: Wet basis concentration by mass

$$C_{wet} = \frac{m_{straw,wet}}{m_{water} + m_{straw,air}} * 100\%$$

Where:

C_{wet} : Concentration, wet mass basis (%)

$m_{straw,wet}$: Mass of wet straw (kg)

m_{water} : Mass of water added to slurry (kg)

$m_{straw,air}$: Mass of air dry straw (kg)

Equation 10: Wet straw mass of air dry straw

$$m_{straw,wet} = \frac{m_{straw,air} * (100\% - MC_{air})}{MC_{straw}}$$

Where:

MC_{air} : Moisture content of air dry straw (%)

MC_{straw} : Moisture content of straw sample (%)

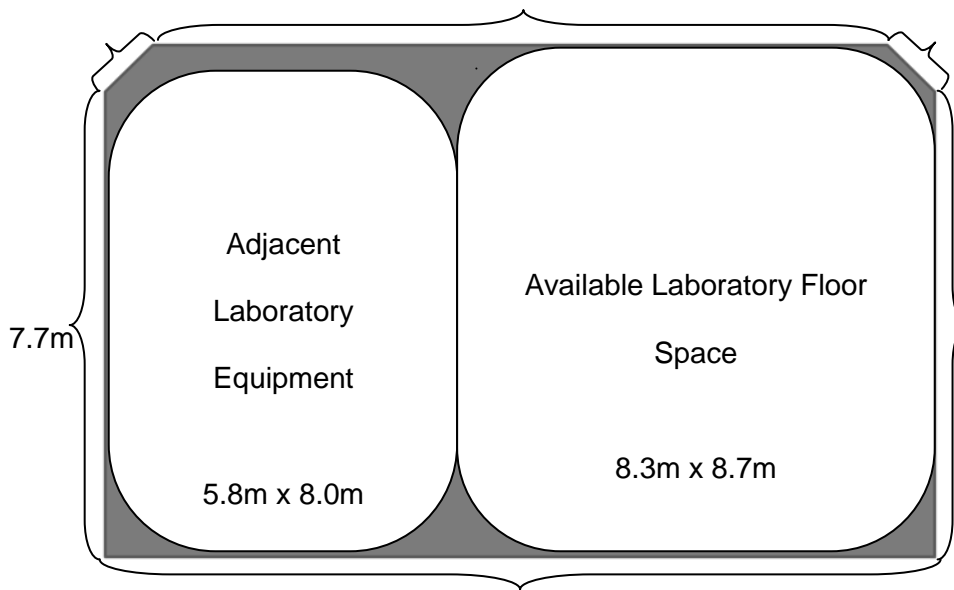


Figure 11: Physical constraints of laboratory floor space

There were several controlled variables to ensure robust results. The pressure loss was to be measured across a section of new commercial steel, as it is a readily available, commonly used material in industrial pipelines. A small diameter pipeline was required due to the laboratory setting, and arbitrarily selected as 2" diameter. Data was to be sampled when the slurry was at room temperature, or 20-25°C, for consistency.

When achieving these design goals, various constraints must also be evaluated. The primary constraint was the overall dimensions of the laboratory space, shown in Figure 11. Also important was the need to avoid, but ultimately remediate congestion, as the system limits are regularly tested during experimentation. Careful consideration of any air content within the system is crucial, as it is inevitably introduced with the dry feedstock material, and must be removed to ensure accurate representation of two phase wheat straw slurry.

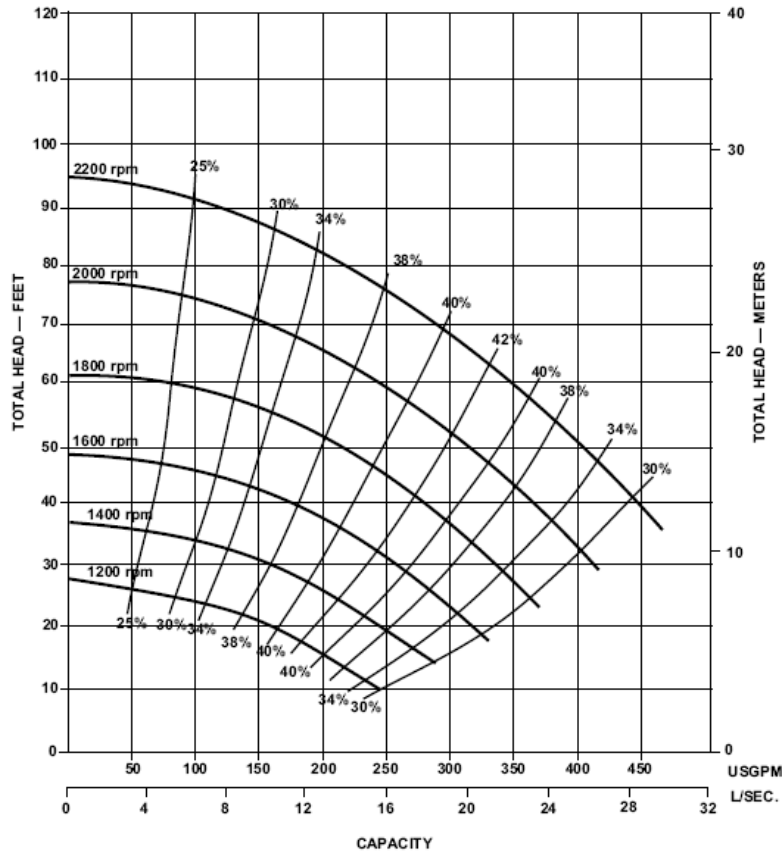


Figure 12: Centrifugal pump curve (Godwin Pumps, 2007)

Finally, there was a limitation of the total head available to pressurize the slurry. The pump curve in Figure 12 is based on the Godwin CD80M centrifugal pump (Godwin Pumps, 2007) which was proven to be successful at handling high concentration slurries (Mohamadabadi, 2009). At 3 m/s, it is able to provide approximately 18.3 m of total head pressure.

2.2. Original Design

The Godwin pump in Figure 13, was connected to the bottom of the mixing tank shown in Figure 14. It was positioned beneath a mixing tank, from which slurry was drawn. At its outlet the 2" steel pipeline loop was installed. Within this loop was pressure, temperature, and flow rate instrumentation, along with a transparent viewing section to monitor the slurry. At the end of the steel pipe section the slurry is returned back into the mixing tank, or diverted into a similar tank which is without a mixer. This superfluous tank was originally intended to strain the solids from the slurry, but for ergonomic reasons, was replaced with a ground level tank installed at the midpoint of the entire system.

To further understand the redesign requirements of the laboratory scale biomass pipeline, this original system was thoroughly examined. This includes both the accuracy of the instrumentation measurements as well as auxiliary concerns.



Figure 13: Godwin CD80M pump

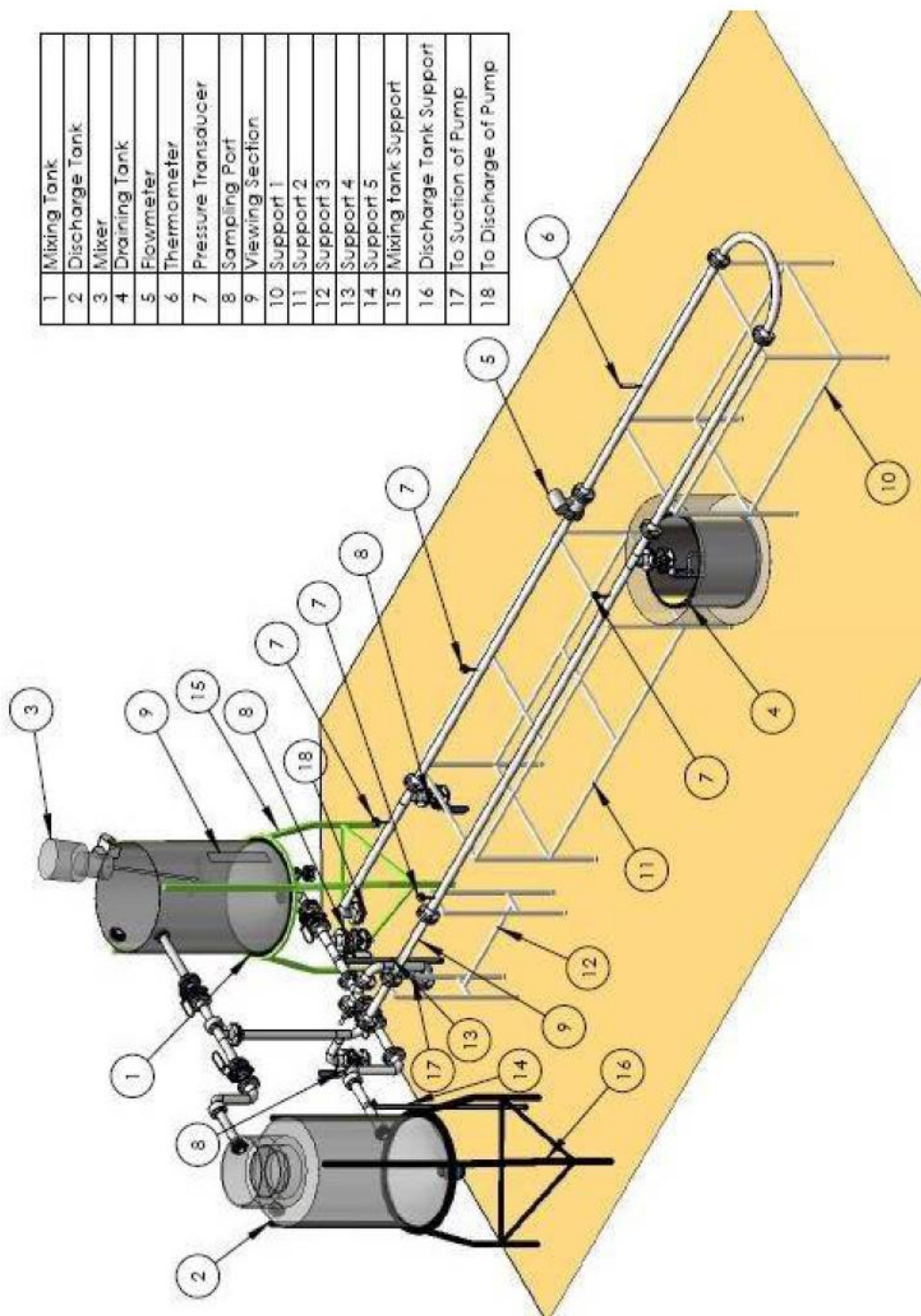


Figure 14: Schematic of original system layout (Mohamadabadi, 2009)

2.2.1. Instrumentation Accuracy

The principal concern was the high volatility of the pressure readings. Figure 15 displays a significant amount of noise in the Viatran 305 piezoelectric pressure transducers (Viatran, 2007) installed in a upstream and downstream position, when the original system operated at 30 Hz (approximately 2 m/s) to pump fresh water. Since the difference of these two instruments is to determine the pressure drop of slurry, it requires a clear discrepancy between the readings. However, gauge pressure spikes of the downstream transducer reaching as high 4.0 psi, which is above minimum 3.9 psi that the upstream transducer reached. The magnitude of the pressure differential was deemed insufficient due to excessive noise.

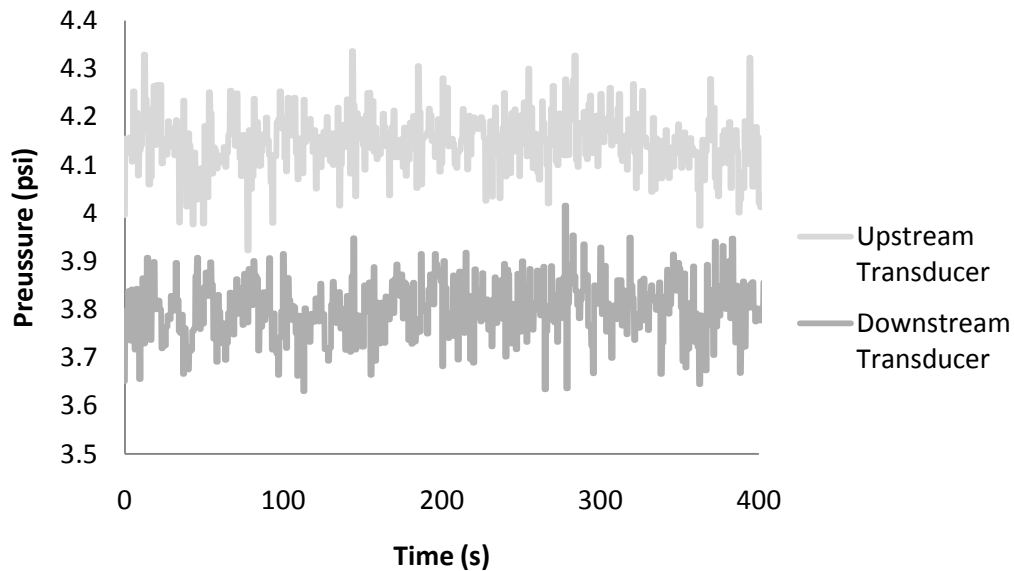


Figure 15: Upstream and downstream pressure transducer noise

2.2.1.1. Proximity to Mechanical Sources of Noise

A potential source of this noise could be the centrifugal pump. As each of its 3 impeller vanes passes the pump outlet, an increase in pressure is experienced in the system. Over long distances, the downstream pressure provided is relatively stable. However the dimensions of the laboratory limited the length of the pipeline system, leading to installation of the pressure transducers in close proximity to the pump.

In addition, the pump was controlled by a variable frequency drive. This allows the pump speed to be manipulated as required for experimentation. At lower input frequencies, there is an increased potential for the electric motor to slip, failing to provide a constant flow rate.

Disturbances from the pump would increase the flow rate along with the pressure simultaneously. Unfortunately the data acquisition system did not have sufficient speed to capture this relation. Each transducer reading is limited to a rate of approximately 1 Hz, and each is iteratively logged with other transducers. Meaning the pressure transducer readings is out of synchronization with that of the flow meter, by up to 1 second. The pump impeller has a rotational velocity of up to 1760 rpm, meaning each of its three vanes produces a small pulse at a rate of 88 Hz.

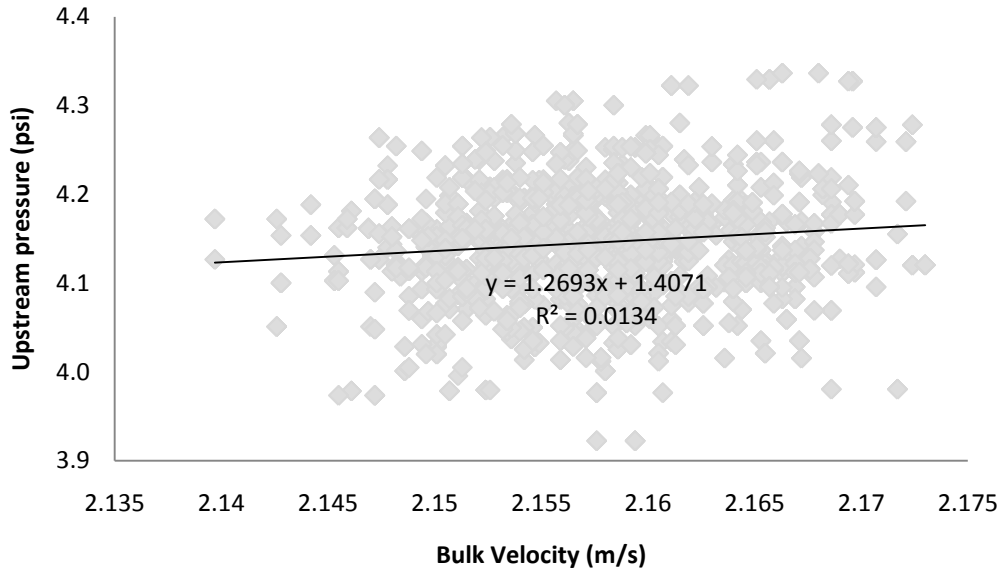


Figure 16: Correlation of pressure transducer and flow rate noise

When the upstream pressure data in Figure 15 is plotted together with flow rate in Figure 16, there is only a weak positive correlation between the two. Thus it is not conclusive evidence of significant instrumentation noise attributed to the pump. Regardless, to minimize any potential impacts it was desired to maximize the distance, and thus frictional losses, between the pump outlet and the transducers.

Likewise, the mixing tank may be a source of noise in the system. The pressure measured within the system is a function of the level of slurry within the mixing tank. Splashing caused by the mixer or slurry from the inlet of the mixing tank, would cause the pressure within the system to fluctuate. However, a means to quantify its contribution to noise in the pressure transducer could not be readily determined. Beyond its proximity to instrumentation, the mixer could be further addressed, by means described in a proceeding section.

2.2.1.2. Electrical and Magnetic Interference

Another source of noise may have been from electrical interference. Although shielded cables were used for the pressure transducers, the readings were fluctuating. Pressure measurements for pure water were inconsistent. Measurements for still, ambient air would stray if the transducers are placed in different locations, possibly due to proximity to other equipment. Pressure gains could be even recorded occasionally measured at low flow rates. Unfortunately, the aforementioned 1 Hz sampling rate was insufficient to quantify frequency aliasing or distortion from electrical interference, at 60Hz.

Mechanical pressure measurement technologies were examined. A WIKA Type 700.01 compression spring and magnetic piston differential pressure gauge (WIKA Instruments, 2010) was selected as a means to avoid electrical interference. While this instrument provided steady readings, they were inconsistent. The issue may have been a result of the electromagnetic flowmeter in close proximity, interfering with the magnetic piston. The presence of small magnets nearby would cause the readings to change.

Electrical and magnetic interference would need to be avoided for instrumentation accuracy.

2.2.1.3. Air Content

When preparing slurry from a dry biomass, the air within the pores of the feedstock is introduced into the system. While the air escapes the particles once water is absorbed, it can remain dissolved within the slurry. At slow velocities, the air is released from the slurry and it is can be seen, as shown in Figure 17. Any additional material distorts the makeup of the slurry. Air bubbles may have been affecting the accuracy of the instrumentation. Vertically installed components, particularly pressure transducers mounted at the top of the pipe, could allow air to accumulate.



Figure 17: Air bubbles seen in viewing section



Figure 18: Slurry splashing caused by mixer and mixing tank inlet

Due to the confines of the available laboratory space, the small scale of the pipeline system requires the slurry to be continuously reintroduced back into the system. The splashing of the slurry upon re-entry into the mixing tank, may have introduced air into the system. Further, while the placement of the mixer impeller in the center of tank, improved the efficacy of the mixer, it was placed high enough to cause a significant amount of surface agitation, creating more splashing. This can be seen in Figure 18.

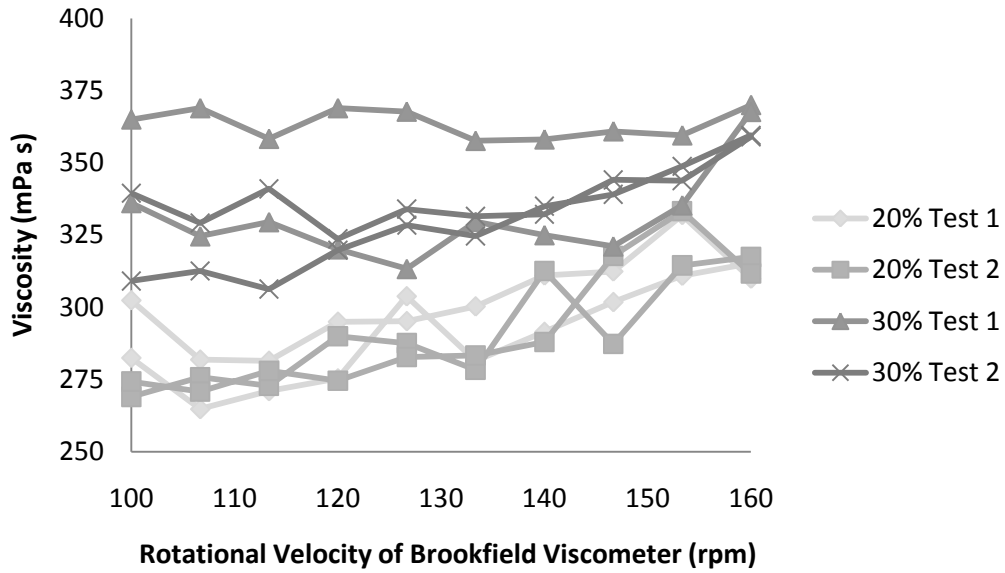


Figure 19: Slurry viscosity experienced by viscometer (Cocirla, 2007)

Along with these qualitative observations, there is also a better understanding of the viscosity of wheat straw slurries. The first iteration of the mixer and mixing tank system was designed before the properties of slurry were understood. Figure 19 shows the increase in viscosity with higher concentrations as determined by a Brookfield viscometer (Cocirla, 2007). The figure also highlights shear thickening properties, where the viscosity increases with velocity. With this information, the mixer and mixing tank system could be redesigned to reduce the introduction of air or conversely allow the dissipation of air out of the system.

2.2.2. Auxiliary Considerations

While the original system was able to pump wet straw at a 30% concentration, it was also highly susceptible to congestion. The narrow outlet of the mixing tank, along with multiple fittings immediately following it, was the most frequent congestion points, particularly during initial slurry preparation. Modifications were required to minimize friction losses between the mixing tank and the pump inlet.

There were also issues during discharge and dewatering. During this process, the continuous flow was impeded. The length of the system downstream of the discharge outlet (approximately half of the system) would be depressurized and left stagnant once the outlet is opened. The stagnant section between the discharge outlet and the inlet to the mixing tank needed to be addressed.

The initial iteration of the system included many supplementary components. This includes those that allowed for alternative flow paths to bypass the mixing tank, or additional drainage points. While these provided flexibility in the system, these components are also left stagnant when not in use. Besides the issue of congestion, these sections could also affect the concentration of straw in the system, should the solids accumulate. This may cause an appreciable difference in the makeup of low concentrations. These risks would need to be minimized.

Aside from these crucial regions of primary concern, the other parts of the system would seldom cause congestion. However, it would still become congested if triggered by other issues. Thus all parts of the pipeline loop would be required to be readily decongested.

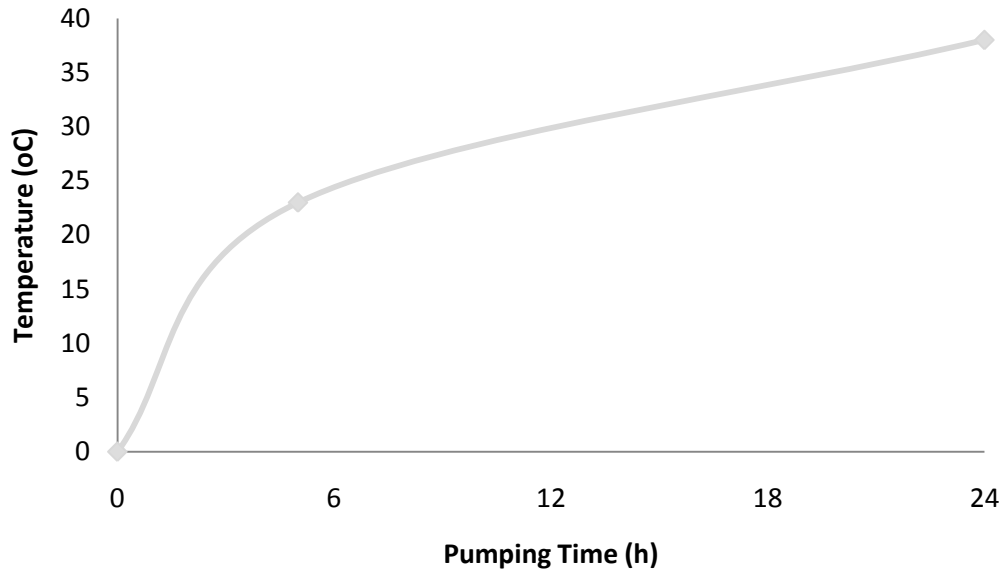


Figure 20: Temperature escalation of ice water pumped in pipeline loop

Temperature control was the final issue raised from the original design. Whereas an industrial pipeline may be buried, utilizing the earth as a natural heat sink (Kumar et al., 2005b), in a laboratory setting the pipeline was simply exposed to ambient room temperature air. This was insufficient to prevent rapid temperature escalations, which could increase several degrees Celsius per hour of operation, before reaching temperatures nearing 40°C, as shown in Figure 20. A source of temperature control would be required in a modified system.

2.3. Modified Design

Table 8: System components

	Component	Description	Source
Pipeline	Pipeline	2" Schedule 40 steel pipe	(Westlund, 2007)
	Fittings	2" & 3" Steel schedule 40 pipe fittings	(Westlund, 2007)
		2" & 3" PVC schedule 40 pipe fittings	(Fabco Plastics, 2009)
		2" & 3" PVC water hose	(Green Line Hose & Fittings, 2009)
Slurry Preparation	Mixing Tank	CB100, 100 Gal, 31" diameter, 30o conical bottom	(Zeebest Plastics, 2009)
	Mixer	EV6P50, 0.5hp Baldor CDP3430 motor, 280 rpm, 12.8" impeller	(Lightnin Mixers, 2009)
System Monitoring	Flow Meter	FMG-401H magnetic flowmeter	(Omega Engineering, 2007)
	Pressure Gauge	WG22699 low pressure diaphragm gauge	(Western Gauge and Instruments, 2005)
	Temperature Transducer	RTD-NPT-72-E-MTP-M	(Omega Engineering, 2007)
	Viewing Section	2" x 0.5m schedule 40 transparent acrylic tube	(Fabco Plastics, 2009)
System Discharge and Slurry Dewatering	Dilution Tank	CB100, 100 Gal, 31" diameter, 30o cone bottom	(Zeebest Plastics, 2009)
	Draining Tank	OTR3, 90 Gal, 36" diameter, round	(Zeebest Plastics, 2009)
	Strainer	Custom-made 16 mesh, 39 Gal, 24 diameter, round	(Faulkner, 2008)
System Control	Water Bath	OTR3, 90 Gal, 36" diameter, round	(Zeebest Plastics, 2009)
	Pump	CD80M electric 10hp centrifugal pump	(Godwin Pumps, 2007)

The key components are compiled in Table 8. All of the aforementioned constraints and limitations were addressed, and the overall length of the system was doubled to 45m. Although the instrumentation was mounted only on carbon steel test sections, many auxiliary components were replaced with low friction PVC to enable the additional length.

Table 9: Minor loss coefficients

Component	Minor Loss, K	Source
31" to 3" diameter 30° bevelled inlet	0.40	(White 2006)
2" steel T branch	1.60	(White 2006)
2" steel T line	0.57	(White 2006)
2" ball valve	0.05	(The Engineering ToolBox 2005)
2" to 3" expansion	0.90	(White 2006)
3" to 2" reduction	0.20	(White 2006)
2" long radius elbow	0.25	(White 2006)
2" 45deg long radius elbow	0.15	(White 2006)
2" 180deg 15" radius bend	0.50	(White 2006)
2" 180deg 15" radius bend	0.50	(White 2006)
3" 45deg 24" radius bend	0.20	(White 2006)
3" 90deg 24" radius bend	0.30	(White 2006)
Sudden expansion	1.00	(White 2006)

Table 10: Major loss factors

Material	Roughness, ϵ (mm/mm)	Source
New commercial steel pipe	0.046	(White 2006)
Plastic drawn tubing	0.0015	(White 2006)
Smoothed rubber	0.01	(White 2006)

Calculations to estimate head loss of water in the pipeline loop were completed using Equation 11 through Equation 13. The major friction loss factors and minor loss coefficients are found in Table 9 and Table 10.

Equation 11: Head loss formula

$$h = \frac{v_m^2}{2g} \left(\frac{f * l}{D_{pipe}} + \sum K \right)$$

Where:

- h : Head loss (m of water)
- v_m : Mean velocity of slurry (m/s)
- f : Friction factor (dimensionless)
- l : Length of pipe (m)
- g : Gravity acceleration (m/s²)
- D_{pipe} : Inside diameter of pipe (m)
- K : Minor head loss coefficient (dimensionless)

Equation 12: Friction factor formula

$$f = \frac{1.325}{\left[\ln \left(\frac{e}{3.7 * D_{pipe}} + \frac{5.74}{Re^{0.9}} \right) \right]^2}, \text{ for } 5000 < Re < 10^8 \text{ and } 10^{-6} \leq \frac{e}{D_{pipe}} \leq 10^{-2}$$

Where:

- Re : Reynold's number (dimensionless)

Equation 13: Reynolds number formula

$$Re = \frac{\rho * v_m * D_{pipe}}{\mu}$$

Where:

- ρ : Density of fluid (kg/m³)
- μ : Viscosity of liquid (Pa*s)

Several approximations of wheat straw slurry head losses were also included Table 11. These are based on laboratory scale woodchip slurry pipeline experiments by Equation 14 by Hunt (Hunt, 1976), Equation 18 by Faddick (Hunt, 1976) and Equation 19 from PAPRICAN (Elliot and Montmorency, 1963).

Equation 14: Hunt's equation (Hunt 1976)

$$\left(\frac{i_m - i}{i}\right) = 197 * \left(\frac{D_{pipe}^{0.970} * g^{1.312} * v^{0.342}}{v_m^{2.964}}\right) \left(\frac{C_{vol}}{1 - C_{vol}}\right)^{0.838 + 0.930 \ln(1-k)}$$

Where:

- i_m : Pressure drop of slurry (m of water per m of pipe length)
- i : Pressure drop of clear water (m of water per m of pipe length)
- v : Kinematic viscosity of carrier fluid (m²/s)
- C_{vol} : Volumetric concentration of solids (dimensionless)
- k : Ratio of particle dimensions to diameter of pipe (dimensionless)

Equation 15: Kinematic viscosity formula

$$v = \frac{\mu}{\rho}$$

Equation 16: Volumetric concentration

$$C_{vol} = \frac{C_{wet} * \rho_{slurry}}{\rho_{straw}}$$

Where:

- C_{wet} : Concentration, wet mass basis (%)
- ρ_{slurry} : Density of slurry (kg/m³)
- ρ_{straw} : Particle density of wet straw (kg/m³)

Equation 17: Slurry density

$$\rho_{slurry} = \frac{\rho_{water} * \rho_{straw} * 100\%}{(\rho_{straw} * 100\%) - C_{wet}(\rho_{straw} - \rho_{water})}$$

Where:

ρ_{water} : Density of water (kg/m³)

Equation 18: Faddick's equation (Hunt 1976)

$$\left(\frac{i_m - i}{i}\right) = 2.51 * C_{vol} * \left(\frac{4 * g * D_{pipe}}{v_m^2}\right)^{1.42}$$

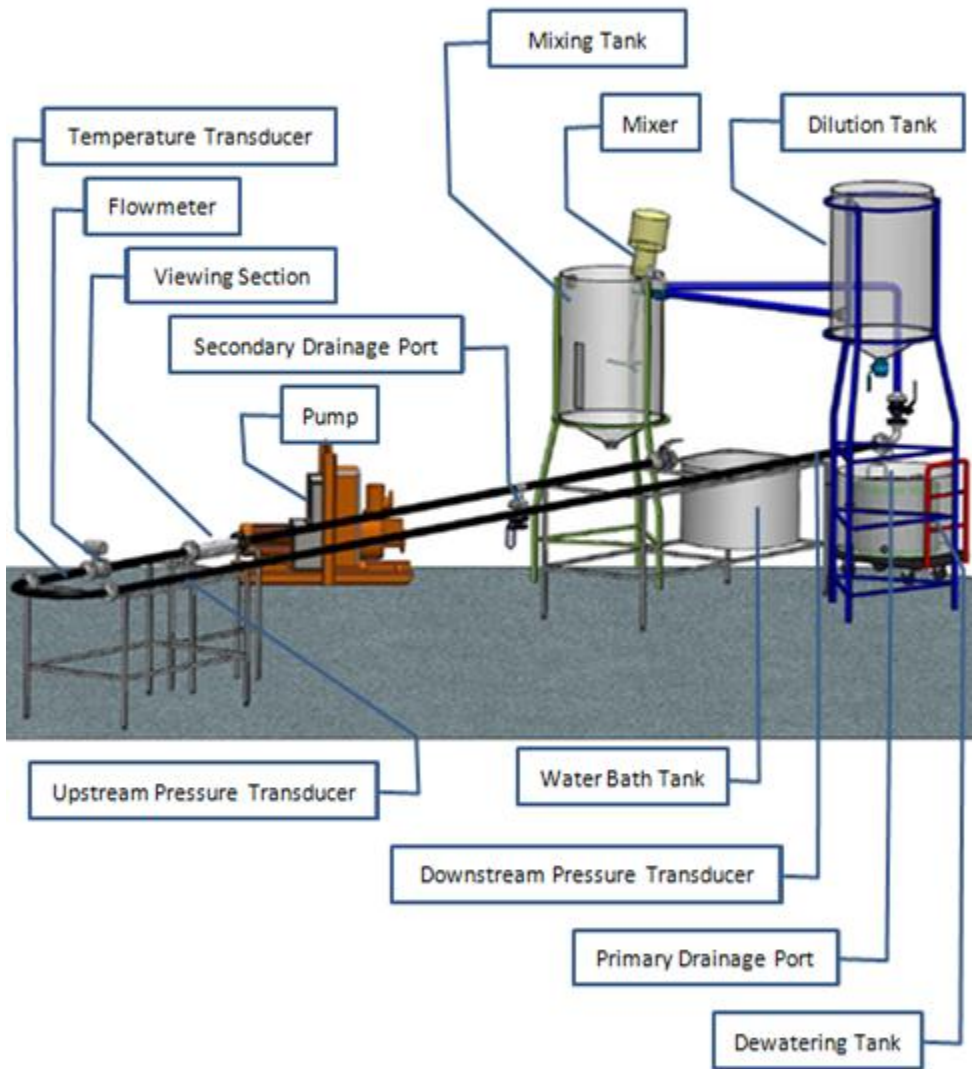
Equation 19: PAPRICAN equation (Elliot and Montmorency 1963)

$$\left(\frac{i_m - i}{i}\right) = 211 * C_{vol} * \left(\frac{\sqrt{D_{pipe}}}{v_m}\right)^{2.25}$$

The largest head loss was calculated with PAPRICAN's equation. To remain conservative, this formula was used in conjunction with a 20% safety factor during the design process. The final design was approximated to have a 15.2m head loss using PAPRICAN's formula, equalling 18.3m the Godwin CD80M pump was able to provide, after the safety factor was included. These hydraulic head losses of water pumped at 3 m/s are detailed in Table 11. A schematic of the modified pipeline system can be seen in Figure 21. Detailed design drawings are round in the Appendix.

Table 11: 3 m/s System Head Loss

Component	Description	Head loss (m)
Mixing tank outlet	Sudden Contraction	0.18
Mixing tank outlet valve	Fully open ball valve	0.02
Pump inlet hose	3" x 1.5m rubber hose	0.17
	3" 90deg 24" radius bend	0.14
Pump outlet hose	3" x 1.5m rubber hose	0.17
	3" 45deg 24" radius bend	0.09
Pump outlet reducer	3" to 2" Reduction	0.09
Pump outlet valve	Fully open ball valve	0.002
Water bath	2" x 20m rubber hose	3.16
	16 x 2" 180deg 15" radius bend	3.67
Water bath outlet valve	Fully open ball valve	0.002
Decongestion outlet section	Tee line flow	0.09
	2" x 5.26m steel pipe	1.01
Viewing section	2" x 0.417m plastic pipe	0.06
	2" x 1.11m steel pipe	0.21
Flow meter	2" x 0.2m plastic pipe	0.03
RTD section	2" x 0.74m steel pipe	0.14
Pipe bend	2" x 1.2m steel pipe	0.23
	2" 180deg 15" radius bend	0.23
Test section	2" x 9.77m steel pipe	1.87
Discharge outlet section	2" x 0.13m steel pipe	0.02
	Tee line flow	0.09
	2" 90deg long radius elbow	0.11
Test section outlet valve	Fully open ball valve	0.002
Return line section	2" x 0.87m plastic pipe	0.13
	2" 90deg long radius elbow	0.11
	2" x 1.796m plastic pipe	0.27
Mixing tank inlet	2" 45deg long radius elbow	0.07
	Sudden expansion	0.46
System total	Water	12.8
	Slurry (Hunt formula)	13.3
	Slurry (Faddick formula)	13.9
	Slurry (PAPRICAN formula)	15.2
Maximum head	Godwin CD80M pump	18.3



Note: Soft hose fittings from mixing tank to pump and pump to water bath tank are not shown

Figure 21: Schematic of modified system layout

2.3.1. Instrumentation Accuracy

To decrease the significance of instrumentation noise, the magnitude of the pressure loss was increased. This was achieved by re-orienting the test section diagonally across the laboratory space, allowing an 8.5m length of straight pipe. Pressure gauge fittings installed at either end of this length, allowed a minimum of 20 pipe diameters after and 5 pipe diameters before obstructions (shown in Figure 22), as determined through engineering consultation (Mohamadabadi, 2009), to reduce influence of fittings by allowing the flow to develop.

Simple spring compression pressure gauges were installed in these mounts. Although measurements could only be recorded within 0.5 kPa, these avoid electrical and magnetic interference. This allows for highly repeatable readings. Accuracy is improved despite having a lower resolution.



Figure 22: Pressure taps and flow meter are placed away from bends

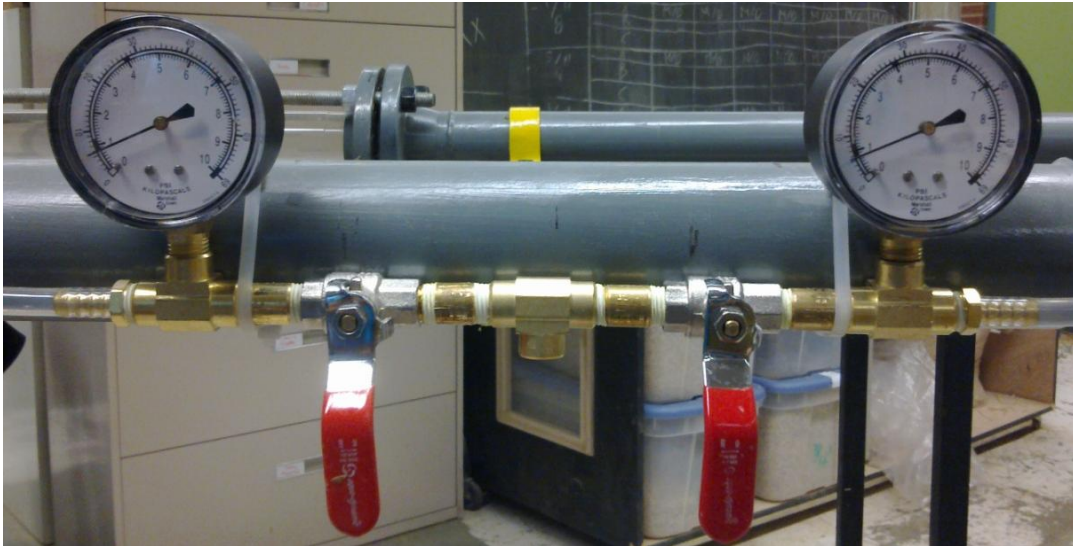


Figure 23: Mechanical pressure gauges adjoined by bleed valves

The pressure gauges were mounted horizontally into the pipe, using brass pipe nipples. Installing the units on the top or bottom of the pipe would increase the likelihood of either air or solids accumulating, respectively. The brass fittings resist the corrosion which would otherwise occur within the threaded female steel fittings, and promote the build up of fine solids.

As shown in Figure 23, clear vinyl hose connected the brass fittings to the pressure gauges. The length of hose is filled with water, buffering the gauge from direct contact with solids in the slurry. The transparency allowed visual inspection of unwanted air bubbles or solids, which could then be purged via in-line brass ball valves. To prevent head loss or gain from having the two pressure gauges at different heights, they were affixed to each other before being strapped to the steel pipe test section. (Note that the use of differential pressure gauges would also avoid this head loss issue. However locally sourced units, without any electrical or magnetic components, could not provide adequate resolution at low differential pressures).



Figure 24: Coils of long radius hose in line with pipeline

To reduce the contribution of the centrifugal pump to instrumentation noise, friction was maximized between pressure gauges and pump outlet. As shown in Table 19, this section was designed to comprise of 72% of total friction loss across the entire system. In addition, the friction losses were not concentrated in short radius elbows or other fittings highly susceptible to congestion. Rather, the long 15" radius loops of low friction 2" PVC hose in Figure 24 was installed between the pump and before the steel pipe sections. This allowed the friction losses to be dispersed over a longer length, while remaining within the limited confines of the laboratory space.



Figure 25: Mixing tank inlet submerged to allow air bubbles to dissipate

To reduce the introduction of additional air content, the inlet of the mixing tank was modified to allow an extension to reach below the surface of the slurry during data collection. Figure 25 displays its ability to eliminate splashing previously caused by the inlet, which introduces air into the system, altering the makeup of the slurry. However, this extension does impede on the ability of the mixer to agitate the slurry, so it is able to be disconnected and re-installed after the initial slurry preparation, during which greater turbulence is required.



Figure 26: Air dissipating from slurry accumulates as bubbles on surface

A replacement mixer was also installed in the mixing tank. The impeller was extended to the bottom of the tank, and a larger gear box reducer allows it to operate with sufficient torque at a lower rotational velocity. Both of these reduce excessive turbulence which induces air into the slurry. Further, the mixer speed can also be reduced after initial slurry preparation. When operating at the minimum turbulence to maintain particle suspension, the slurry is slowed sufficiently to allow dissolved air to dissipate from the system, as seen in Figure 26.

2.3.2. Auxiliary Considerations

To prevent congestion, the friction losses between the mixing tank and the pump were minimized. Positioning the mixing tank above the pump would allow the pump to be primed by gravity and reduce drag on the performance. The mixing tank outlet was expanded from 2" diameter to 3", matching that of the pump inlet. All tees and elbows were removed in the direct connection to the pump, which previously increased friction losses to allow alternate pipeline flows. As shown in Figure 27. The connection was also made completely with low friction PVC hose, gradually curved in a long radius bend, to further prevent clogging.

To purge slurry from the system, two discharge valves were integrated within the system. The discharge valve further upstream, was installed as a means to aid in decongestion. This emergency outlet was placed at the onset of the instrumented mounted steel pipeline section. This allows for unobstructed operation of the instrumentation, while providing the ability to decongest the upstream end of the higher friction steel pipe.

To prevent congestion due to stagnation the main discharge valve, was placed downstream all instrumentation, as shown in Figure 28. By being located in close proximity to the mixing tank, the length of the return line is minimized. Additionally, the return line was constructed out of PVC pipe and extends vertically from the main discharge valve. When the valve is open, the force exerted by gravity is sufficient to reverse the flow of slurry in the low friction return line.



Figure 27: Hose bend in wide radius connects the pump to mixing tank

As the inlet of the mixing tank is extended beneath the surface of the slurry (Figure 25), a siphon is created, which drains slurry out the top of the mixing tank. Figure 29 depicts how this maintains the flow through the return line, again preventing stagnation. During this process, the mixing tank is gradually diluted until the risk of congestion is removed.

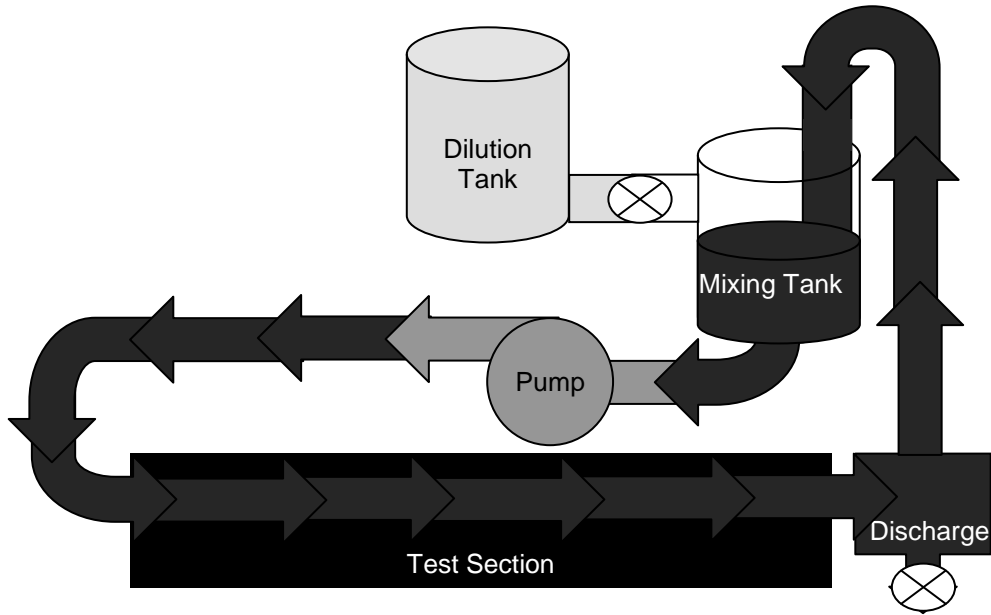


Figure 28: Slurry cycles through the entire system during normal operation

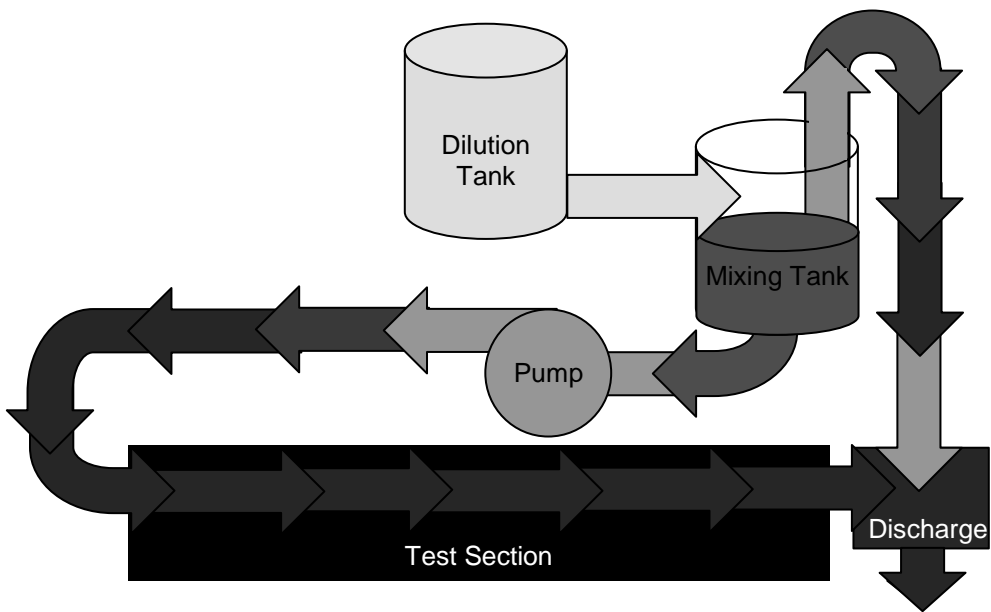


Figure 29: A siphon reverses the slurry in the return line during discharge



Figure 30: The dilution tank is elevated above the mixing tank

To overcome the relatively slow municipal water source, the reservoir shown in Figure 30 was attached to the mixing tank to acting as a dilution tank. This supplementary component was an identical 100 gallon tank, but elevated to allow gravity fed draining into the mixing tank through a 2" PVC hose. The diameter of this hose enables the slurry to be diluted much more rapidly than is possible from directly using municipal tap water.



Figure 31: Transparent PVC return line links discharge valve to mixing tank

Increased visibility within the system allows the ability to identify the sections of concern. With the exception of the necessary steel components, transparent materials were utilized, such as in Figure 31. Clear water hose was used, although a solid helix was required to provide the necessary strength. The strength of rigid clear PVC pipe was sufficient without reinforcement, allowing complete transparency. This enabled the entire section of stagnant materials to be viewed.

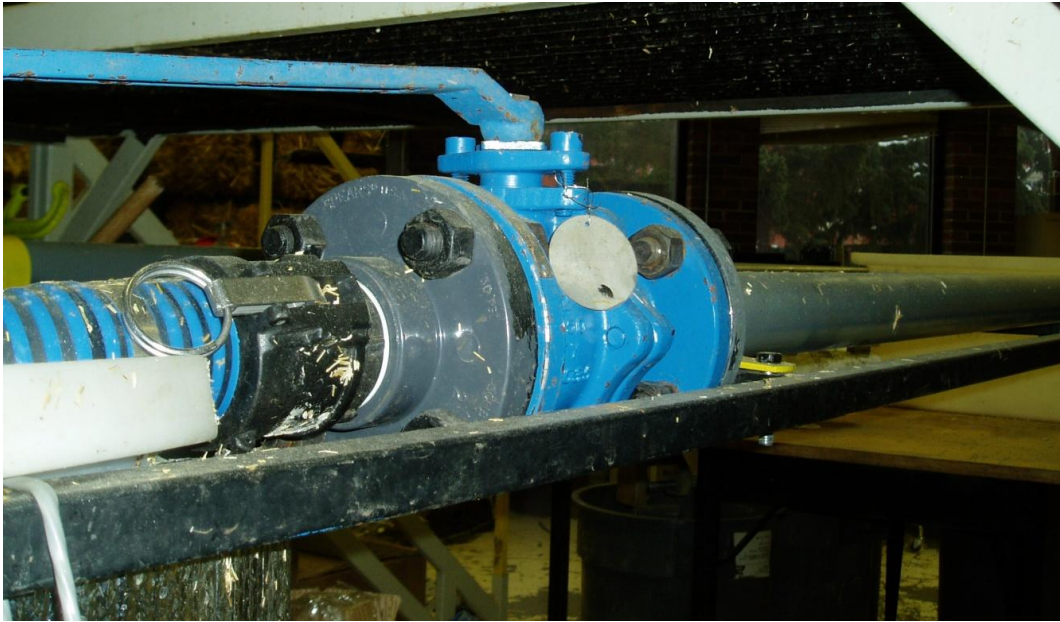


Figure 32: PVC hose, cam lock and ball valve in-line with steel pipe

After identifying congestion issues, access to the clog would be required. PVC connections were created with cam-locks as in Figure 32, which enabled efficient, tool free disconnection. Finally, inline ball valves are able to isolate clogs. This enables a flanged connection to the high pressure tap water, to remove clogs within the large sections of steel pipe to be removed simply with water pressure. This method avoids the need to dismantle individual heavy steel components.

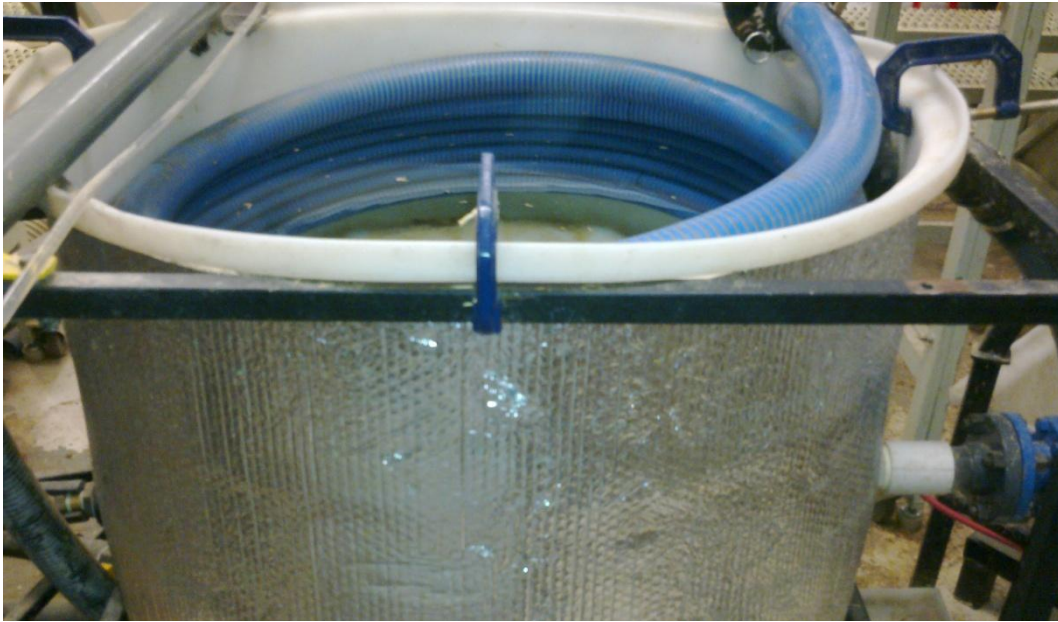


Figure 33: Insulated 90 gallon water bath

The water bath in Figure 33 was selected as a practical heat sink. This design utilizes the passive heat absorption of the cold municipal tap water (5-20°C). The previously mentioned 20 m of 2" PVC water hose was connected in line with the pipeline. The hose was placed in wide radius coils within a 90 gallon cylindrical tank and filled with water. Although steel would be able to conduct of heat more efficiently, flexible PVC hose was more readily integrated within the compact dimensions water bath limited by the available laboratory space. The risk of congestion occurring within the water bath is reduced by the use of the low friction material. In addition, utilizing a low friction material enabled a significantly longer length. This further increased distancing of instrumentation and the viewing section from the turbulence generated at the centrifugal pump and mixer. By doubling the length of the system, the frequency of the slurry passing the pump or mixer is also halved. This reduces the potential impact of particle degradation from these components.

3. Results and Discussion

3.1. Instrumentation Accuracy

The accuracy in the pressure measurements has been addressed with the redesign of the system. In Figure 34, fresh water was pumped from 1.5 m/s to 2.9 m/s, in three separate trials. The velocity of the water is converted into its Reynolds number, and the pressure drop readings are used to calculate the Darcy-Weisbach friction factor using Equation 20. Although the pressure measurements could only be recorded to the nearest 0.5 kPa, the data points are seen to follow the upper boundary of what can be expected for turbulent flow through new commercial steel. The curves are calculated using the textbook value for roughness of 0.046 mm $\pm 30\%$, (White 2006), and Haaland's equation, Equation 21, to approximate the turbulent region of the Moody charts.

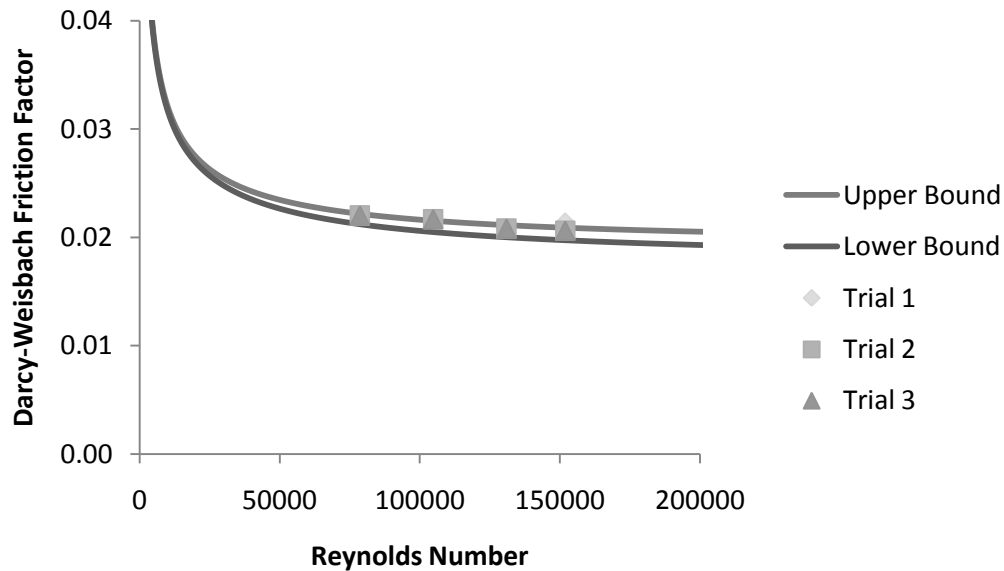


Figure 34: Theoretical and experimental friction factors

Equation 20: Friction factor as a function of pressure drop

$$f = \frac{\Delta P}{l} \frac{2D_{pipe}}{\rho_{water} v_m^2}$$

Where:

f : Darcy-Weisbach friction factor (dimensionless)

ΔP : Pressure drop (Pa)

l : Length of pipe (m)

D_{pipe} : Inside diameter of pipe (m)

ρ_{water} : Density of water (kg/m³)

v_m : Mean velocity of slurry (m/s)

Equation 21: Haaland equation for friction as a function of Reynolds number

$$\frac{1}{\sqrt{f}} = -1.8 \log_{10} \left[\left(\frac{\varepsilon/D_{pipe}}{3.7} \right)^{1.11} + \frac{6.9}{Re} \right]$$

Where:

Re : Reynold's number (dimensionless)

ε : Roughness (mm)

While the estimates for major losses may have been accurate, minor losses may not have been fully accounted for. The centrifugal pump was to provide 18.3 m of head at a 3 m/s bulk velocity, while water pumped through the system at that flow rate was calculated result in 12.8 m of head loss. The final design of the system however would see a maximum flow rate for water of only 2.9 m/s.



Figure 35: Inner diameter of cam lock fittings are 1/4" less than steel pipe

As seen in Figure 35, a major cause of this discrepancy may have been from the cam lock connections, used to expedite the decongestion of the system. While they were assumed to have an internal diameter near the nominal diameter of 2", a 1/4" narrower opening was discovered upon ordering. The minor effect of flanged connections were also ignored, however their cumulative impact have been more substantial.

The design successfully addressed the issue of air content. In experimenting with slurry, after the initial preparation is complete, the mixer speed can now be lowered and the mixing tank inlet extension is installed to prevent splashing. The volume of the slurry in the system can be seen to decrease by 5% to 10% once air is allowed to dissipate from the mixing tank. Instrumentation measurements of slurries can now be made with greater confidence.

3.2. Auxiliary Considerations

With slurries created from the various particle sizes, the flowability of different wet basis concentrations were examined in increments of approximately 5%. The maximum concentrations consistently achieved without congestion by each particle size are displayed in Figure 36. The greatest concentration achieved was 30% using the 1/8" particle size. The largest particle size successfully pumped was 3/4", although it would only reach a concentration of 10% before congestion.

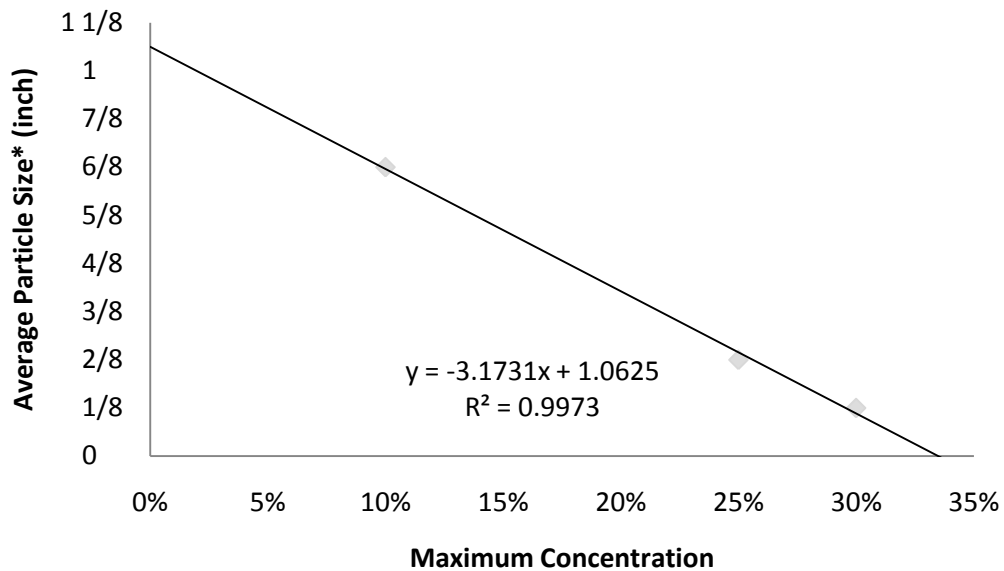


Figure 36: Maximum flowable concentration at different particle sizes

*Average particle size sample as classified in Table 1



Figure 37: 40% concentration slurries are not flowable

When the result of the intermediate 3/4" particle size is included, a relationship between maximum concentration and particle size can be plotted. A linear trend line results in a lower coefficient of determination of 0.9973. An increase of 1/8" of particle size results in a decrease of approximately 5% in maximum concentration. This infers that it may be possible to near a 33% concentration, with a sufficiently fine particle size, but no more as shown in Figure 37. Conversely, a particle size of 1", or half the pipeline diameter could be achieved at an exceedingly low concentration. Although it is not possible to extrapolate this trend line to other pipeline diameters at this point, this is the first step in establishing a relationship between particle and pipeline size. Further experimentation is required to determine the appropriate particle size and concentration relationship which can be pumped through a particular pipeline.

Chapter IV:

Hydraulic-transport Characterization

In order to determine the feasibility of a wheat straw biomass slurry pipeline, the hydraulic transport characteristics must be determined. Pressure drop gradients were created at various particle sizes and solids concentrations. This is done by determining the pressure drop of the slurry over a given length of straight pipe, at different velocities. This critical information aids in the selection of pumps and in understanding the power consumption required to transport these materials over long distances. The ultimate aim is to understand the cost structure of the biomass transport through pipelines as compared to other modes.

1. Methodology

In Chapter 3, the modified design of the laboratory scale pipeline loop improved the accuracy of the instrumentation measurements. It was found that the noise in the measurements has been reduced. However, this can be further addressed by optimizing the operating conditions of the system.

1.1. Operating Conditions

An increased volume of slurry in the system allows an increased duration of time the slurry resided in the mixing tank. Slurry within the pipeline cannot dissipate any unintentionally induced air from the system. An addition, a higher level of

fluid in the mixing tank provides additional head for the system, reducing the impact of splashing on instrumentation noise.

However, increased volumes of slurries require a greater rotational velocity of the mixer impeller to maintain suspension of solid particles. The impeller creates turbulence which limits the ability for air to dissipate from the slurry. Excessive mixer speeds can even induce additional air into the slurry. At lower mixing tank volumes, splashing at the surface can capture air into the mixing tank. At higher volumes, vortices could form around the mixer shaft and allow air to be pulled into the pump.

With these qualitative observations were considered, a 50 gallon (out of a 120 gallon maximum) mixing tank volume and 140 rpm (out of 280 rpm maximum) mixer speed was selected as the optimum set of operating conditions during data collection. The moderate mixer speed also enables turbulence to be increased substantially by increasing the mixer speed temporarily during initial slurry preparation. The moderate mixing tank volume also allows room in the mixing tank for fresh water to be added to dilute the slurry concentration as required.

1.2. Material Introduction

An industrial scale system could be a continuous process, with material gradually loaded and discharged. A large mixing tank could have dry material and carrier fluid constantly added, while uninterrupted slurry discharge could maintain the system in equilibrium. The volume of the tank could be large enough to allow for the average time the material resides in the tank, to be sufficient to ensure near

saturation before being introduced into the pipeline (as well as allowing for air to dissipate from the slurry).

In this laboratory system, the volume of the mixing tank is insufficient. Even while pumped at a slow flow rate of 1.5 m/s, the compact mixing tank would be fully discharged within several minutes, whereas rapid water absorption continues for hours. Thus water was run at a high 2.9 m/s flow rate through the entire system in a continuous loop, as dry material was added to the mixing tank to create the desired concentration. The high flow rate is required, as the dry feedstock quickly absorbs water, and the rapidly expanding solid particles are susceptible to congestion in the narrow pipeline. Dry straw is also more rigid, exacerbating the difficulties in preparing the slurry in confined space.

1.3. Sample Preparation

In Chapter 2, it was determined that water absorption increases the particle density of mixed wheat straw throughout the first 24 hours. Although the straw could be successfully pumped at low flow rates after significantly less processing time, all data sets were collected near saturation. This also ensures it more accurately represents material transported in long distance pipelines which would reach saturation within the pipeline.

Due to temperature, air and practical considerations, data was collected within 2 hours of the targeted 24 hour preparation time. Several steps were taken to prepare the slurry to data collection. Should the slurry temperature fall outside the 20-25°C desired range, warm or cold municipal tap water would be added to

the water bath accordingly. To enable air to dissipate, the mixer impeller is slowed to 140 rpm, and the mixing tank inlet extension is added to prevent splashing. The justification for these measures was further discussed in Chapter 3. The flow rate is also slowed to a 1.5 m/s bulk velocity. This was previously found to be sufficiently slow for air to be released from the slurry (Mohamadabadi, 2009).

Visual inspection was used to qualitatively determine when the air had dissipated. Bubbles would cease to form at the surface of the slurry in the mixing tank. The slurry seen through the various transparent sections within the pipeline would be without bubbles at the top, as well as being the same color as seen through the viewing section in the mixing tank. Dissolved air bubbles make the slurry appear more white or yellow in color, as opposed to brown.

1.4. Data Collection

Measurements of slurries were first taken at the maximum concentration for their respective particles size. These concentrations were determined in Chapter 3, and with calculations outlined in Chapter 2. Data were taken at each of four flow rate intervals; from 1.5 m/s (critical velocity before material begins to settle), 2.0 m/s, 2.5 m/s and the maximum flow rate of each slurry (as limited by the pump power). The upstream and downstream pressure gauge readings were recorded within 0.5 kPa, while the flow rate was within 0.1 m/s.

After data was collected, the slurry was diluted to reduce the wet mass basis concentration by 5%. The system was then drained until the slurry returned to the

50 gallon mark within the mixing tank. The pressure measurements were recorded at the four flow rates. This process was repeated until the concentration reached 0%. At 0%, the pressure drop data was then be compared to that of water to ensure the performance of the system.

Following this testing, the entire system, including the lead lines to the pressure gauges, was purged with water. Fresh straw could then be added, and the methodology repeated for a total three independent trials of each particle size and concentration. A summary of the methodology can be seen in Figure 38 as a flowchart.

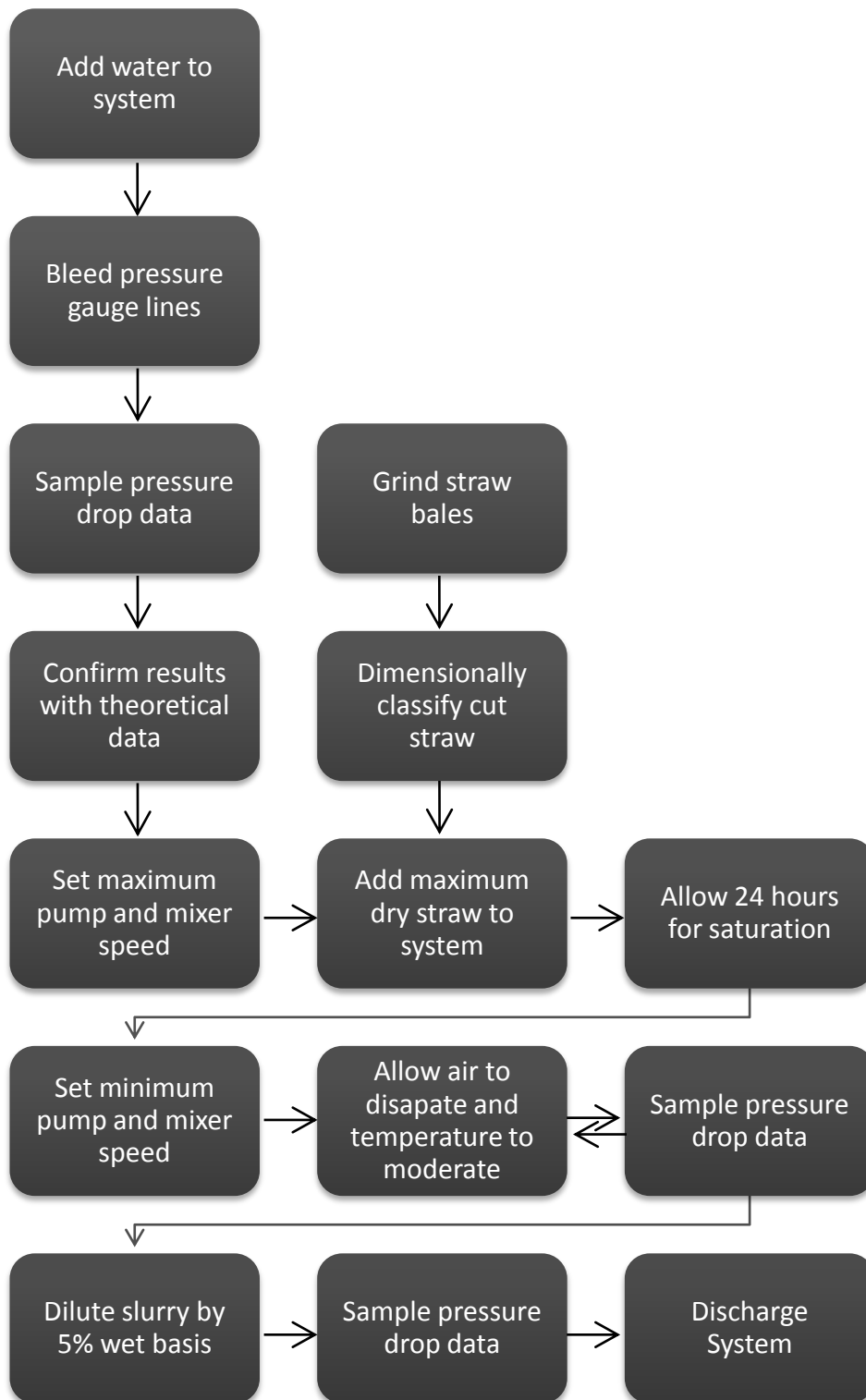


Figure 38: Flowchart depicting experimental methodology for measuring hydraulic transport properties

2. Results and Discussion

Table 12: Power law approximation for pressure loss gradients

Average Particle Size	Wet Mass Basis Concentration	Pressure Drop Gradient (kPa/m)	Coefficient of Determination (R^2)	95% Confidence Interval (kPa/m)
*1/8"	30%	$0.4273v_m^{1.1250}$	0.979	± 0.084
*1/8"	25%	$0.2841v_m^{1.4997}$	0.990	± 0.097
*1/8"	20%	$0.2307v_m^{1.7748}$	0.996	± 0.063
*1/8"	15%	$0.2234v_m^{1.8433}$	0.998	± 0.051
*1/8"	10%	$0.2230v_m^{1.8640}$	0.999	± 0.042
*1/8"	5%	$0.2223v_m^{1.8658}$	0.998	± 0.059
*1/4"	25%	$0.3806v_m^{1.2197}$	0.958	± 0.153
*1/4"	20%	$0.2399v_m^{1.6317}$	0.995	± 0.055
*1/4"	15%	$0.2335v_m^{1.7219}$	0.998	± 0.056
*1/4"	10%	$0.2236v_m^{1.8072}$	0.999	± 0.033
*1/4"	5%	$0.2218v_m^{1.8395}$	0.997	± 0.071
*3/4"	10%	$0.2512v_m^{1.6424}$	0.991	± 0.066
*3/4"	5%	$0.2218v_m^{1.8199}$	0.998	± 0.049
Water	0%	$0.2174v_m^{1.9089}$	n/a	n/a

The collected pressure drop data from the flowable slurries were compiled to produce pressure drop gradients. A power-law approximation was used to create lines of best fit, which has been proposed for slurries by Clift (Wilson et al., 2010). The power law pressure drop gradients in Table 12, resulted in high coefficients of determination above 97%. Most 95% confidence intervals, which are determined from the student-t test, comparable to the resolution of the measurements of 0.059 kPa/m. Detailed data, used to create this table and all other figures in this chapter, can be found in Table 13 through Table 25.

*Average particle size sample as classified in Table 1

Table 13: *1/8" 30% Concentration slurry pressure drop data

Measure	Bulk Velocity	Pressure Gauge Readings	Absolute Pressure Drop	Relative Pressure Drop	Specific Pressure Drop	Effective Viscosity
Unit	m/s	kPa / 8.5m	kPa / m	kPa slurry / kPa water	kPa / m / kg straw	mPa*s
Trial A	1.5	6.00	0.71	1.50	2.35	8.45
	2.0	8.00	0.94	1.15	3.14	2.78
	2.5	10.00	1.18	0.94	3.92	0.19
	2.6	10.50	1.24	0.92	4.12	-0.07
Trial B	1.5	4.50	0.71	1.50	2.35	8.45
	2.0	7.00	0.88	1.08	2.94	1.78
	2.5	10.00	1.24	0.99	4.12	0.68
	2.7	12.00	1.35	0.93	4.51	0.06
Trial C	1.5	4.00	0.65	1.37	2.16	5.86
	2.0	7.00	0.88	1.08	2.94	1.78
	2.5	10.00	1.18	0.94	3.92	0.19
	2.6	12.50	1.29	0.96	4.31	0.36
Average	1.5	n/a	0.69	1.46	2.29	7.53
	2.0	n/a	0.90	1.10	3.01	2.09
	2.5	n/a	1.20	0.96	3.99	0.34
	2.6	n/a	1.29	0.94	4.31	0.11

**Average particle size sample as classified in Table 1*

Table 14: *1/8" 25% Concentration slurry pressure drop data

Measure	Bulk Velocity	Pressure Gauge Readings	Absolute Pressure Drop	Relative Pressure Drop	Specific Pressure Drop	Effective Viscosity
Unit	m/s	kPa / 8.5m	kPa / m	kPa slurry / kPa water	kPa / m / kg straw	mPa*s
Trial A	1.5	4.00	0.53	1.12	2.12	2.12
	2.0	7.00	0.82	1.01	3.29	0.97
	2.5	10.50	1.18	0.94	4.71	0.21
	2.8	13.50	1.41	0.91	5.65	-0.18
Trial B	1.5	4.00	0.53	1.12	2.12	2.12
	2.0	7.00	0.76	0.94	3.06	0.29
	2.5	10.50	1.12	0.89	4.47	-0.22
	2.8	13.50	1.35	0.87	5.41	-0.52
Trial C	1.5	4.00	0.53	1.12	2.12	2.12
	2.0	7.00	0.76	0.94	3.06	0.29
	2.5	10.00	1.06	0.85	4.24	-0.58
	2.8	14.00	1.29	0.82	5.18	-0.81
Average	1.5	n/a	0.53	1.12	2.12	2.12
	2.0	n/a	0.78	0.96	3.14	0.50
	2.5	n/a	1.12	0.89	4.47	-0.22
	2.8	n/a	1.35	0.87	5.41	-0.52

*Average particle size sample as classified in Table 1

Table 15: *1/8" 20% Concentration slurry pressure drop data

Measure	Bulk Velocity	Pressure Gauge Readings	Absolute Pressure Drop	Relative Pressure Drop	Specific Pressure Drop	Effective Viscosity
Unit	m/s	kPa / 8.5m	kPa / m	kPa slurry / kPa water	kPa / m / kg straw	mPa*s
Trial A	1.5	4.00	0.47	1.00	2.35	0.88
	2.0	7.00	0.82	1.01	4.12	1.00
	2.5	10.50	1.18	0.94	5.88	0.24
	2.8	14.50	1.47	0.95	7.35	0.23
Trial B	1.5	5.50	0.47	1.00	2.35	0.88
	2.0	7.50	0.82	1.01	4.12	1.00
	2.5	10.50	1.18	0.94	5.88	0.24
	2.9	11.50	1.53	0.92	7.65	-0.07
Trial C	1.5	4.00	0.47	1.00	2.35	0.88
	2.0	6.50	0.76	0.94	3.82	0.31
	2.5	9.50	1.12	0.89	5.59	-0.19
	2.8	11.00	1.41	0.91	7.06	-0.16
Average	1.5	n/a	0.47	1.00	2.35	0.88
	2.0	n/a	0.80	0.98	4.02	0.76
	2.5	n/a	1.16	0.93	5.78	0.09
	2.8	n/a	1.47	0.93	7.35	0.00

**Average particle size sample as classified in Table 1*

Table 16: *1/8" 15% Concentration slurry pressure drop data

Measure	Bulk Velocity	Pressure Gauge Readings	Absolute Pressure Drop	Relative Pressure Drop	Specific Pressure Drop	Effective Viscosity
Unit	m/s	kPa / 8.5m	kPa / m	kPa slurry / kPa water	kPa / m / kg straw	mPa*s
Trial A	1.5	4.00	0.47	1.00	3.14	0.91
	2.0	6.50	0.82	1.01	5.49	1.03
	2.5	10.00	1.24	0.99	8.24	0.78
	2.9	12.00	1.59	0.96	10.59	0.35
Trial B	1.5	4.00	0.47	1.00	3.14	0.91
	2.0	6.50	0.82	1.01	5.49	1.03
	2.5	10.00	1.24	0.99	8.24	0.78
	2.9	13.00	1.59	0.96	10.59	0.35
Trial C	1.5	4.00	0.47	1.00	3.14	0.91
	2.0	6.50	0.76	0.94	5.10	0.34
	2.5	10.00	1.18	0.94	7.84	0.27
	2.8	13.50	1.47	0.95	9.80	0.26
Average	1.5	n/a	0.47	1.00	3.14	0.91
	2.0	n/a	0.80	0.98	5.36	0.78
	2.5	n/a	1.22	0.97	8.10	0.60
	2.9	n/a	1.55	0.95	10.33	0.32

**Average particle size sample as classified in Table 1*

Table 17: *1/8" 10% Concentration slurry pressure drop data

Measure	Bulk Velocity	Pressure Gauge Readings	Absolute Pressure Drop	Relative Pressure Drop	Specific Pressure Drop	Effective Viscosity
Unit	m/s	kPa / 8.5m	kPa / m	kPa slurry / kPa water	kPa / m / kg straw	mPa*s
Trial A	1.5	4.00	0.47	1.00	4.71	0.93
	2.0	7.00	0.82	1.01	8.24	1.06
	2.5	10.50	1.24	0.99	12.35	0.81
	2.9	14.00	1.59	0.96	15.88	0.38
Trial B	1.5	4.50	0.47	1.00	4.71	0.93
	2.0	7.00	0.82	1.01	8.24	1.06
	2.5	10.00	1.24	0.99	12.35	0.81
	2.9	12.50	1.65	0.99	16.47	0.82
Trial C	1.5	4.00	0.47	1.00	4.71	0.93
	2.0	6.50	0.82	1.01	8.24	1.06
	2.5	10.00	1.24	0.99	12.35	0.81
	2.9	13.50	1.59	0.96	15.88	0.38
Average	1.5	n/a	0.47	1.00	4.71	0.93
	2.0	n/a	0.82	1.01	8.24	1.06
	2.5	n/a	1.24	0.99	12.35	0.81
	2.9	n/a	1.61	0.97	16.08	0.52

**Average particle size sample as classified in Table 1*

Table 18: *1/8" 5% Concentration slurry pressure drop data

Measure	Bulk Velocity	Pressure Gauge Readings	Absolute Pressure Drop	Relative Pressure Drop	Specific Pressure Drop	Effective Viscosity
Unit	m/s	kPa / 8.5m	kPa / m	kPa slurry / kPa water	kPa / m / kg straw	mPa*s
Trial A	1.5	4.00	0.47	1.00	9.41	0.95
	2.0	7.00	0.82	1.01	16.47	1.09
	2.5	10.50	1.18	0.94	23.53	0.32
	2.9	14.00	1.65	0.99	32.94	0.86
Trial B	1.5	0.00	0.47	1.00	9.41	0.95
	2.0	0.00	0.82	1.01	16.47	1.09
	2.5	0.00	1.24	0.99	24.71	0.84
	2.9	0.00	1.65	0.99	32.94	0.86
Trial C	1.5	0.00	0.47	1.00	9.41	0.95
	2.0	0.00	0.82	1.01	16.47	1.09
	2.5	0.00	1.24	0.99	24.71	0.84
	2.8	0.00	1.47	0.95	29.41	0.32
Average	1.5	n/a	0.47	1.00	9.41	0.95
	2.0	n/a	0.82	1.01	16.47	1.09
	2.5	n/a	1.22	0.97	24.31	0.66
	2.9	n/a	1.59	0.98	31.76	0.68

**Average particle size sample as classified in Table 1*

Table 19: *1/4" 25% Concentration slurry pressure drop data

Measure	Bulk Velocity	Pressure Gauge Readings	Absolute Pressure Drop	Relative Pressure Drop	Specific Pressure Drop	Effective Viscosity
Unit	m/s	kPa / 8.5m	kPa / m	kPa slurry / kPa water	kPa / m / kg straw	mPa*s
Trial A	1.5	0.00	0.65	1.37	2.59	5.92
	2.0	0.00	0.88	1.08	3.53	1.82
	2.5	0.00	1.24	0.99	4.94	0.72
	2.7	0.00	1.35	0.93	5.41	0.09
Trial B	1.5	0.00	0.65	1.37	2.59	5.92
	2.0	0.00	0.94	1.15	3.76	2.82
	2.5	0.00	1.18	0.94	4.71	0.21
	2.7	0.00	1.35	0.93	5.41	0.09
Trial C	1.5	0.00	0.59	1.25	2.35	3.79
	2.0	0.00	0.82	1.01	3.29	0.97
	2.5	0.00	1.06	0.85	4.24	-0.58
	2.7	0.00	1.18	0.81	4.71	-0.91
Average	1.5	n/a	0.63	1.33	2.51	5.16
	2.0	n/a	0.88	1.08	3.53	1.82
	2.5	n/a	1.16	0.93	4.63	0.06
	2.7	n/a	1.29	0.89	5.18	-0.29

**Average particle size sample as classified in Table 1*

Table 20: *1/4" 20% Concentration slurry pressure drop data

Measure	Bulk Velocity	Pressure Gauge Readings	Absolute Pressure Drop	Relative Pressure Drop	Specific Pressure Drop	Effective Viscosity
Unit	m/s	kPa / 8.5m	kPa / m	kPa slurry / kPa water	kPa / m / kg straw	mPa*s
Trial A	1.5	0.00	0.47	1.00	2.35	0.88
	2.0	0.00	0.76	0.94	3.82	0.31
	2.5	0.00	1.12	0.89	5.59	-0.19
	2.8	0.00	1.29	0.83	6.47	-0.79
Trial B	1.5	0.00	0.47	1.00	2.35	0.88
	2.0	0.00	0.71	0.86	3.53	-0.23
	2.5	0.00	1.06	0.85	5.29	-0.56
	2.8	0.00	1.29	0.83	6.47	-0.79
Trial C	1.5	0.00	0.47	1.00	2.35	0.88
	2.0	0.00	0.71	0.86	3.53	-0.23
	2.5	0.00	1.06	0.85	5.29	-0.56
	2.8	0.00	1.29	0.83	6.47	-0.79
Average	1.5	n/a	0.47	1.00	2.35	0.88
	2.0	n/a	0.73	0.89	3.63	-0.07
	2.5	n/a	1.08	0.86	5.39	-0.45
	2.8	n/a	1.29	0.83	6.47	-0.79

**Average particle size sample as classified in Table 1*

Table 21: *1/4" 15% Concentration slurry pressure drop data

Measure	Bulk Velocity	Pressure Gauge Readings	Absolute Pressure Drop	Relative Pressure Drop	Specific Pressure Drop	Effective Viscosity
Unit	m/s	kPa / 8.5m	kPa / m	kPa slurry / kPa water	kPa / m / kg straw	mPa*s
Trial A	1.5	0.00	0.47	1.00	3.14	0.91
	2.0	0.00	0.76	0.94	5.10	0.34
	2.5	0.00	1.18	0.94	7.84	0.27
	2.9	0.00	1.41	0.85	9.41	-0.69
Trial B	1.5	0.00	0.47	1.00	3.14	0.91
	2.0	0.00	0.76	0.94	5.10	0.34
	2.5	0.00	1.12	0.89	7.45	-0.17
	2.9	0.00	1.47	0.89	9.80	-0.39
Trial C	1.5	0.00	0.47	1.00	3.14	0.91
	2.0	0.00	0.76	0.94	5.10	0.34
	2.5	0.00	1.12	0.89	7.45	-0.17
	2.8	0.00	1.41	0.91	9.41	-0.13
Average	1.5	n/a	0.47	1.00	3.14	0.91
	2.0	n/a	0.76	0.94	5.10	0.34
	2.5	n/a	1.14	0.91	7.58	-0.03
	2.9	n/a	1.43	0.88	9.54	-0.41

**Average particle size sample as classified in Table 1*

Table 22: *1/4" 10% Concentration slurry pressure drop data

Measure	Bulk Velocity	Pressure Gauge Readings	Absolute Pressure Drop	Relative Pressure Drop	Specific Pressure Drop	Effective Viscosity
Unit	m/s	kPa / 8.5m	kPa / m	kPa slurry / kPa water	kPa / m / kg straw	mPa*s
Trial A	1.5	0.00	0.47	1.00	4.71	0.93
	2.0	0.00	0.76	0.94	7.65	0.36
	2.5	0.00	1.18	0.94	11.76	0.30
	2.9	0.00	1.53	0.92	15.29	-0.01
Trial B	1.5	0.00	0.47	1.00	4.71	0.93
	2.0	0.00	0.76	0.94	7.65	0.36
	2.5	0.00	1.18	0.94	11.76	0.30
	2.9	0.00	1.53	0.92	15.29	-0.01
Trial C	1.5	0.00	0.47	1.00	4.71	0.93
	2.0	0.00	0.76	0.94	7.65	0.36
	2.5	0.00	1.18	0.94	11.76	0.30
	2.8	0.00	1.47	0.95	14.71	0.29
Average	1.5	n/a	0.47	1.00	4.71	0.93
	2.0	n/a	0.76	0.94	7.65	0.36
	2.5	n/a	1.18	0.94	11.76	0.30
	2.9	n/a	1.51	0.93	15.10	0.09

**Average particle size sample as classified in Table 1*

Table 23: *1/4" 5% Concentration slurry pressure drop data

Measure	Bulk Velocity	Pressure Gauge Readings	Absolute Pressure Drop	Relative Pressure Drop	Specific Pressure Drop	Effective Viscosity
Unit	m/s	kPa / 8.5m	kPa / m	kPa slurry / kPa water	kPa / m / kg straw	mPa*s
Trial A	1.5	0.00	0.47	1.00	9.41	0.95
	2.0	0.00	0.76	0.94	15.29	0.38
	2.5	0.00	1.18	0.94	23.53	0.32
	2.9	0.00	1.59	0.96	31.76	0.41
Trial B	1.5	0.00	0.47	1.00	9.41	0.95
	2.0	0.00	0.76	0.94	15.29	0.38
	2.5	0.00	1.18	0.94	23.53	0.32
	2.9	0.00	1.53	0.92	30.59	0.02
Trial C	1.5	0.00	0.47	1.00	9.41	0.95
	2.0	0.00	0.82	1.01	16.47	1.09
	2.5	0.00	1.24	0.99	24.71	0.84
	2.8	0.00	1.53	0.99	30.59	0.78
Average	1.5	n/a	0.47	1.00	9.41	0.95
	2.0	n/a	0.78	0.96	15.69	0.60
	2.5	n/a	1.20	0.96	23.92	0.49
	2.9	n/a	1.55	0.95	30.98	0.39

*Average particle size sample as classified in Table 1

Table 24: *3/4" 10% Concentration slurry pressure drop data

Measure	Bulk Velocity	Pressure Gauge Readings	Absolute Pressure Drop	Relative Pressure Drop	Specific Pressure Drop	Effective Viscosity
Unit	m/s	kPa / 8.5m	kPa / m	kPa slurry / kPa water	kPa / m / kg straw	mPa*s
Trial A	1.5	0.00	0.53	1.12	5.29	2.22
	2.0	0.00	0.82	1.01	8.24	1.06
	2.5	0.00	1.18	0.94	11.76	0.30
	2.9	0.00	1.47	0.89	14.71	-0.36
Trial B	1.5	0.00	0.47	1.00	4.71	0.93
	2.0	0.00	0.76	0.94	7.65	0.36
	2.5	0.00	1.12	0.89	11.18	-0.15
	2.6	0.00	1.18	0.87	11.76	-0.36
Trial C	1.5	0.00	0.47	1.00	4.71	0.93
	2.0	0.00	0.76	0.94	7.65	0.36
	2.5	0.00	1.12	0.89	11.18	-0.15
	2.8	0.00	1.35	0.87	13.53	-0.45
Average	1.5	n/a	0.49	1.04	4.90	1.31
	2.0	n/a	0.78	0.96	7.84	0.58
	2.5	n/a	1.14	0.89	11.37	-0.01
	2.8	n/a	1.33	0.88	13.33	-0.38

**Average particle size sample as classified in Table 1*

Table 25: *3/4" 5% Concentration slurry pressure drop data

Measure	Bulk Velocity	Pressure Gauge Readings	Absolute Pressure Drop	Relative Pressure Drop	Specific Pressure Drop	Effective Viscosity
Unit	m/s	kPa / 8.5m	kPa / m	kPa slurry / kPa water	kPa / m / kg straw	mPa*s
Trial A	1.5	0.00	0.47	1.00	9.41	0.95
	2.0	0.00	0.76	0.94	15.29	0.38
	2.5	0.00	1.18	0.94	23.53	0.32
	2.9	0.00	1.59	0.96	31.76	0.41
Trial B	1.5	0.00	0.47	0.00	9.41	0.95
	2.0	0.00	0.76	0.94	15.29	0.38
	2.5	0.00	1.18	0.94	23.53	0.32
	2.6	0.00	1.24	0.92	24.71	0.06
Trial C	1.5	0.00	0.47	1.00	9.41	0.95
	2.0	0.00	0.76	0.94	15.29	0.38
	2.5	0.00	1.18	0.94	23.53	0.32
	2.8	0.00	1.47	0.95	29.41	0.32
Average	1.5	n/a	0.47	1.00	9.41	0.95
	2.0	n/a	0.76	0.94	15.29	0.38
	2.5	n/a	1.18	0.94	23.53	0.32
	2.8	n/a	1.43	0.94	28.63	0.29

*Average particle size sample as classified in Table 1

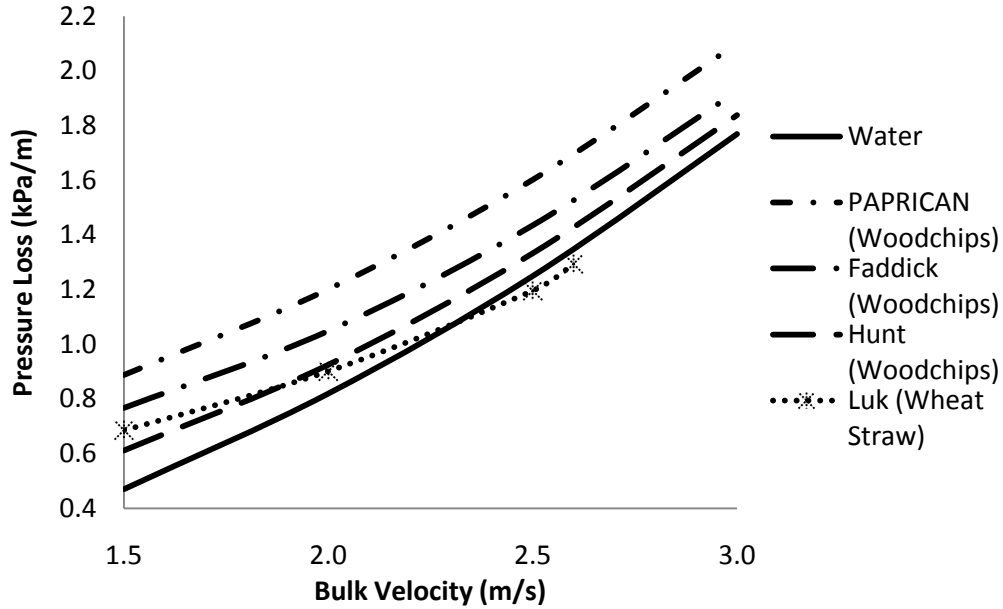


Figure 39: 30% *1/8" Average size woodchip and straw slurries

None of the woodchip biomass slurry approximations used in past studies accurately represented performance of wheat straw slurry. While all woodchip estimates were above the pressure drop of water, straw slurries have a more complex relationship. All of the wheat straw slurry samples resulted in a lower pressure drop than water at certain velocities. It can be seen that this is true at velocities above 2.5 m/s, for the maximum 30% concentration of 1/8" wheat straw particles in Figure 39.

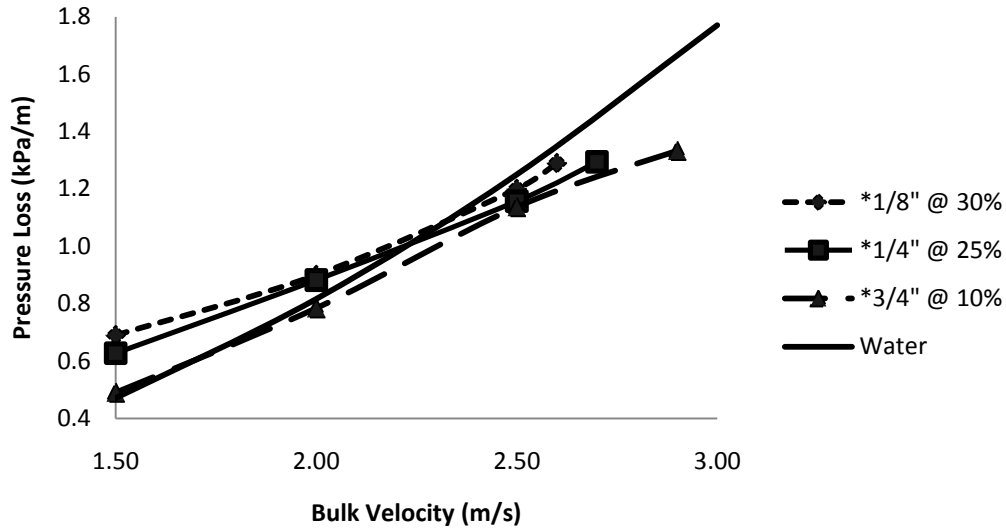


Figure 40: Maximum flowable slurry concentration pressure losses

With woodchips equations, pressure loss increases with concentration, and continue to diverge at greater flow rates. When comparing only the maximum concentrations of each of the three wheat straw particle size slurries, in Figure 40, there is a general trend which saw pressure drop increase with solids content. However, the pressure drop gradients converge as flow rates increase, and each intersects with that of water. The intersection points ranges from approximately 2.0 m/s for the 3/4" 10% slurry to 2.3 m/s for the 1/8" 30% slurry.

These findings follow that of fibre suspension flows. At these high concentrations, there may be networks of straw, which create plugs in the flow (Lee and Duffy, 1976). This is qualitatively seen during discharge, when slurries do not flow out smoothly. An annulus of water is formed around the flocs, while the network of straw suppresses turbulence and the momentum of the flow. At higher velocities, sufficient turbulence at the walls can begin to tear apart the flocs, gradually altering the nature of the flow.

2.1. Concentration Comparison

At lower concentrations or higher velocities, the trend is completely reversed, with pressure losses decreasing with additional solids content. It can be seen in the 1/8", 1/4", and 3/4" particle slurries in Figure 41 to Figure 43. For clarity only Table 12 power law approximations are plotted. This is consistent through much of the flow rate interval examined, although the low resolutions of the pressure gauges blur the differences between low concentrations and low flow rates.

Sufficiently low concentrations or high velocities, do not allow plugs to form. The long fibre-like particles however, continue to interact with each other differently than shorter rounder woodchips. The suspended fibres continue to suppress turbulence, although it occurs throughout the cross-section of the flow (Vaseleski and Metzner, 1974). This is opposed to only interfering with turbulence within the core of the flow, at lower velocities of the maximum concentration slurries.

Suppressing turbulence reduces the amount of energy lost by viscous shear (Lee and Duffy, 1976). This allows the pressure drop to be less than what would occur with the carrier fluid alone. Increasing the concentration of long slender solids further dampens turbulence and reduces the pressure losses.

The pressure losses of these slurries diverged with increased flow rates. This divergence occurs as there is increased turbulence at higher velocities. Thus, there is a greater potential for turbulence to be interfered by the straw particles. At higher velocities, the difference in the ability for the solids to suppress turbulence is magnified.

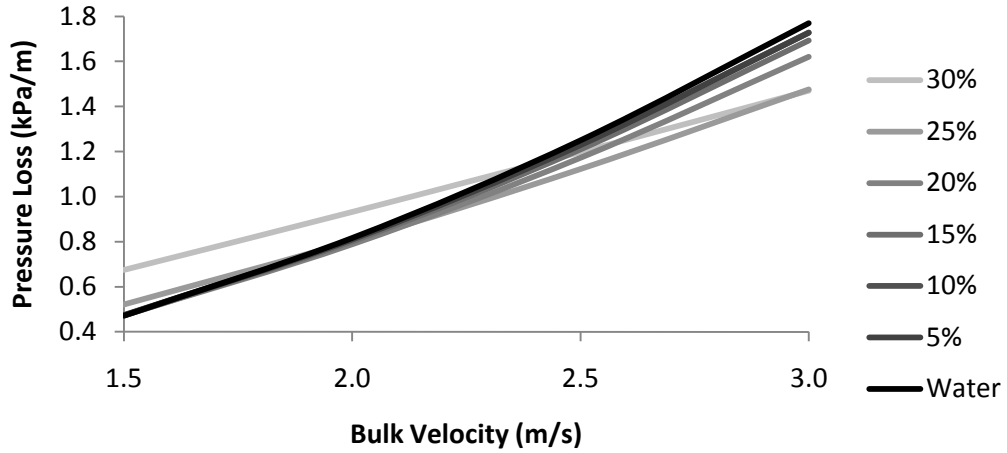


Figure 41: *1/8" Particle slurry pressure losses, exhibiting 25% & 30% plugs

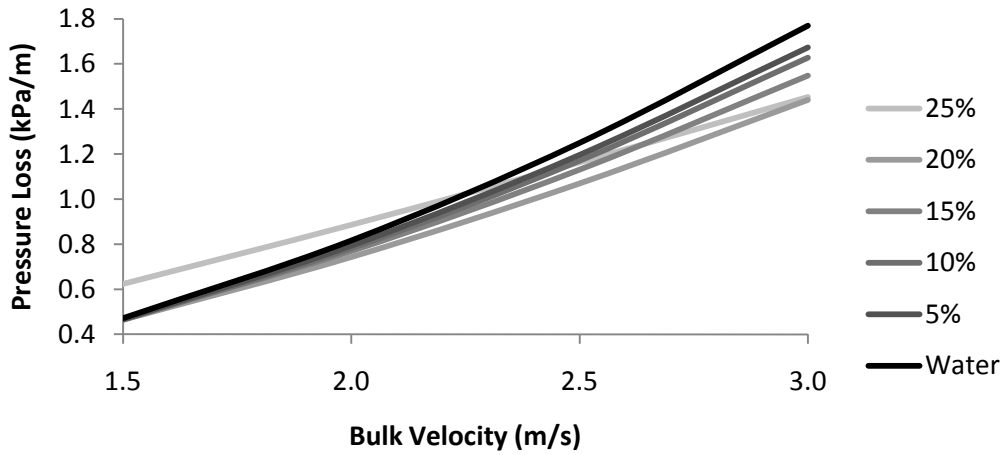


Figure 42: *1/8" Particle slurry pressure losses, exhibiting 25% plug

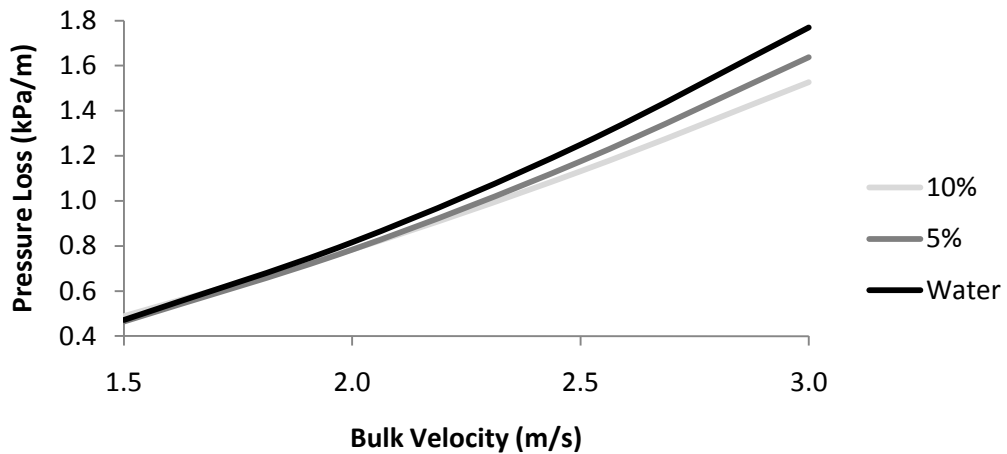


Figure 43: *3/4" Particle slurry pressure losses, exhibiting 10% plug

2.2. Particle Size Comparison

Figure 44 to Figure 49 compare different particle sizes of three common slurry concentrations. To closer examine the subtle patterns between each particle size, these figures display pressure losses relative to that of water. Unlike pressure drop gradients which were graphed with exponential lines of best fit, as determined in past studies, these figures do not depict lines of fit. Instead, straight lines are drawn through the average values at each of the four bulk velocity intervals. Certain slurries depict wavy, oscillating patterns, similar to what was found in other experiments with fibres (Kazi et al., 1999). The range of flow rates examined in this study is insufficient to conclude these trends however, which may be simply a product of the resolution of the pressure gauges used.

Longer particles have lower pressure losses, than those shorter. This pattern is impeded only when plugs are formed in the flow, (when 1/8" particles at 25% and 30%, 1/4" at 25% and 3/4" at 10%). However as the flow rates increase and the plugs are removed, pressure losses quickly fall below that of water, and begins to align with the pattern.

Shorter particles are more similar in geometry to the round woodchips which do not suppress turbulence. As with the trend observed by comparing different concentrations, the ability to suppress turbulence is magnified at greater velocities (when turbulence in the carrier fluid would otherwise be greater) resulting in diverging pressure drop gradients.

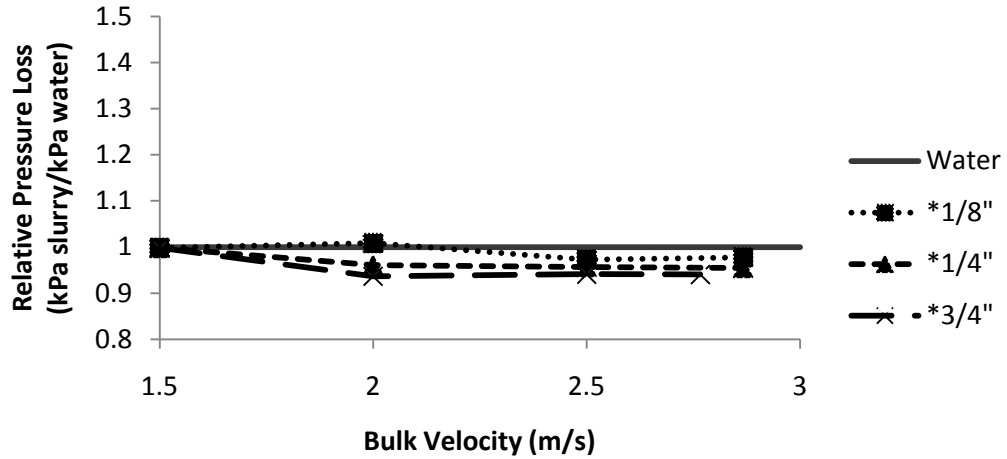


Figure 44: 5% Relative pressure losses, exhibiting no plugs

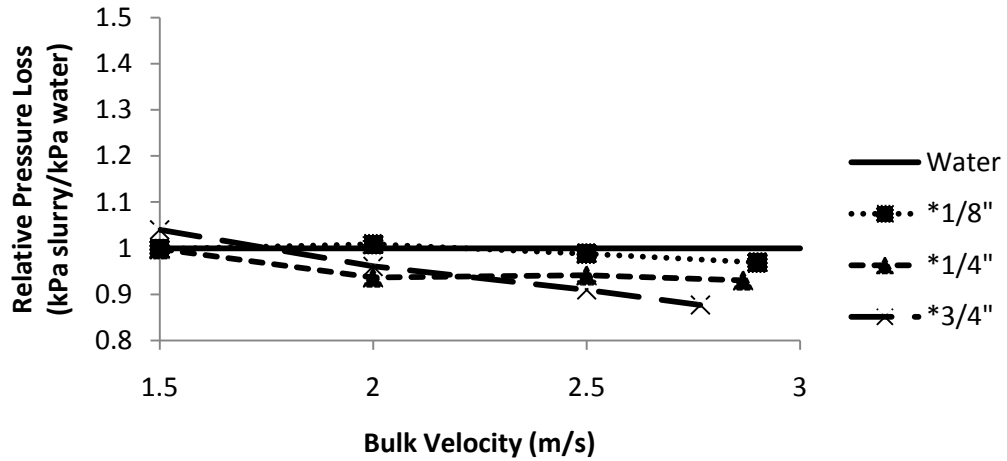


Figure 45: 10% Relative pressure losses, exhibiting *3/4" plug

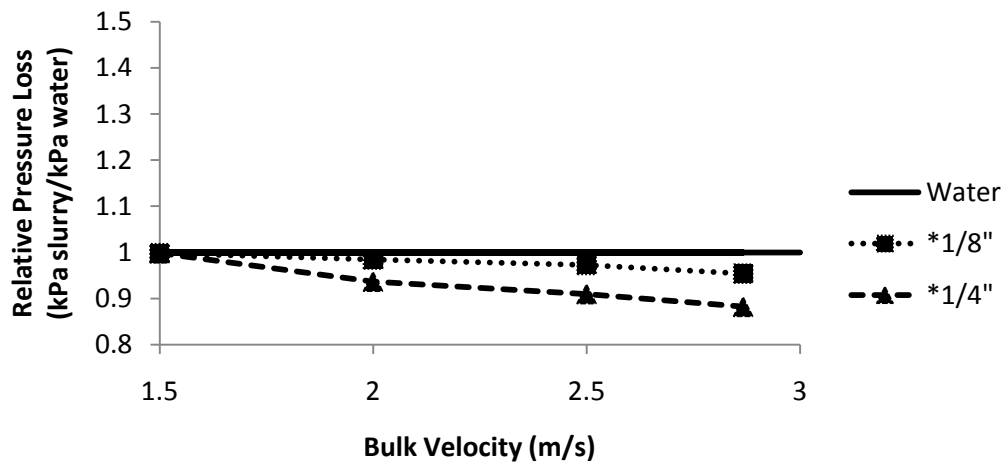


Figure 46: 15% Relative pressure losses, exhibiting no plugs

*Average particle size sample as classified in Table 1

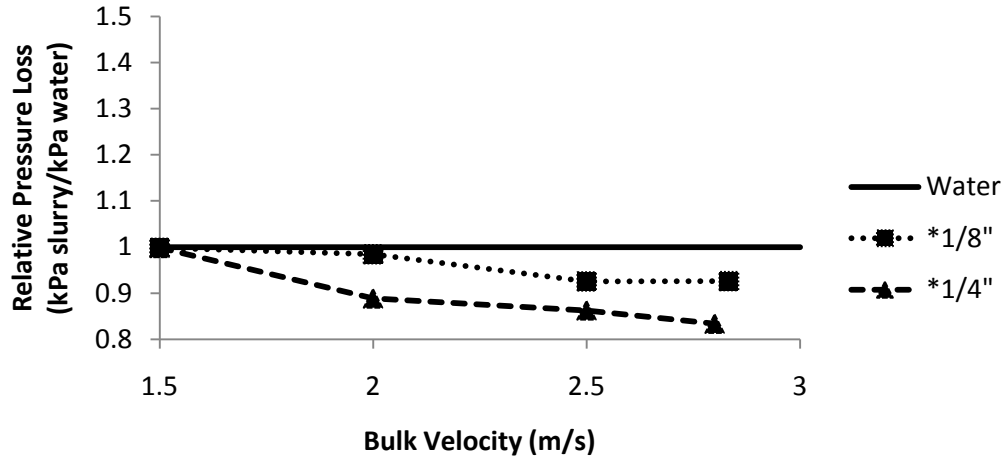


Figure 47: 20% Relative pressure losses, exhibiting no plugs

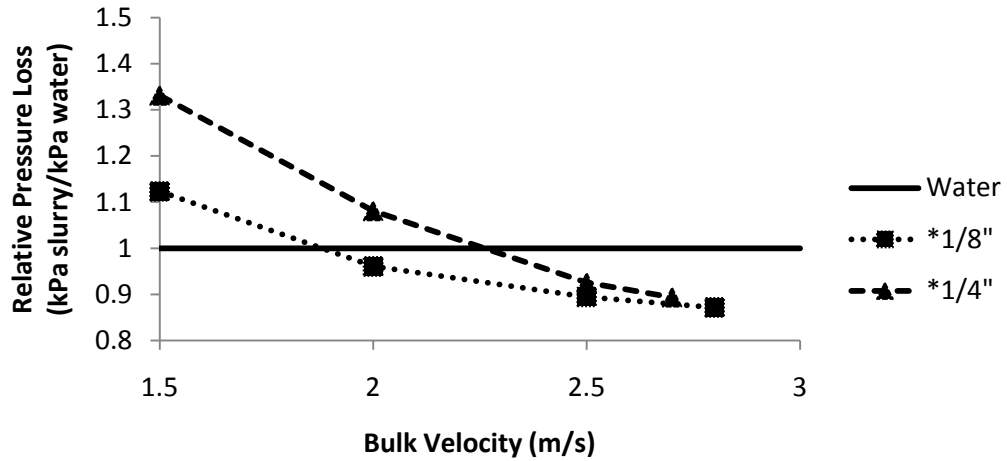


Figure 48: 25% Relative pressure losses, exhibiting *1/8" & *1/4" plugs

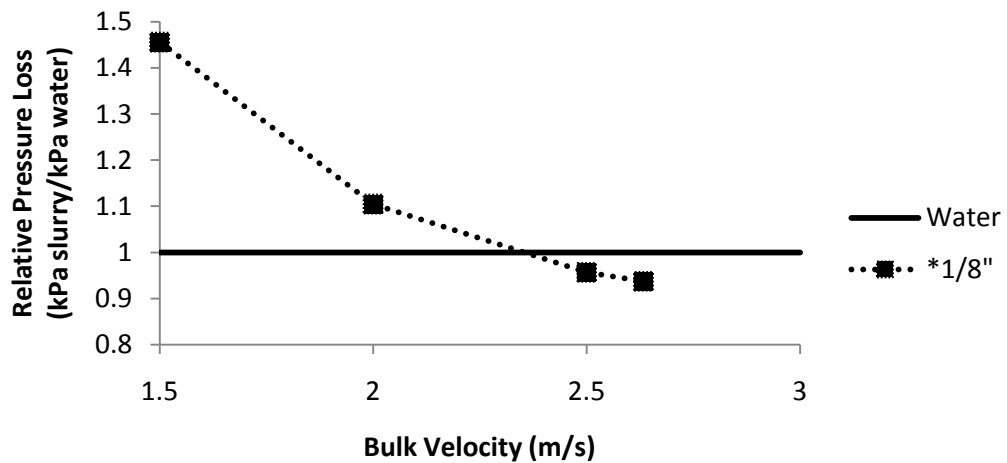


Figure 49: 30% Relative pressure losses, exhibiting 1/8" plug

*Average particle size sample as classified in Table 1

2.3. Drag Reducing Fibre Suspension

The drop gradients patterns between different concentrations and particle sizes in this study are not typical of industrial slurry pipelines. This is due to the long slender geometry of the particle sizes examined. Wheat straw behaves more similarly to fibres which have been analyzed in experimental settings, than rounder particles such as woodchips, or coal and sand which can be found in industrial slurry pipelines (Liu, 2003).

The ability for suspended fibres to reduce the drag resistance of a liquid through a pipe has been known for decades. Vaseleski and Metzner (1974) experimented on nylon fibres (Figure 50a), and various diameters of PVC tubing. They determined that because the drag reduction occurs at turbulent core of the system, that it is independent of the scale of the system (Vaseleski and Metzner, 1974). Conversely, if the reduction occurred along the walls of the pipe, it would have a diminishing effect with increased pipe diameter. Their experiments also determined that turbulence suppression increased with the aspect ratio (length over width) of the particles.

An industrial scale wheat straw biomass pipeline would have a pipe diameter greater than what was used in this study. Vaseleski and Metzner's findings infer that it would still experience pressure losses below that of pure water. In addition, the longer particles used may further reduce losses beyond what was achievable on a laboratory scale.

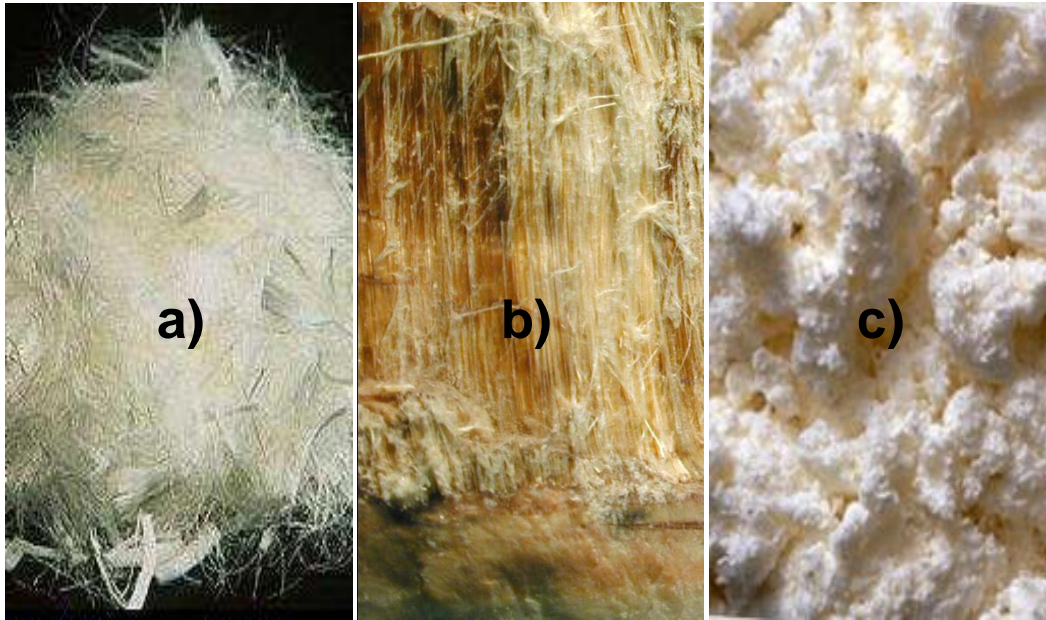


Figure 50: a) nylon (Fiber Depot, 2001), b) asbestos fibres (Glendale Community College, n.d.) and c) wood pulp (U-Haul, 2007)

This allows for savings on several fronts. Smaller or fewer pumping stations reduce capital costs, as well as power consumption throughout the life of the system. Similarly, the ability to use larger particles sizes minimizes both upfront and ongoing expenses required to process the straw before slurring.

Past studies have also been extended to natural fibres. Kato and Mizunuma experimented on using asbestos fibres (Figure 50b) within pipeline flows, with similar findings (Kato and Mizunuma,1983). However, they noted that unlike synthetic materials, asbestos fibres degrade during pumping. Therefore, over time the effectiveness for natural fibres to suppress turbulence decreases. With asbestos fibres, this significantly slowed after the first 2-3 hours, with 5-10% degradation. If this pattern extends to wheat straw, the data which was collected after 24 hours should be applicable to pressure losses that would occur over long distance transportation.

While nylon and asbestos fibres were considered as additives, wood pulp (Figure 50c) is an example of a freight material which acts as a drag reducing fibre. Kazi, Duffy and Chen determined that turbulence is further suppressed with increased flexibility of the fibres, which is a function of the fibre wall thickness (Kazi et al., 1999). Therefore as natural fibres degrade, drag reduction diminishes with a decreased length, but improves with the thinning of the material's wall. Thus it would be difficult to determine how the resultant drag reduction of wheat straw is affected overtime, without experimentation.

2.4. Other Drag Reducing Mechanisms

Other drag reducing mechanisms were also considered, as a possible explanation of the recorded results. This includes the near wall model, bubbly flows, and polymer solutions.

2.4.1. Near Wall Model

Sufficiently heavy solid particles settle to create a sliding bed of material independent of local fluidic forces. Additional material would generate greater sliding friction losses. Conversely, sufficiently small and light solid particles can create homogeneous slurries which behave similar to that of the carrier fluid itself, albeit with an increased density. The increased density would result in greater pressure losses.

Intermediate particles are too large or heavy to produce truly homogeneous slurries, and may be subject to a near-wall effect (Wilson et al., 2010). Shook

examined the concentration profiles of slurries and found that the particles avoid the pipe wall (Shook et al., 1968). This could be the result of turbulence in the viscous sub-layer along the wall being eliminated, which Newitt found creates a buffer region of reduced turbulence (Newitt et al., 1955). Intermediate particles are not sufficiently small enough to enter this viscous sub-layer (Wilson et al., 2010). The local fluidic forces which cause or are caused by the particles lifting away from the pipe wall, in turn may be reducing the friction losses of the slurry.

This, however, can only reduce the frictional drag below that of the equivalent fluid model. In this situation, the equivalent fluid model is a Newtonian fluid with the higher density of wheat straw slurry, but otherwise similar properties to that of the water carrier fluid. While it may play a role in the drag reduction seen in this study, the near wall model cannot account for pressure losses which are below the water carrier fluid.

2.4.2. Micro-bubbles

Air bubbles on the other hand, can account for significant drag reductions (Mohanarangam et al., 2009) (Murai et al., 2008) (Ceccio, 2010) (Bernal 2004). Micro-bubbles have been found to reduce the frictional drag in a channel by up to 38% (Bernal, 2004). These results have been achieved by continually releasing, or creating through electrolysis, a concentration of micro-bubbles at the solid surfaces. This layer of gas creates a buffer region with substantially lower density, which reduces friction losses along the walls of the flow. In practical scenarios this technology may best be suited for external flows, such as water around a ship hull, where the air could freely dissipate.

Although great care, as described previously in the slurry preparation methodology, has been taken to prevent and remove any air content within the slurries examined, a limited volume may still be present. However, dissolved air is dispersed throughout the flow, which is believed to be the case in this study, would not provide a significant drag reducing effect. Rather than provide a significant decrease in density along the walls, the density of the entire slurry would be lowered by a slight degree, resulting in a similarly minor impact on pressure losses.

(Note that completely replacing water with air as the carrier fluid would markedly decrease the pressure loss at a given flow rate. However, the lower density fluid would require substantially higher velocities to propel solid particles. This relegates the use economic of pneumatic pipelines for short distances, of typically less than a kilometre (Liu, 2003).)

2.4.3. Polymer

Another means of achieving drag reductions of this magnitude, is through the introduction of polymer additives (Jubran et al., 2005). Polymer solutions, like fibre suspensions, dampen turbulence to reduce frictional drag. Although, wheat straw is not a polymer, it may be possible to benefit from the technology. The drag reduction capabilities of polymer-fibre mixtures, is greater than the sum of the drag reduction achieved by each additive individually (Reddy and Singh, 1985). In 1979, polymer additives were first used industrially with the 1.2 m diameter Trans-Alaskan pipeline, and achieved a 50% drag reduction. If combined with fibre suspensions, substantial drag reductions could be achieved.

Sugars released from the solid particles into the carrier fluid could be contributing to this phenomenon. It could explain the lower pressure drop of higher concentration slurries, which would release more material into the water. Longer particle slurries also exhibited lower pressure drop than that of shorter particles, however. Unless there is a mechanism which causes larger particles to breakdown more rapidly than those smaller, the patterns which arose from examining different particle sizes are not explained by the presence of polymers. More experimentation would be required to determine the impact of sugar releases, on pressure losses.

2.5. Efficiency Comparison

Figure 51 compares the pumping requirements to transport a unit of wet straw at the minimum flow rate. The concentration of the slurries has been divided out of its respective pressure loss, at the critical velocity. This results with a minimum pressure loss per unit straw for slurries with concentrations just below that of its maximum. The exception is of the largest $\frac{3}{4}$ " particles, in which there was insufficient number of concentrations examined to produce a curve. More nuances were able to be captured at smaller particle sizes. For $\frac{1}{8}$ " particles size slurry at a 25% concentration has the lowest pumping requirements. This reduces the formation of flocs in the flow, while still maintaining a high concentration. This does not consider other requirements, such as water supply, which are minimized with higher concentrations.

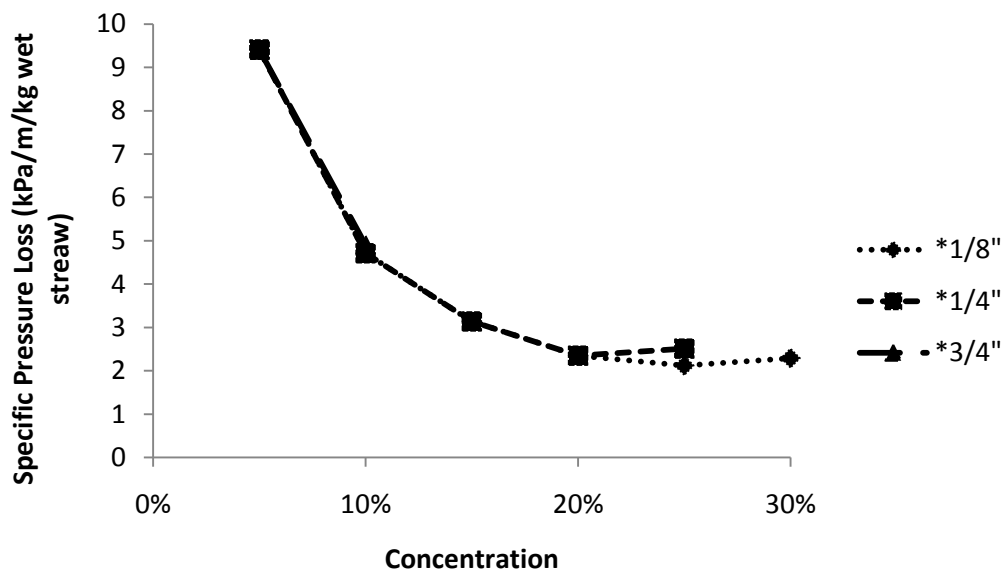


Figure 51: Specific pressure loss by concentration at 1.5 m/s

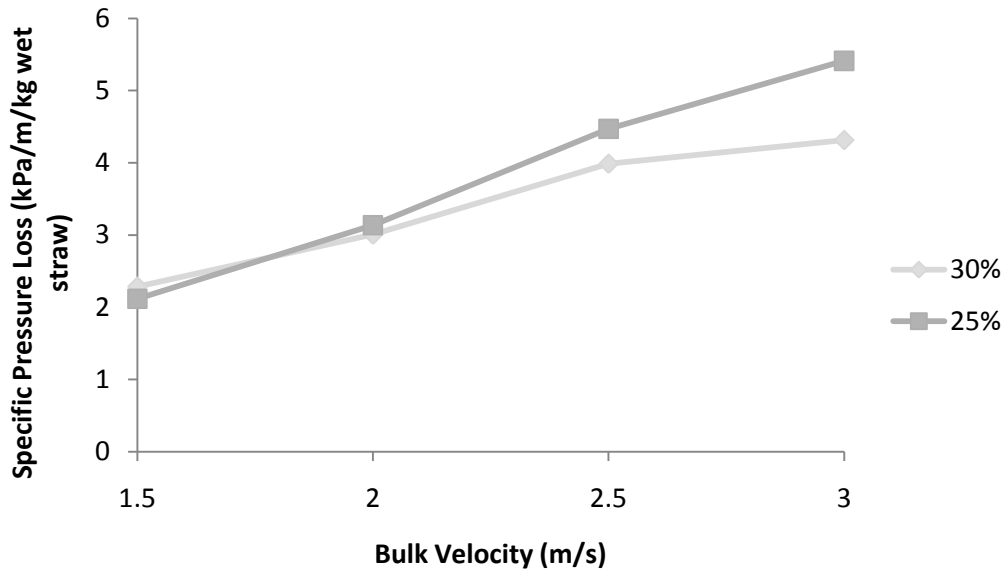


Figure 52: *1/8” particle size specific pumping requirements by velocity

While slower flow rates minimize the pumping requirements of slurry, it also reduces the feedstock available to the end user, while increasing the risk of congestion. Figure 52 examines the impact of increasing slurry velocities on the pumping requirements. Due to the fact that the pressure losses of high concentration slurries do not increase at nearly the same rate as water, their curves are relatively flat. Increasing the flow rate within mechanical constraints may be a feasible means to increase the capacity of the pipeline system, without the need to invest in a larger pipe diameter. When the bulk velocity reaches 2 m/s, 30% concentrations begin to have lower specific pressure losses than that at 20%.

**Average particle size sample as classified in Table 1*

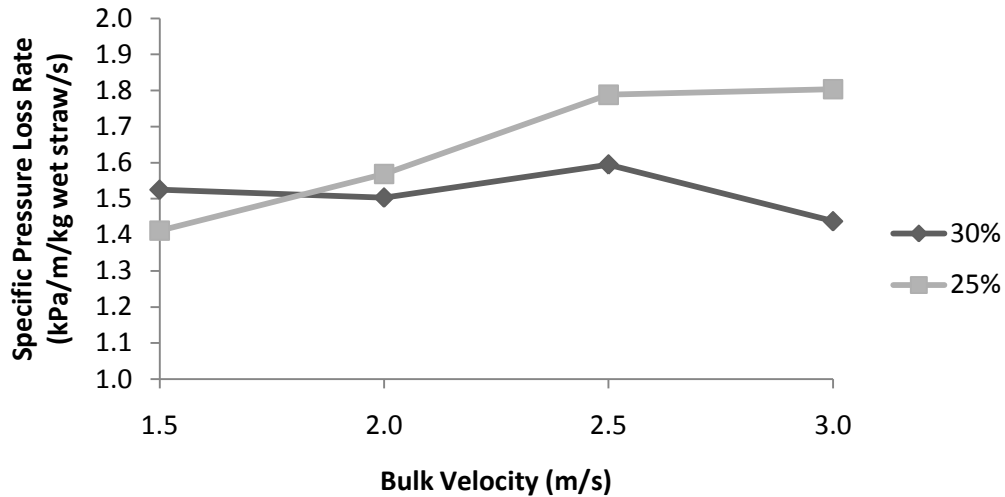


Figure 53: *1/8” particle size specific pumping requirements, per unit time

When the time required to transport a unit of straw is factored, Figure 53 is produced. It highlights the specific pressure losses which occur to deliver a kilogram of straw in one second. For 30% slurries, but not for lower concentrations, the losses remain similar with increased flow rate. Thus doubling the flow rate in a pipeline of a given diameter is approximately as efficient as installing a second pipeline with the slower flow rate.

As previously demonstrated, when increasing velocity to gain additional capacity, overall pumping requirements per unit straw is still escalating. Increasing the diameter of a pipeline to double its cross sectional area would decrease surface friction. However, larger diameters have been found to increase critical velocity (Brebner 1964), the minimum flow rate required to avoid congestion. The effect of pipeline diameter has not been evaluated in this study, but is critical in understanding the feasibility of biomass pipelines. Another important consideration which has not been taken into account here is the impact of erosion at higher flow rates.

**Average particle size sample as classified in Table 1*

2.6. Effective Viscosity

Although this study does not quantify the impact of pumping straw slurry through larger diameter pipelines, some insights have been gained. By using Equation 20 and Equation 21, an effective viscosity can be calculated. As shown in Figure 54, the slurries do appear to exhibit shear thinning properties, as the effective viscosity decreases with increased velocity. As these values do fall below zero with certain slurries, it is strongly emphasized that is not the actual viscosity. Rather this calculated data, tabulated in Table 13 through Table 25, is only provided as a means to calculate initial approximations of the pumping requirements of larger scale system.

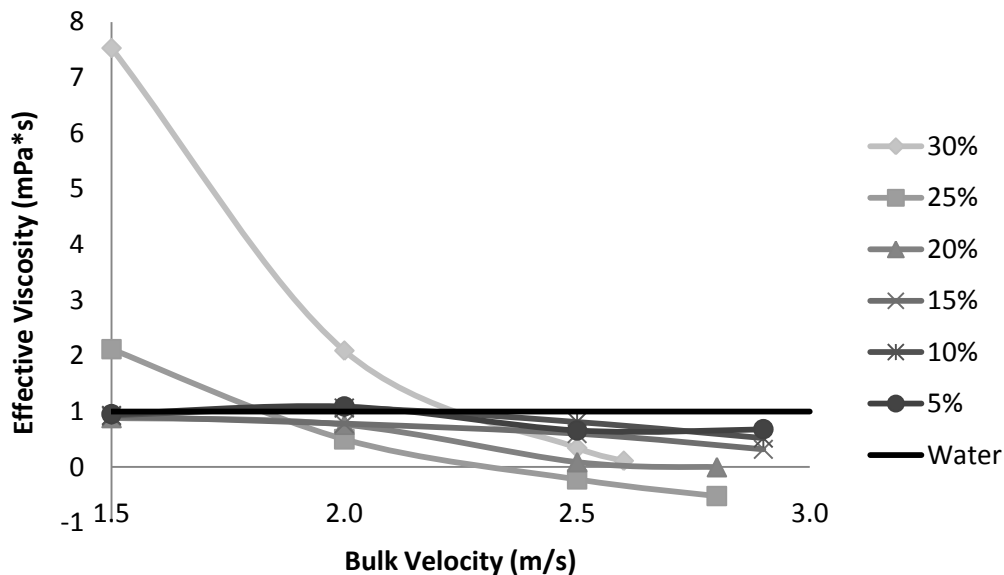


Figure 54: Effective viscosity of *1/8" average particle size straw slurry

2.7. Uncertainty Analysis

The replication of tests in this study was conducted to address the uncertainty of the pressure drop gradient results. While relatively constant flow rate could be maintained, the repeatability was reduced by the uncertainty in pressure measurements. The resolution of the pressure data was 0.5 kPa (or 0.06 kPa/m), while the pressure gauge could oscillate by up to 1 kPa (or 0.12 kPa/m).

The trend between coefficients of determination using a power law approximation itemized in Table 12 and concentration highlights these uncertainties. A coefficient of determination (R^2) is a measure between 0 and 1, of the ability for the line of fit to predict the data, with a value of 1 representing a perfect fit. Lower concentrations were better fitted to a pressure drop gradient, than that of higher concentrations as seen in Figure 55. Smooth downward parabolas are created with more dilute slurries, with a sharper drop off once the maximum concentrations are reached.

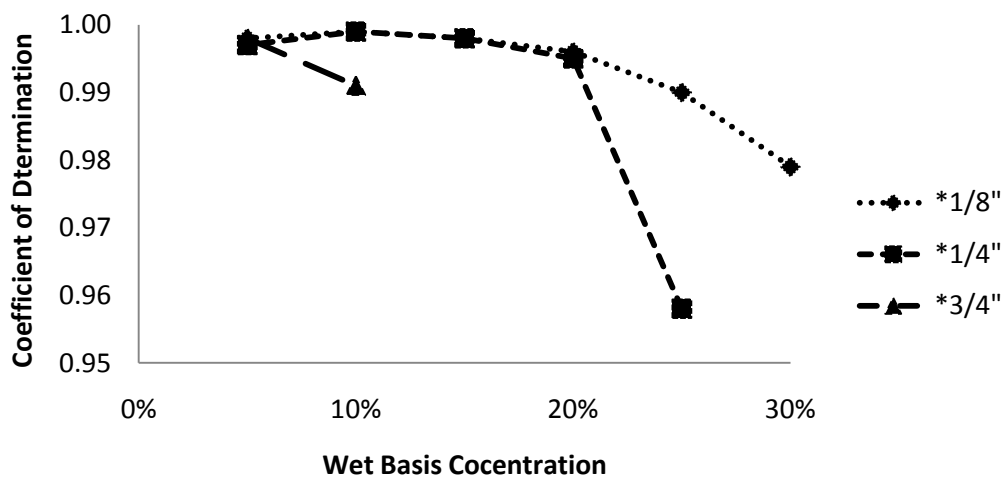


Figure 55: Coefficient of determination by wet basis concentration

**Average particle size sample as classified in Table 1*

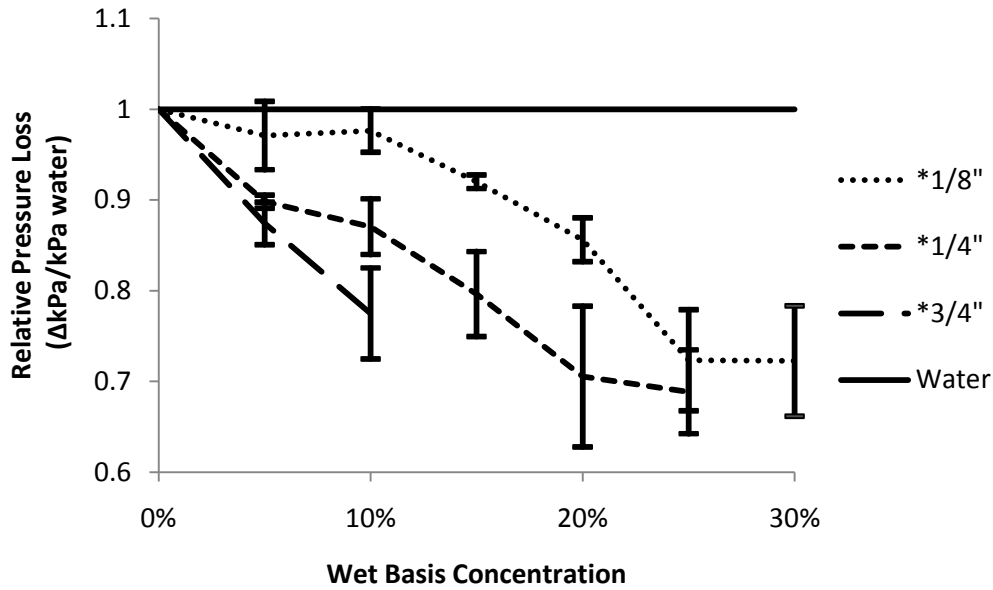


Figure 56: Relative pressure drop 95% confidence interval at 3 m/s

This may be due to the presence of plugs in the flow, which drastically alter the characteristics of the slurry. Minor changes in concentrations, flow rates or particle sizes would have marked differences in pressure losses. Lower concentrations without plugs, or that have plugs broken up at lower flow rates, experience more consistent pressure losses. Regardless, the coefficients of determination remained high, with all slurries above 0.95.

The implications of these uncertainties on the confidence intervals were more complex. For reasons of clarity, confidence intervals were not included in previous sections, but are compared in Figure 56. The pressure loss of each slurry is graphed, relative to water. All data is extrapolated with the power law approximations in Table 12, to 3 m/s when plugs in the flow are largely torn apart, and a 95% confidence interval shown for comparison.



Figure 57: A mix of straw reveals green and golden material

With the exception of dilute (5% and 10%) 1/8" slurries, all have pressure losses below that of water at a 95% confidence interval. Moderate concentrations of a particular particle size measure a more distinct pressure drop, while higher and lower mixtures are more similar. The trend of larger particles dampening more turbulence is strongly evident.

The slurries produced for these experiments introduce further uncertainties as well. While all feedstock was harvested outside Westlock Alberta in 2009 and delivered the first half of 2010, there may be a measureable natural variability across even a single harvest. The properties of wheat straw changes while in storage (Sebastian et al., 2006). Bales piled under large stacks are stored under compression. Exterior bales are exposed to ambient air. A large mix of straw in Figure 57 reveals material that can appear either fresh and green, or dry and golden.

Furthermore, process, measurement and calculation of large volumes of material will have contributed additional errors. Uncertainties in the size distribution of straw would occur from both the grinding and screen shaking process. The weighing of large volumes of material, in small containers can propagate measurement errors. Material splashing out from the mixing tank also distorts concentrations. The calculated moisture content and particle density of straw over time is approximate, but the error was limited by allowing the straw to approach saturation after 24 hours, avoiding a period of rapid water absorption. The mixture of straw may not be completely uniform throughout the slurry, as some bundles of straw can entangle with each other, or momentarily get interrupted by fittings. Other sources of uncertainty were discussed with the design considerations in Chapter 3.

Chapter V:

Conclusions

1. Particle Characterization

Determination of particle characteristics is critical for pipeline transport of biomass to a biorefinery. In this study physical characterization were carried out as the first step towards understanding pipeline transport of biomass. The physical characteristics of chopped wheat straw within a mixing tank were determined. Larger particles were found to be able to absorb an increased amount of the carrier fluid. Particles of 3/4" size reached $79.5 \pm 0.3\%$ saturated moisture content after 2 days of mixing, whereas smaller 1/8" size particles achieved a lower moisture content level of $78.5 \pm 1\%$ after 4 days. The resolution of the particle density experiments however, could not measure the subtle difference between the particle sizes. The saturation levels of the smaller and larger particles are similar at $1,060 \pm 9 \text{ kg/m}^3$ and $1,060 \pm 5 \text{ kg/m}^3$ respectively, after only 24 hours within the mixing tank.

Time and particle size were factors found to have an influence on the uncertainty level in this study. Impurities within the carrier fluid increase over time and settle upon straw surfaces after straining. This is an obstacle in achieving surface dry conditions of the straw, necessary to properly measure internal moisture content and particle density. Smaller particles compound this problem by having increased surface area which allow more fine impurities to be released into the carrier fluid, and additional area for surface moisture to reside on. The

significance of excess surface moisture on characterization calculations, are two orders of magnitude greater for moisture content, than it is for particle density.

2. Hydraulic-transport Design

The laboratory scale pipeline loop designed to operate with wheat straw biomass slurries was significantly modified. Carbon steel was used for the test sections, as it is a typical material for industrial pipelines. A 2" diameter was selected based on the limitation of the available space. Unique considerations of a laboratory system included thermal heat and air absorption, as well as the need for decongestion. The results from previous studies completed on woodchip slurries were used to estimate the power requirements of this system.

Ultimately the design of the pipeline loop was conservative. Straw slurries proved to have lower head losses than what was predicted from woodchip slurry formulas. The goal of achieving a 30% maximum concentration was reached for 1/8" particles, while 1/4" and 3/4" particles attained 25% and 10% concentrations respectively. The instrumentation noise was successfully reduced, and air content could be dissipated from the system. Both the magnitude and uncertainty of the measurements were improved.

3. Hydraulic-transport Characterization

The principle aim of this study was to characterize the hydraulic pipeline transport requirements of wheat straw biomass. The direct measure of this was in the form of pressure loss over a length of straight pipe. The effect of different particle sizes and concentrations were examined; three trials were conducted for each slurry make up.

At high concentrations, the straw particles mesh together to form plugs. Surrounding these plugs is highly turbulent annular flow, which produces high the pressure losses. By increasing the flow rate, the plugs are gradually torn apart, and individual particles become freely suspended in the carrier fluid. The long fiber like particles can then dampen turbulence, lowering pressure losses below that of pure water at the same flow rate. This is depicted in Figure 58, where the maximum flowable concentration of particle size slurry is compared.

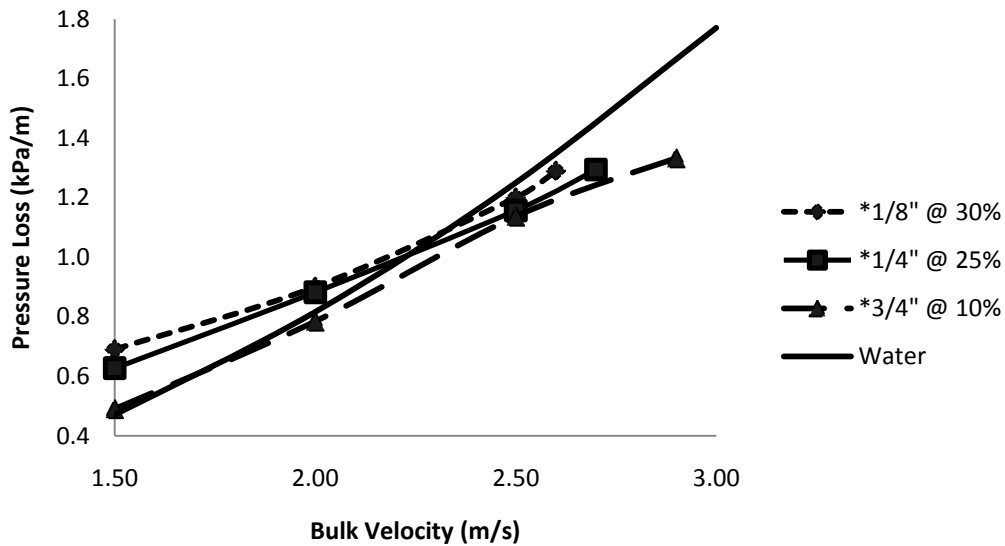


Figure 58: Pressure loss of maximum flowable concentrations

*Average particle size sample as classified in Table 1

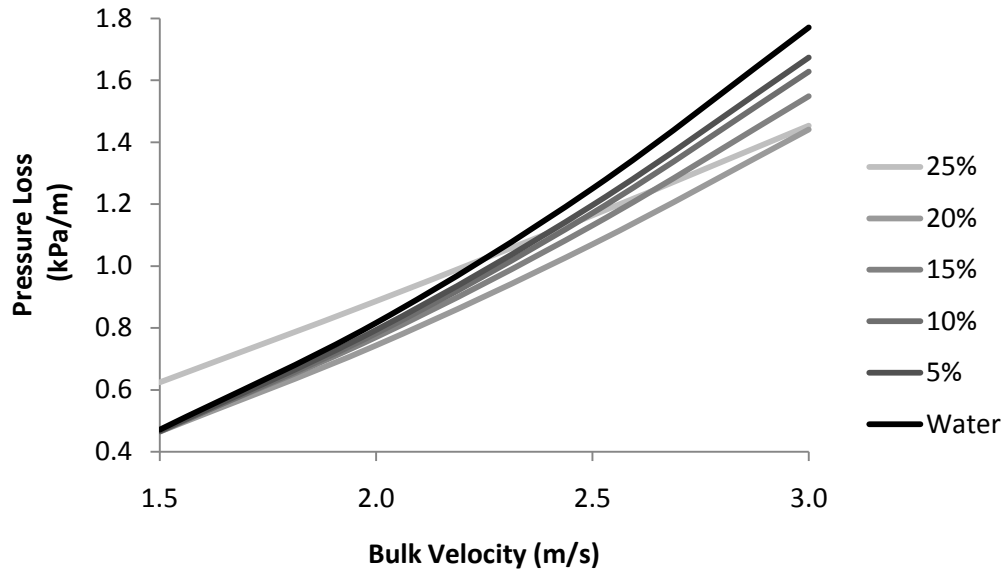


Figure 59: Pressure loss of *1/4" particle size slurry

Once the bulk velocity reaches 3m/s, none of the slurries examined would form plugs in the flow. At this flow rate, a comparison can be made between different concentrations of freely suspended particles. It can be seen in Figure 59 that higher concentrations exhibit lower pressure losses. This is due to the presence of more fibers which can further dampen turbulence.

**Average particle size sample as classified in Table 1*

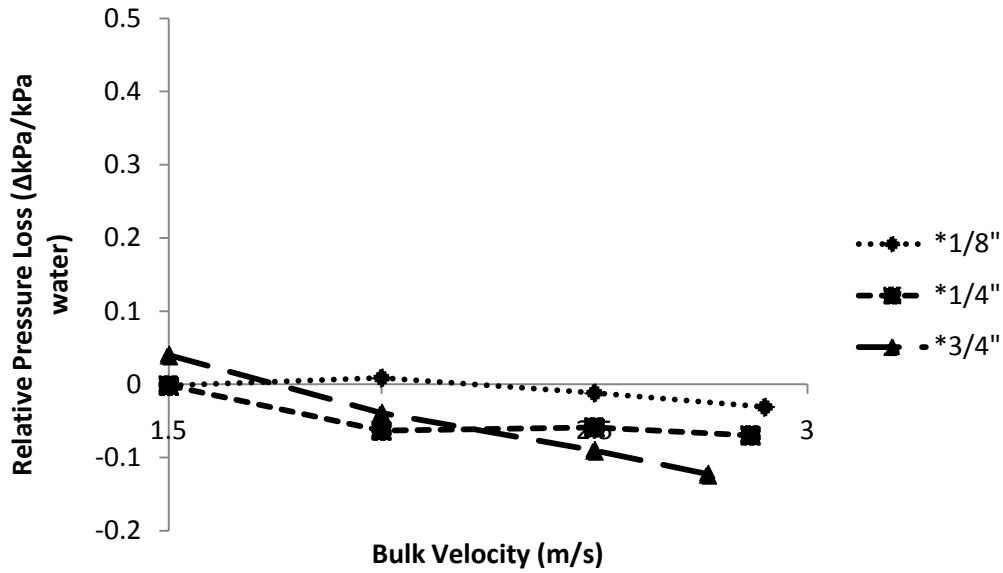


Figure 60: Pressure loss of 10% concentration slurry

The effect of particle size on pressure loss was more subtle. When the relative pressure loss, as compared to water, is compared in Figure 60, these differences in pressure losses are magnified. It can be seen that freely suspended larger particle sizes have lower pressure losses. Longer fibers have increased ability to dampen turbulence at higher flow rates, but are more susceptible to forming plugs at low velocities.

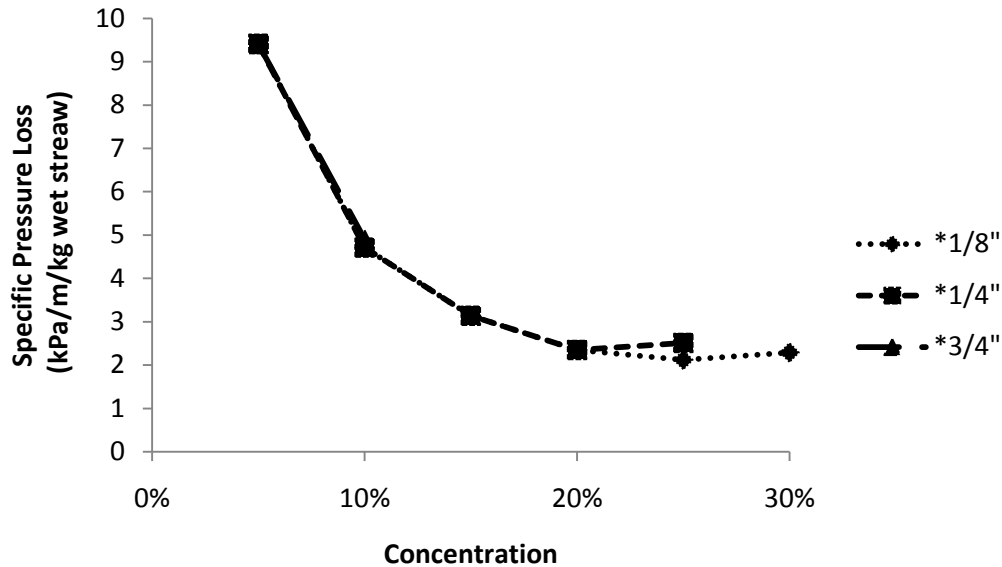


Figure 61: Pumping requirements of 1.5 m/s slurry

When taking all of these trends into account, it was determined that slurry concentrations that fall just below the maximum, would yield the lowest pumping requirements. In Figure 61 it is seen that 1/8" particles in a 25% concentration wet basis slurry at 1.5 m/s was the most efficient means to pump straw. This is due to the fact that 1.5 m/s is the minimum bulk velocity before particles fall out of suspension. 1/8" particle size slurries are able to flow at higher concentrations, than slurries of larger particle sizes. The 25% concentration is transports solid material more rapidly than more dilute slurries, while the addition of more straw would decrease efficiency by with the formation of plugs in the flow.

Table 26: Optimum conditions to minimize specific pumping requirements

Operating Variable	Optimum Condition	Physical Impact	Capital Impact	Operating Impact
Flow Rate	Minimum (1.5m/s)	Minimum erosion	Thinner pipe wall requirements	Lower maintenance
		Minimum pressure loss	Fewer/Smaller pumping stations	Lower power consumption
Concentration	5% Below maximum (25%)	Lower carrier fluid volume	Lower pipeline capacity	Lower water processing requirements
		Higher concentration	Lower pipeline capacity	Lower power consumption
Particle size	Minimum (1/8")	Higher concentration	Lower pipeline capacity	Lower power consumption

Table 26 summarizes the set of optimum conditions to minimize specific pumping requirements, as well as residual capital and operating cost implications. However, to minimize overall financial costs and environmental impact of a wheat straw slurry pipeline, a balance between several factors must be achieved. Processing feedstock further than is currently done, to reduce the average particle size, could minimize the volume of carrier fluid that must be transported. Increasing the carrier fluid above the minimum, could prevent plugs in the flow, to reduce friction losses. In addition, longer particles further suppress turbulence, to frictional drag losses.

4. Recommendations for Future Work

The following are recommendations for future work:

- Additional research could be conducted to further understand the slurry preparation process. The moisture content of wheat straw is known to change during storage (Russell and Buxton, 1985). The effect of these initial conditions on the rate of water absorption could impact the required slurry preparation time prior to being introduced into the pipeline.
- To further define the physical properties of wheat straw, samples could be placed under a scanning electron microscope (SEM). Average particle sizes may be determined with improved precision, as can particle size gradients within the samples used. The porosity of wheat straw may also be observed.
- An optimization of operational variables was beyond the scope of this project. An industrial scale system would be substantially larger than the 2" diameter pipeline loop used in these experiments. Slurries with larger particle sizes would be flowable at greater concentrations, and further suppress turbulence to reduce drag. It is not evident from these tests, to what degree the drag reducing effectiveness of wheat straw is improved at larger scales. Examination of larger diameter pipelines is essential to understand the implications of operating a full scale commercial wheat straw biomass pipeline.

- The change of properties of the lignocellulosic biomass slurry within the system will need to be studied further. Degradation of the physical properties will occur over time to alter turbulence suppression. The chemical makeup of the slurry over time can be analyzed, to develop a greater understanding of the impact of pipelining materials on the potential end uses. In particular, sugar losses into the carrier fluid, changes in the digestibility of lignocellulosic biomass and its effect on the cellulosic ethanol production.
- The effect of additives within the system would alter the results of the study. Polymer powders or gels could further reduce pressure losses, to minimize pumping requirements. Additives in the slurry to induce fermentation or saccharification (process of breaking down cellulose) would reduce the need for processing of the delivered material.
- These experiments will also be completed on other biomass materials as well. Woodchip slurries will be re-evaluated, to evaluate repeatability of previous results. Switch grass and corn stover are other abundant potential sources of biomass which are of interest to this project. The successful commissioning of this pipeline loop will serve as a platform for ongoing research.

Bibliography

ASABE. (2008). *S358.2: Moisture measurement-forages*. St. Joseph, MI: American Society of Agricultural and Biological Engineers.

ASABE. (2007). *S424.1: Method of determining and expressing particle size of chopped forage materials by screening*. St. Joseph, MI: American Society of Agricultural and Biological Engineers.

ASTM. (2007). *C125-07: Standard terminology relating to concrete and concrete aggregates*. West Conshohocken, PA.: ASTM International.

ASTM. (2004). *C566-97: Standard test for total evaporable moisture content of aggregate by drying*. West Conshohocken, PA: ASTM International.

Banerjee, S., Mudliar, S., Sen, R., Giri, B., Satpute, D., Chakrabarti, T., et al. (2010). Commercializing lignocellulosic bioethanol: technology bottlenecks and possible remedies. *Biofuels, Bioproducts & Biorefining* , 77-93.

Bernal, J. A. (2004). *Microbubble Drag Reduction Phenomenon Study in a Channel Flow*. College Station: Texas A&M University.

Bi, Y., Gao, C., Wang, Y., & Li, B. (2009). Estimation of straw resources in China. *Transactions of the Chinese Society of Agricultural Engineering* , 211-217.

BM&M Screening Solutions. (2007). *Chip Classifiers*. Retrieved April 20, 2010, from BM&M Website: <http://www.bmandm.com/c-class.htm>

Brebner, A. (1964). On the pumping of wood chips through a four-inch aluminum pipe-line. *The Canadian Journal of Chemical Engineering* , 139-142.

Canadian Renewable Fuels Association. (2009, September). *Industry Information*. Retrieved August 1, 2010, from <http://www.greenfuels.org/lists.php>

Ceccio, S. L. (2010). Frictional Drag Reduction of External Flows with Bubble and Gas Injection. *Annual Review of Fluid Mechanics* , 183-203.

Chum, H., & Overend, R. (2001). Biomass and Renewable Fuels. *Fuel Processing Technology* , 187-195.

Cocirla, E. O. (2007). *Wheat straw slurry viscosity*. Oakville, ON: Can-Am Instruments.

Desseault Farms. (2009). Westlock, AB.

Elliot, D. R., & Montmorency, W. H. (1963). *The transport of pulpwood chips in pipelines*. Montreal, QC: Pulp and Paper Research Institute of Canada.

Energy Manager Training. (n.d.). *Fan Engineering*. Retrieved August 31, 2010, from Energy Manager Training Web Site: <http://www.emt-india.net/Documents/CS19Oct09/Equipment/Fans/Fans-2.pdf>

Fabco Plastics. (2006). *Contact Us*. Retrieved August 9, 2010, from Fabco Plastics Website: <http://www.fabcoplastics.com/contact.html>

Farrell, A., Plevin, R., Turner, B., Jones, A., O'Hare, M., & Kammen, D. (2006). Ethanol can contribute to energy and environmental goals. *Science* , 506-508.

Faulkner, B. (2008). Retrieved from <http://www.uofaweb.ualberta.ca/mece/nav03.cfm?nav03=93505&nav02=41013&nav01=24236&CFNoCache=TRUE>

Geller, H., Schaeffer, R., Szklo, A., & Tolmasquim, M. (2004). Policies for advancing energy efficiency and renewable energy use in Brazil. *Energy Policy* , 1437-1450.

Ghafoori, E., Flynn, P. C., & Feddes, J. J. (2007). Pipeline vs. truck transportation of beef cattle manure. *Biomass and Bioenergy* , 168-175.

Glendale Community College. (n.d.). *Earth Science Image Archive*. Retrieved August 9, 2010, from Glendale Community College Website: <http://gccweb.gccaz.edu/earthsci/imagearchive/asbestos.htm>

Gnansounou, E. (2010). Production and use of lignocellulosic bioethanol in Europe: Current situation and perspectives. *Bioresource Technology* , 4842-4850.

Gnansounou, E., & Dauriat, A. (2010). Techno-economic analysis of lignocellulosic ethanol: A review. *Bioresource Technology* , 4980-4991.

Godwin Pumps. (2007). *CD80M Dri-Prime Pump*. Retrieved April 20, 2010, from Godwin Website: http://www.godwinpumps.com/_CD_Pages/cd80m.html

Green Line Hose & Fittings. (2009). *Locations*. Retrieved August 9, 2010, from Green Line Website: <http://www.greenlinehose.com/locations.htm>

GS Caltex. (2005). *About GS Caltex: Overview*. Retrieved April 19, 2010, from http://www.gscaltex.com/About/gs_Overview.asp

Hajimiragha, A., Caizares, C. A., Fowler, M. W., & Elkamel, A. (2010). Optimal Transition to Plug-In Hybrid Electric Vehicles in Ontario, Canada, Considering the Electricity-Grid Limitations. *IEEE Transactions on Industrial Electronics* , 690-701.

Hunt, W. (1976). Friction factors for mixtures of wood chips and water flowing in pipelines. *Fourth International Conference on the Hydraulic Transport of Solids in Pipes*. Banff, AB.

Jubran, B. A., Zurigat, Y. H., & Goosen, M. F. (2005). Drag Reducing Agents in Multiphase Flow Pipelines: Recent Trends and Future Needs. *Petroleum Science and Technology* , 1403-1424.

Kato, H., & Mizunuma, H. (1983). Frictional Resistance in Fiber Suspensions. *Bulletin of the Japan Society Mechanical Engineers* , 231-238.

Kazi, S. N., Duffy, G. G., & Chen, X. D. (1999). Heat Transfer in the Drag Reducing Regime of Wood Pulp Fibre Suspensions. *Chemical Engineering Journal* , 247-253.

Kumar, A., & Flynn, P. C. (2006). Uptake of fluids by boreal wood chips: implications for bioenergy. *Fuel Processing Technology* , 605-608.

Kumar, A., Cameron, J. B., & Flynn, P. C. (2003). Biomass power cost and optimum plant size in western Canada. *Biomass and Bioenergy* , 445-464.

Kumar, A., Cameron, J. B., & Flynn, P. C. (2005). Large-scale ethanol fermentation through pipeline. *Applied Biochemistry and Biotechnology* , 47-54.

Kumar, A., Cameron, J. B., & Flynn, P. C. (2005). Pipeline transport and simultaneous saccharification of corn stover. *Bioresource Technology* , 819-829.

Kumar, A., Cameron, J. B., & Flynn, P. C. (2004). Pipeline transportation of biomass. *Applied Biochemistry and Biotechnology* , 24-39.

Lee, P. F., & Duffy, G. G. (1976). Relationship Between Velocity Profiles and Drag Reduction in Turbulent Fiber Suspension Flow. *AIChE Journal* , 750-753.

Libecap, G. (2003). Agricultural programs with dubious environmental benefits: the political economy of ethanol. *Agricultural policy and the environment* , 89-106.

Lightnin Mixers. (2010). *Contact Us*. Retrieved August 9, 2010, from Lightnin Website: <http://www.lightninmixers.com/contact-us/how-buy>

Liu, H. (2003). Freight Pipelines: An Overview. *Proceedings of International Conference on Pipeline Engineering and Construction* (pp. 1603-1614). Baltimore, MD: American Society of Civil Engineers.

Luk, J. M., Fernandez, H., & Kumar, A. (2009). Characterization of biomass material during pipeline transport. *CSBE/SCGAB Technical Conference*. Brudenell River, PEI: The Canadian Society for Bioengineering.

Mohamadabadi, H. S. (2009). *Characterization and Pipelining of Biomass Slurries*. Edmonton: University of Alberta.

Mohanaragam, K., Cheun, S., Tu, J., & Chen, L. (2009). Numerical simulation of micro-bubble drag reduction using population balance model. *Ocean Engineering* , 863-872.

Murai, Y., Oiwa, H., & Takeda, Y. (2008). Frictional drag reduction in bubbly Couette-Taylor flow. *Physics of Fluids* , 1-12.

National Energy Board. (2006). *Emerging Technologies in Electricity Generation*. Calgary, AB: The Publications Office National Energy Board.

Newitt, D. M., Richardson, J. F., Abbot, M., & Turtle, R. B. (1955). Hydraulic conveying of solids in horizontal pipes. *Transactions fo the Institution of Chemical Engineers*. London, UK.

Newport Scientific. (2006). *Contact Newport Scientific*. Retrieved August 9, 2010, from Newport Scientific, Inc: <http://www.newport-scientific.com/contact/contact-newport-scientific.php>

Omega Engineering. (2002). *Contact Us*. Retrieved August 9, 2010, from Omega Website: http://www.omega.ca/cservice/contactus_eng.asp

Oosterveer, P., & Mol, P. J. (2010). Biofuels, trade and Sustainability: a review of perspectives for developing countries. *Biofuels, Bioproducts & Biorefining* , 66-76.

Procaccia, I., & L'vov, V. S. (2008). Theory of drag reduction by polymers in wall-bounded turbulence. *Reviews of Modern Physics* , 225-247.

Pryfogle, P. (2009). Biomass Properties for Optimizing Feedstock Handling Operations. *Bioenergy Engineering '09*. Belluevue: American Society of Agricultural and Biological Engineers.

Reddy, G. V., & Singh, R. P. (1985). Drag reduction effectiveness and shear stability of polymer-polymer and polymer-fibre mixtures in recirculatory turbulent flow of water. *Rheologica Acta* , 296-311.

Retsch. (2007). *Cutting Mill SM 100*. Retrieved April 20, 2010, from Retsch Website: <http://www.retsch.com/products/milling/cutting-mills/sm-100/>

Russell, J. R., & Buxton, D. R. (1985). Storage of large round bales of hay harvested at different moisture concentrations and treated with sodium diacetate and/or covered with plastic. *Animal Feed Science and Technology* , 69-81.

Searcy, E., Flynn, P. C., Ghafoori, E., & Kumar, A. (2007). The relative cost of biomass energy transport. *Applied Biochemistry and Biotechnology* , 639-652.

Sebastian, A., Madsen, A. M., Martensson, L., Pomorska, D., & Larsson, L. (2006). ASSESSMENT OF MICROBIAL EXPOSURE RISKS FROM HANDLING. *Annals of Agricultural and Environmental Medicine* , 139-145.

Shook, C. A., Daniel, S. M., Scott, J. A., & Holgate, J. P. (1968). Flow of suspensions of solids in pipelines, Part 2: two mechanisms of particle suspension. *Canadian Journal of Chemical Engineering* , 238-244.

Singh, A., Pant, D., Korres, N., Nizami, A.-S., Prasad, S., & Murphy, J. D. (2010). Key issues in life cycle assessment of ethanol production from lignocellulosic biomass: Challenges and perspectives. *Bioresource Technology* , 5003-5012.

The Engineering ToolBox. (2005). *Minor loss coefficients for common used components in pipe and tube systems*. Retrieved April 20, 2010, from http://www.engineeringtoolbox.com/minor-loss-coefficients-pipes-d_626.html

The Fiber Depot. (2001). *Multifilament Nylon*. Retrieved August 9, 2010, from The Fiber Depot Website: http://www.thefiberdepot.com/multifilament_nylon_1.htm

U-Haul. (2007). *Ice Will Win The War?* Retrieved August 9, 2010, from U Haul Website: http://www.uhaul.com/supergraphics/enhanced.aspx?site_id=169&sort_order=3

Vaseleski, R. C., & Metzner, A. B. (1974). Drag Reduction in Turbulent Flow of Fiber Suspensions. *AIChE Journal* , 301-306.

Viatran. (n.d.). *Contact Us*. Retrieved August 9, 2010, from Viatran Website:
<http://www.viatran.com/>

Western Gauge and Instruments. (2005). *Pressure Gauges*. Retrieved July 1, 2010, from http://www.wgilt.com/pressure_gauges.asp

Westlund. (2004). *Our Locations*. Retrieved August 9, 2010, from Westlund Website: http://www.westlund.ca/en_locations/branches.htm

White, F. (2006). *Fluid Mechanics. 6th ed.* Boston, MA: McGraw-Hill Higher Education.

WIKA Instruments. (2010). *Differential Pressure Gauges*. Retrieved July 1, 2010, from Wika Instruments Website:
http://www.wika.ca/700_0X_en_us.WIKA?ActiveID=23777

Wilson, K. C., Sanders, R. S., Gillies, R. G., & Shook, C. A. (2010). Verification of the near-wall model for slurry flow. *Powder Technology*, 247-253.

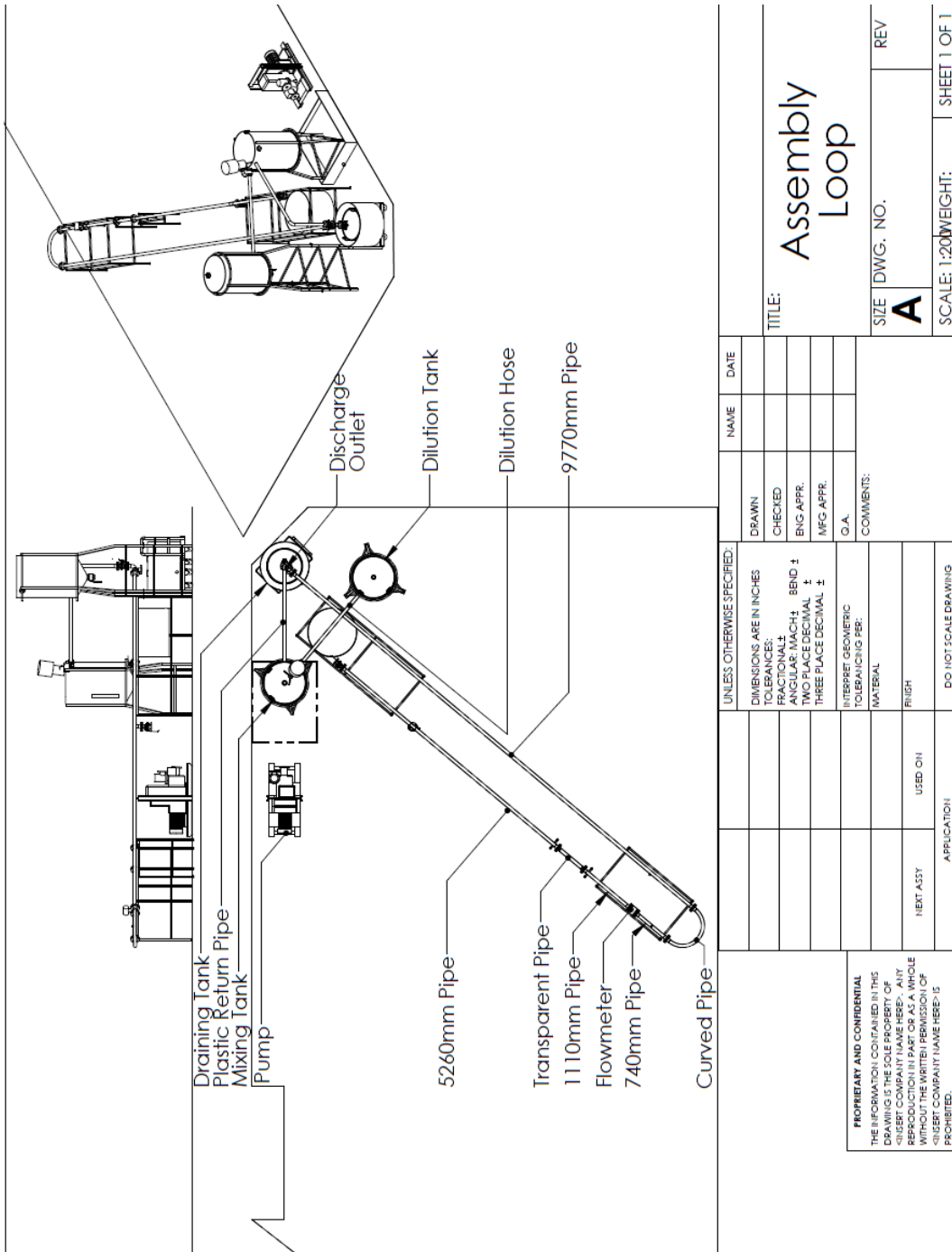
Zeebest Plastics. (2004). *Contact Information*. Retrieved August 9, 2010, from Zeebest Plastics Website: <http://www.zeebest.com/>

Appendix: Detailed Design Drawings

Contents:

- Assembly of loop
- 5260 mm pipe section
- 1110 mm pipe section
- 740 mm pipe section
- 9770 mm pipe section
- Discharge outlet
- Return Line
- Mixing tank
- Discharge tank stand
- Water bath tank

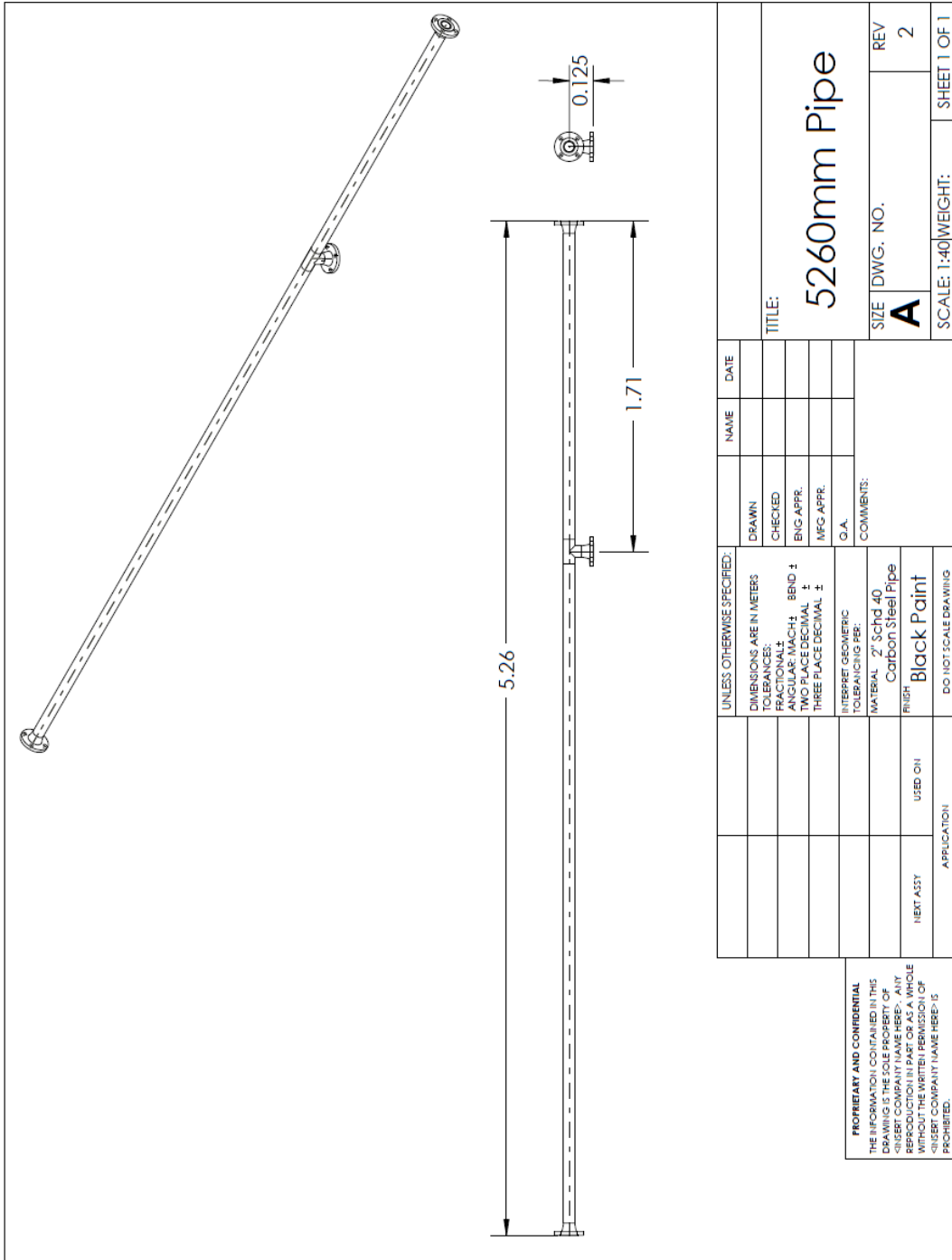
Figure 62: Assembly of loop



UNLESS OTHERWISE SPECIFIED:		NAME	DATE
DIMENSIONS ARE IN INCHES		DRAWN	
TOLERANCES:		CHECKED	
FRACTIONAL ±		ENG. APPR.	
ANGULAR: MACH ± BEND ±		MFG. APPR.	
TWO PLACE DECIMAL ±		G.A.	
THREE PLACE DECIMAL ±		COMMENTS:	
INTERPRET GEOMETRIC TOLERANCING PER:			
MATERIAL			
FINISH			
NEXT ASSY	USED ON		
APPLICATION			

<p>PROPRIETARY AND CONFIDENTIAL THE INFORMATION CONTAINED IN THIS DRAWING IS THE SOLE PROPERTY OF [COMPANY NAME]. IT IS TO BE USED ONLY FOR THE PROJECT AND NOT BE REPRODUCED IN PART OR AS A WHOLE WITHOUT THE WRITTEN PERMISSION OF [COMPANY NAME]. *INSERT COMPANY NAME HERE* IS PROHIBITED.</p>		
<p>TITLE: Assembly Loop</p>		
<p>SIZE: A</p>	<p>DWG. NO.:</p>	<p>REV:</p>
<p>SCALE: 1:200</p>		<p>WEIGHT: SHEET 1 OF 1</p>

Figure 63: 5260 mm pipe section



PROPRIETARY AND CONFIDENTIAL
 THE INFORMATION CONTAINED IN THIS DRAWING IS THE PROPERTY OF [INSERT COMPANY NAME HERE]. ANY REPRODUCTION IN PART OR AS A WHOLE WITHOUT THE WRITTEN PERMISSION OF [INSERT COMPANY NAME HERE] IS PROHIBITED.

Figure 64: 1110 mm pipe section

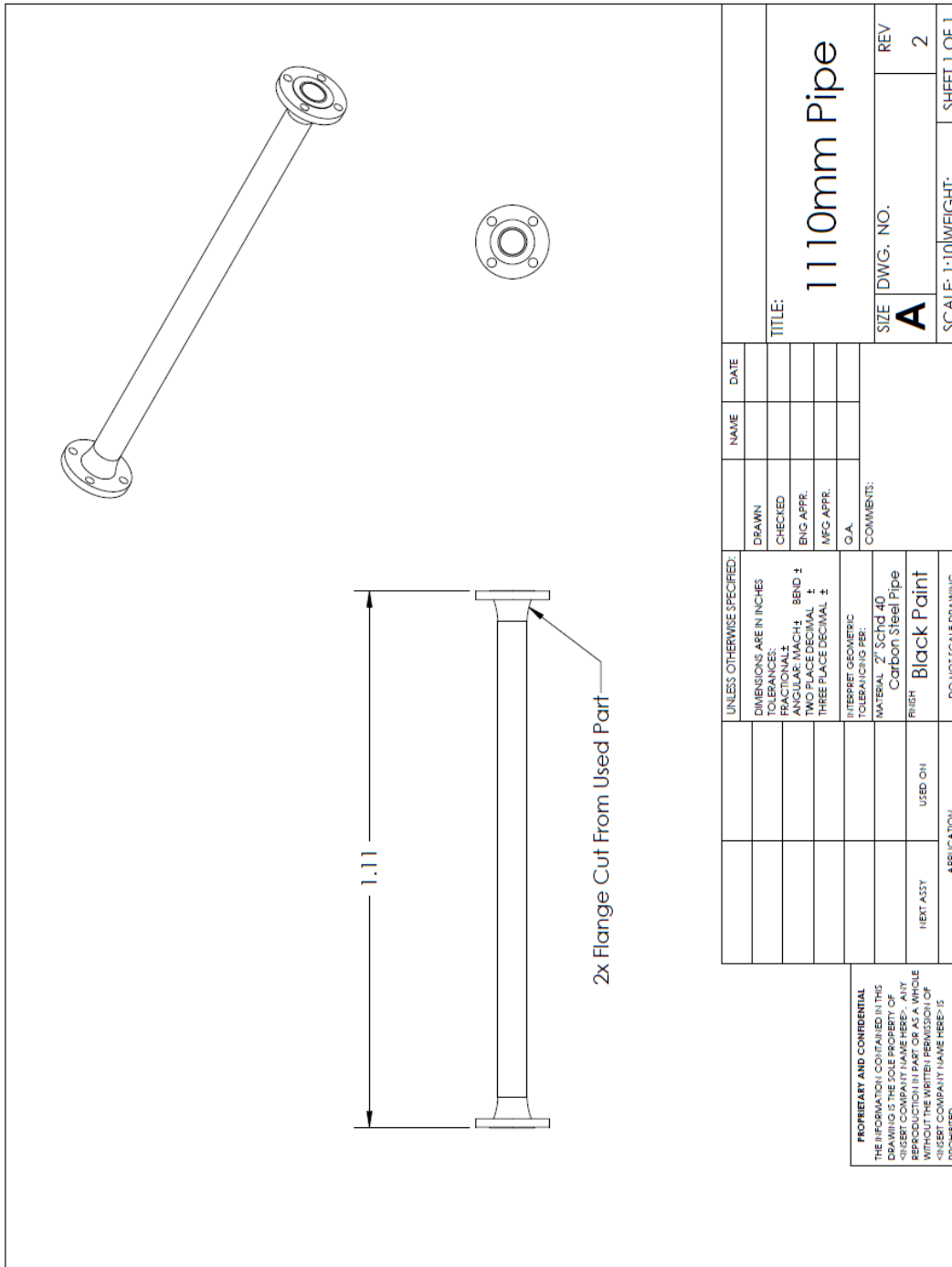


Figure 65: 740 mm pipe section

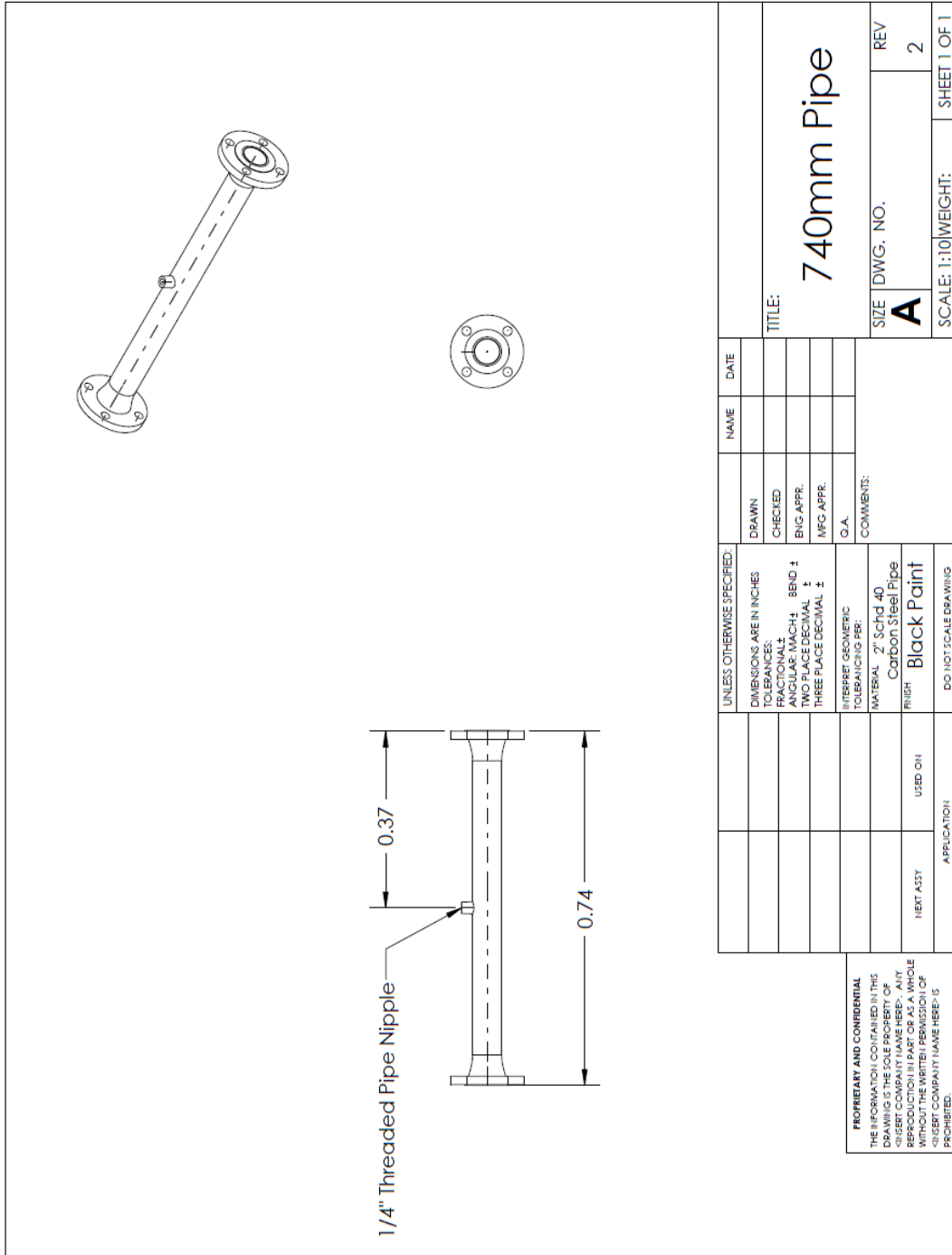


Figure 66: 9770 mm pipe section

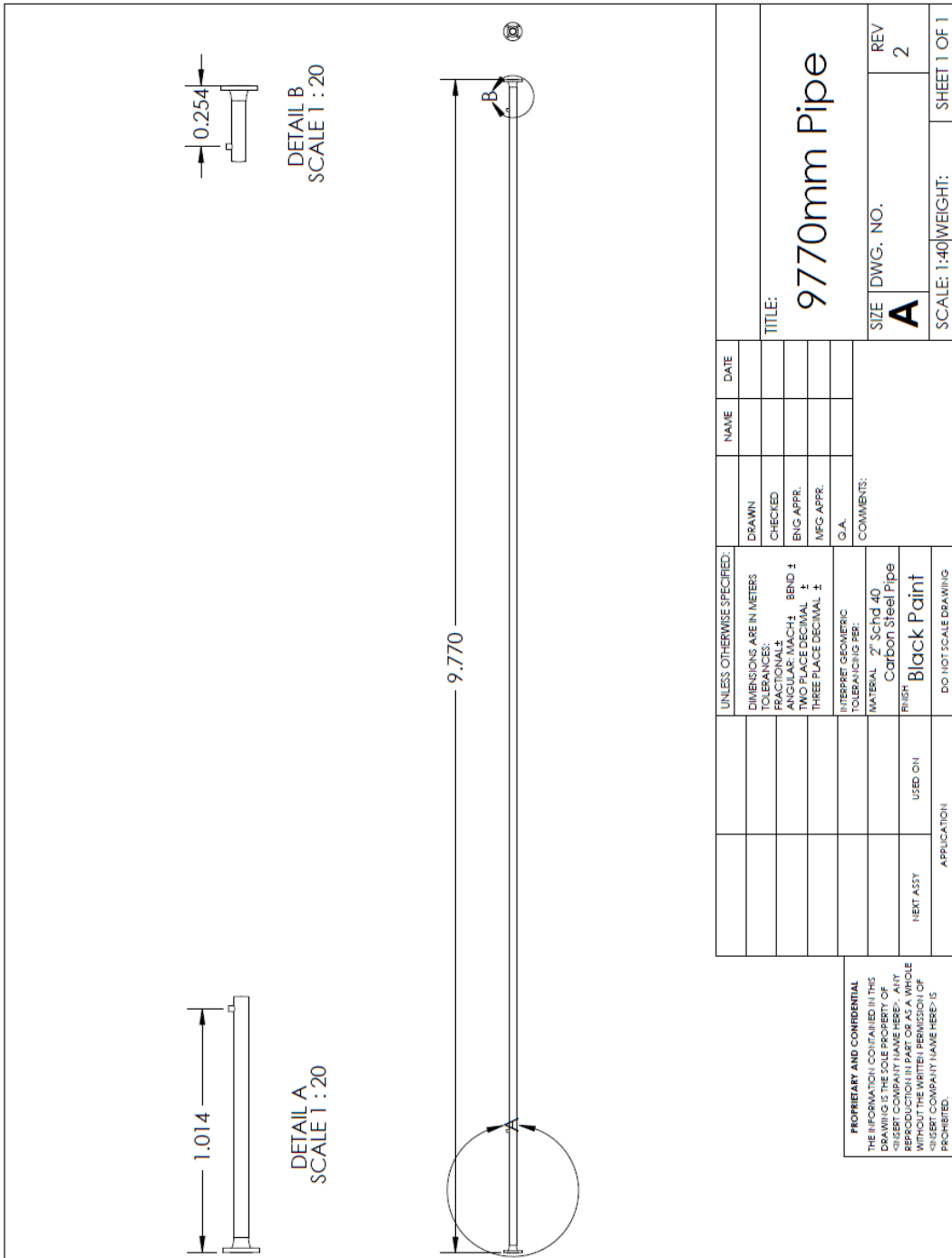
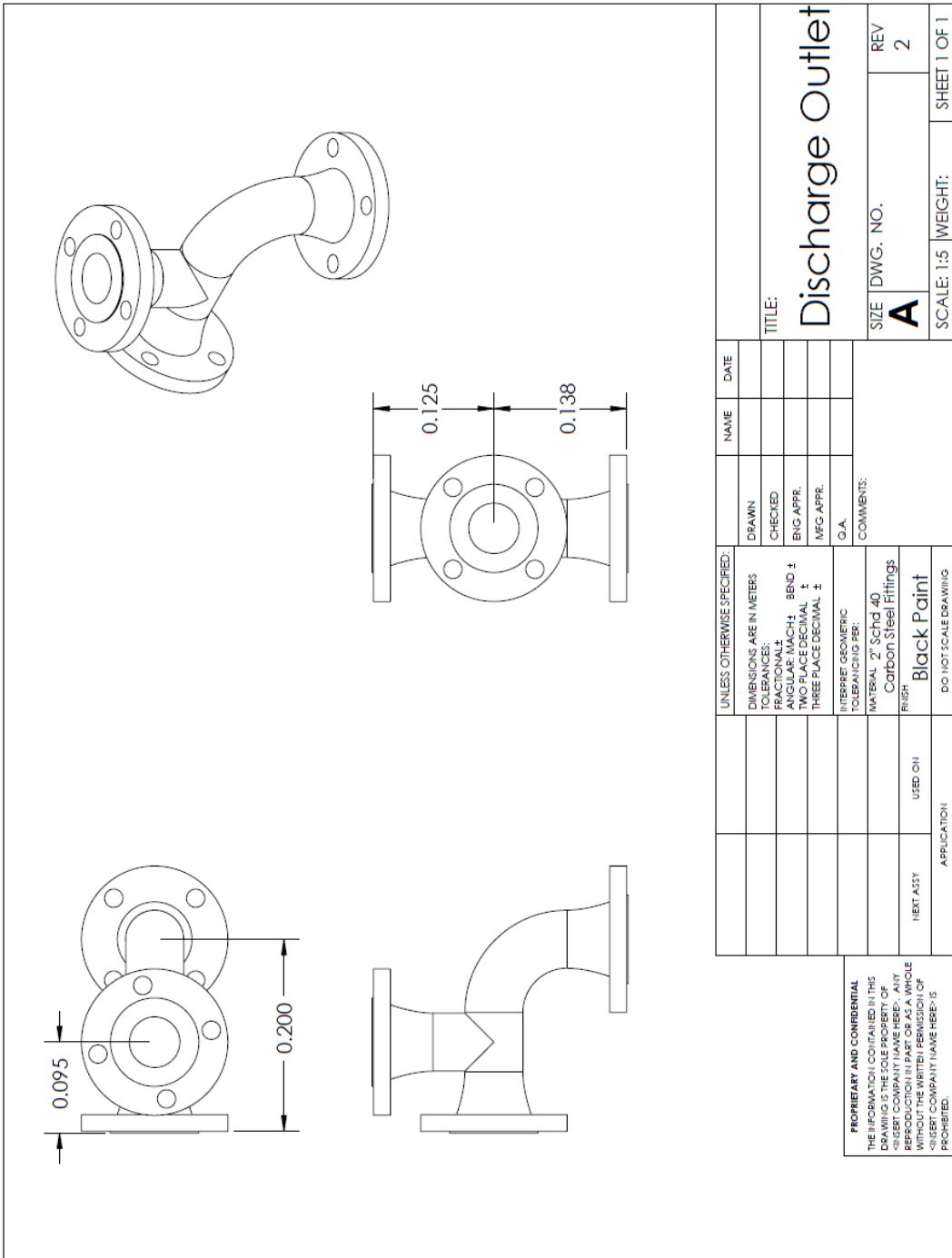


Figure 67: Discharge outlet



UNLESS OTHERWISE SPECIFIED:		NAME	DATE
DIMENSIONS ARE IN METERS	DRAWN		
TOLERANCES:	CHECKED		
FRACTIONAL: ±	ENG. APPR.		
ANGULAR: MACH: ± BEND: ±	MFG. APPR.		
TWO PLACE DECIMAL: ±			
THREE PLACE DECIMAL: ±			
INTERPRET GEOMETRIC TOLERANCES PER:	COMMENTS:		
	MATERIAL: 2" Schd 40 Carbon Steel Fittings		
	FINISH: Black Paint		
	DO NOT SCALE DRAWING		
	APPLICATION:		
	NEXT ASSY	USED ON	
<p>PROPRIETARY AND CONFIDENTIAL</p> <p>THE INFORMATION CONTAINED IN THIS DRAWING IS THE PROPERTY OF [INSERT COMPANY NAME HERE]. ANY REPRODUCTION IN PART OR AS A WHOLE WITHOUT THE WRITTEN PERMISSION OF [INSERT COMPANY NAME HERE] IS PROHIBITED.</p>			
<p>TITLE: Discharge Outlet</p> <p>SIZE: A DWG. NO. [] REV. 2</p> <p>SCALE: 1:5 WEIGHT: [] SHEET 1 OF 1</p>			

Figure 68: Return line

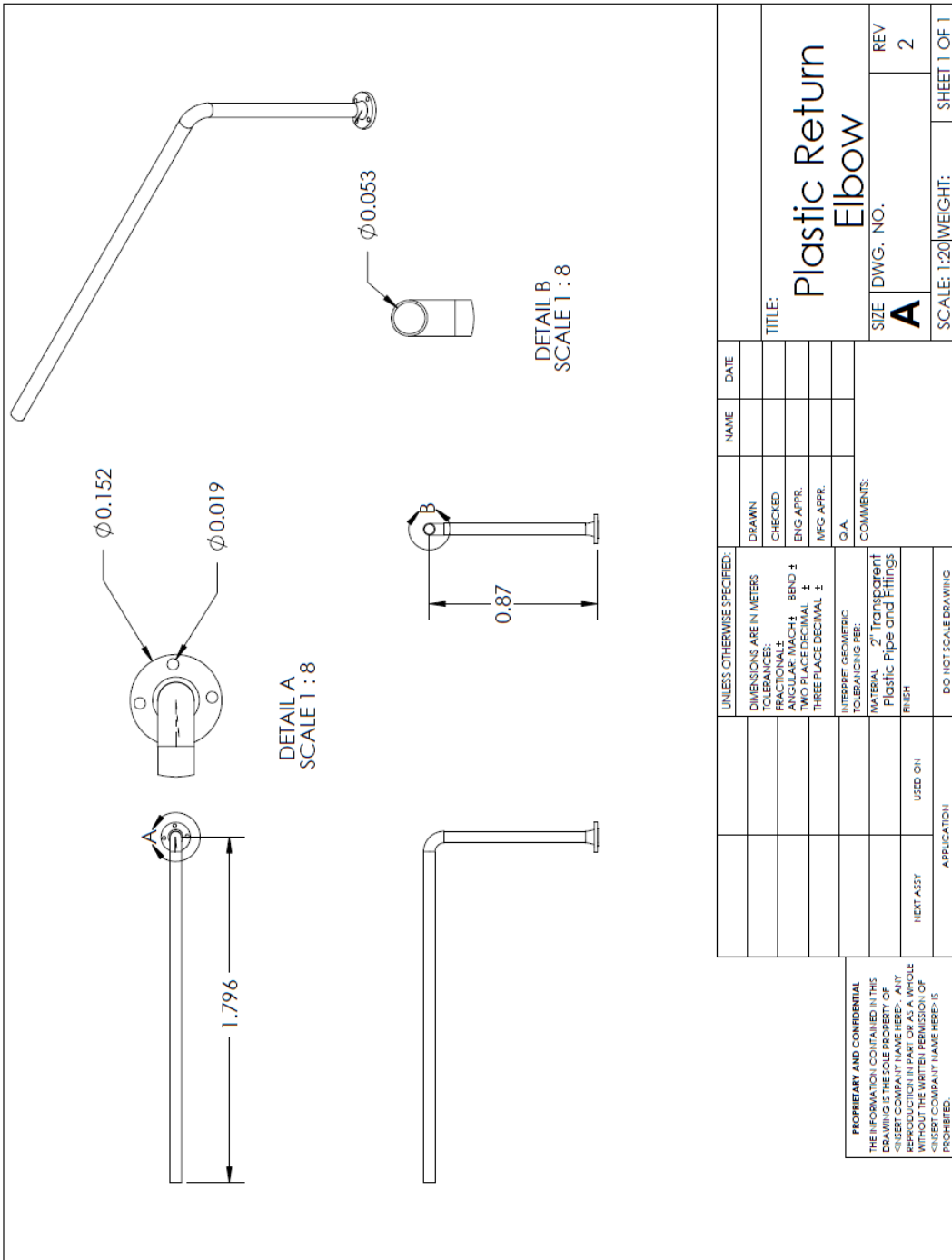


Figure 69: Mixing tank

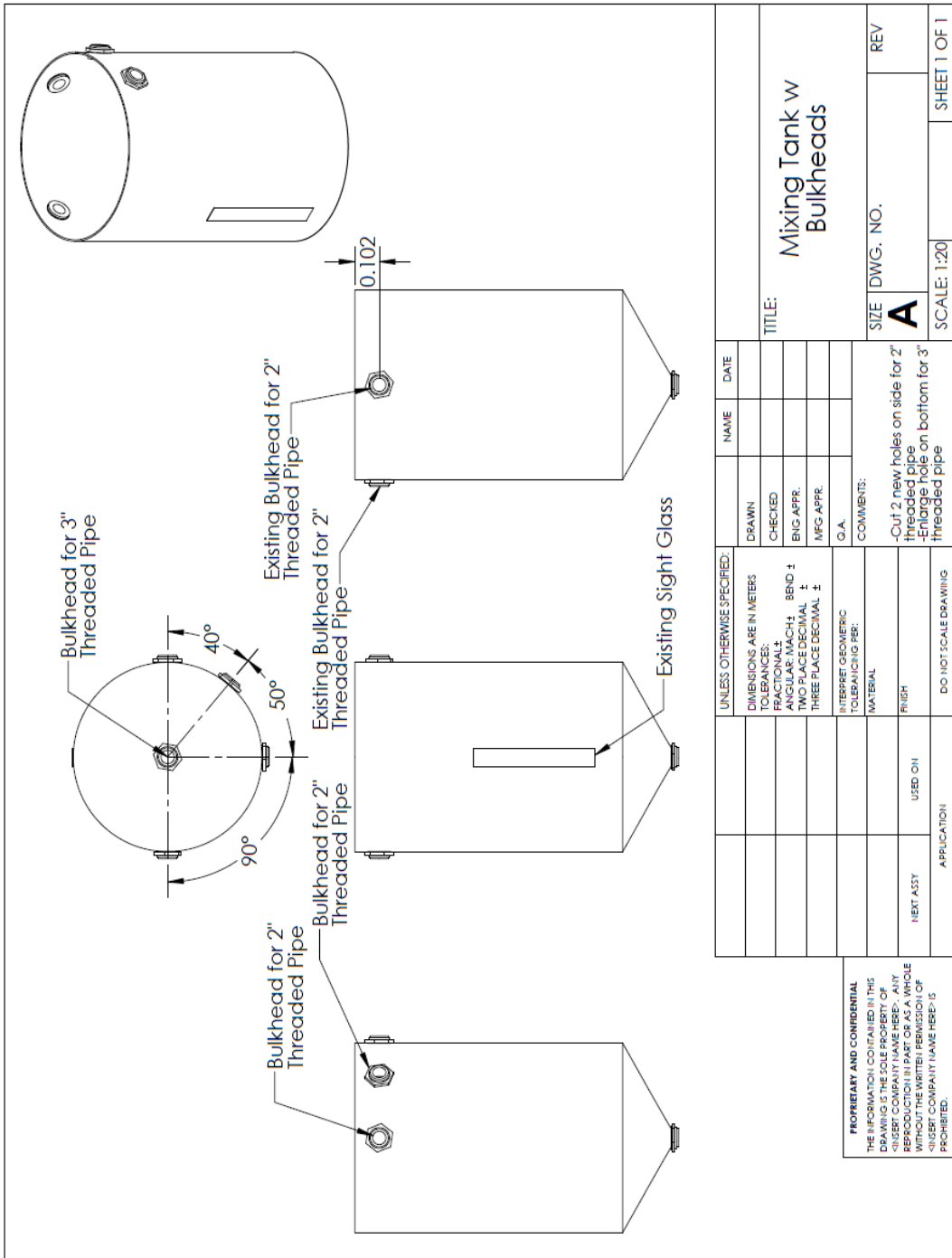


Figure 70: Discharge tank stand

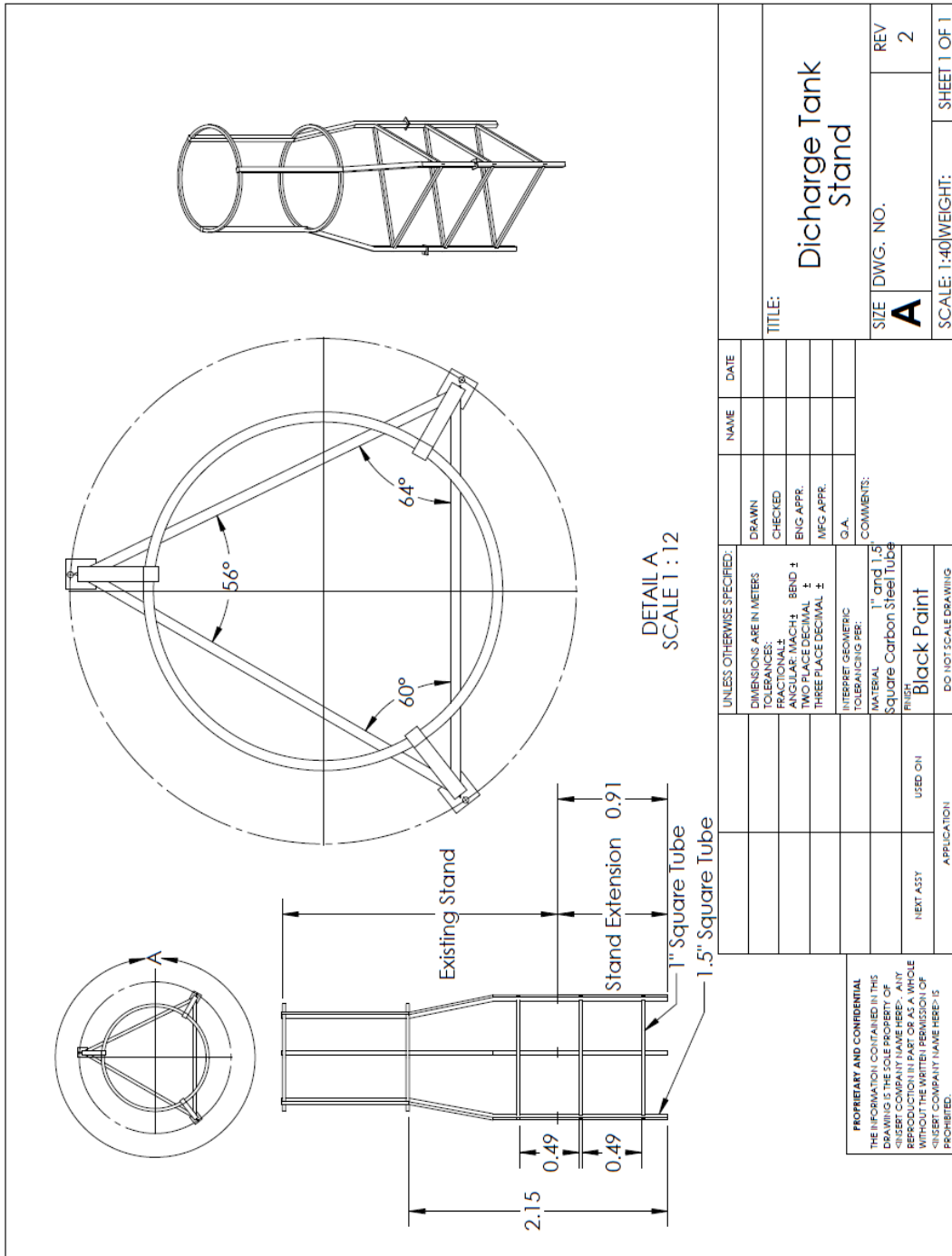


Figure 71: Water bath tank

